Applied Energy (www.elsevier.com/locate/apenergy)

Volume 277, 1 November 2020, 115557

Towards highly efficient electrochemical CO_2 reduction: cell designs, membranes and electrocatalysts[1]

Ramato Ashu Tufa[1,*], Debabrata Chanda[2], Ming Ma[3], David Aili[1,*], Taye Beyene Demissie[4,5], Jan Vaes[6,7], Qingfeng Li[1], Shanhu Liu[2], Deepak Pant[6,7*]

[1] *Department of Energy Conversion and Storage, Technical University of Denmark, Building 310, 2800 Kgs. Lyngby, Denmark*

[2] *Henan Key Laboratory of Polyoxometalate Chemistry, Henan Engineering Research Center of Resource & Energy Recovery from Waste, College of Chemistry and Chemical Engineering, Henan University, Kaifeng, 47504, P. R. China*

[3] *Department of Physics, Technical University of Denmark, Building 311, 2800 Kgs. Lyngby, Denmark*

[4] *Materials Science Program, Department of Chemistry, Addis Ababa University, P. O. Box 1176, Addis Ababa, Ethiopia*

[5] *Institute of Organic Chemistry and Biochemistry, Czech Academy of Sciences, Flemingovo nám. 2, 16610, Prague, Czech Republic*

[6] *Flemish Institute for Technological Research (VITO), Separation and Conversion Technology, Boeretang 200, Mol 2400, Belgium*

[7] *Centre for Advanced Process Technology for Urban Resource Recovery (CAPTURE), 9000 Ghent, Belgium*

***Corresponding authors**

Email: deepak.pant@vito.be; larda@dtu.dk; rastu@dtu.dk

[1]DOI: 10.1016/j.apenergy.2020.115557

Abstract

An increase in atmospheric CO_2 concentration is directly associated with the rising concerns of climate change and energy issues. The development of effective technologies for capture and utilization of atmospheric CO_2 is required to mitigate these global challenges. Electrochemical CO_2 reduction (eCO_2R) is one of the most promising approaches for the conversion of excess renewable energy sources into storable fuels and value-added chemicals. This field has recently advanced enormously with impressive research achievements aiming at bringing the technology on the brink of commercial realization. Herein, we present a comprehensive review analyzing the recent progress and opportunities of using different cell designs with the main focus on membrane-based flow cells for eCO_2R, along with the required system-level strategies for optimal engineering to enhance electrocatalytic selectivity and efficiency. Research advance on the use of different polymer electrolyte membranes for CO_2 electrolyzers is updated. Main achievements in new catalyst discoveries are assessed in terms of activity, selectivity, stability together with CO_2R reaction kinetics. This was supported by the analysis of the computational studies performed to devise the effective catalyst design routes and to understand the pathways for CO_2Rs. The interactive effect of the design of reactors and gas diffusion electrodes with catalysts is analyzed for different operating conditions (like pH, temperature and pressure) of CO_2 electrolyzers. Finally, an outlook on future research directions in terms of material and process design for a breakthrough in eCO_2R technologies is provided.

Keywords: Electrochemical CO_2 reduction; Membranes; Electrocatalysts; Cell designs; Cell optimization; Product selectivity

Contents Page

List of abbreviations

AEM	Anion exchange membrane
BPM	Bipolar membrane
CEM	Cation exchange membrane
COF	Covalent organic framework
CO_2R	CO_2 reduction
CO_2RR	CO_2 reduction reaction
DFT	Density functional theory
GDE	Gas diffusion electrodes
SHE	Standard hydrogen electrode
MFR	Microfluidic reactor
MR	Membrane flow reactors
eCO_2R	Electrochemical CO_2 reduction
eCO_2RR	Electrochemical CO_2 reduction reaction
FE	Faradaic efficiency
MEA	Membrane electrode assembly
MOF	Metal organic framework
NP	Nanoparticle
PEM	Polymer electrolyte membrane
PGH	Porphyrin graphene hydrogel
RHE	Reversible Hydrogen Electrode
RVC	Reticulated vitreous carbon
TCPP	4,4´,4´´,4´´´-(porphyrin-5,10,15,20-tetrayl)-tetra benzoate
TMD	Transition metal chalcogenide
TOF	Turn-over frequency
TPP	Tetraphenylporphyrin

1. Introduction

The increasing concentration of greenhouse gases along with the depletion of fossil fuels, which is strongly linked to global warming and climate change issues, is a serious challenge for humankind. In the past decades, atmospheric CO_2 levels have increased drastically, reaching 411.85 ppm in 2019 [1]. It has been recognized that the CO_2 emissions should be reduced by at least 50%, from the level in 2011, to reach the target set by the International Energy Agency, i.e. < 2 °C rise in global temperature by 2050 [2, 3]. In this regard, tremendous effort is required to reduce the rate of global CO_2 emissions and hence limit the impact of global warming. As a potential solution to this challenge, the scientific community has outlined different strategies for CO_2 capture and sequestration, that can mitigate the environmental impact as well as promote sustainable energy supply chain. The vision is to close the carbon cycle, as illustrated in Fig. 1. Here, the conversion of CO_2 into value-added chemicals and fuels can be done through different CO_2 conversion technologies driven by renewable energy sources such as wind and solar. The produced chemicals and fuels can be used for different purposes, including mobility and households, whereafter, the emitted CO_2 is recovered [4].

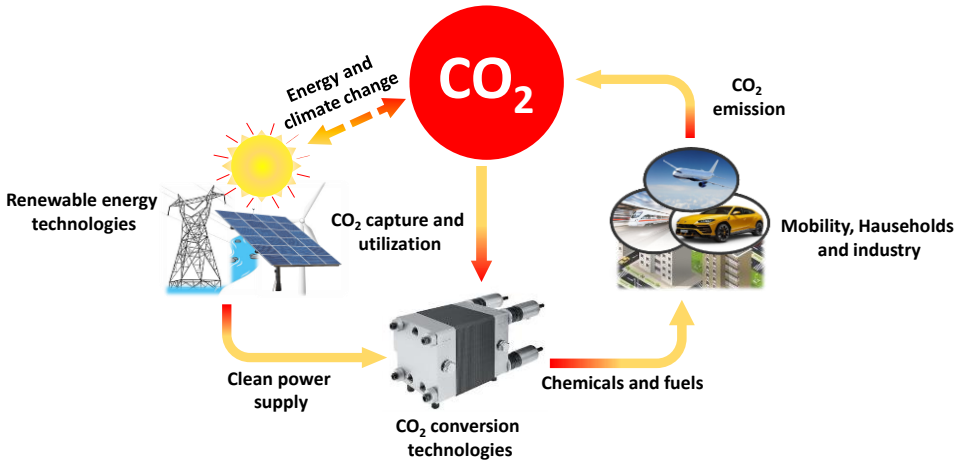

Fig 1. Anthropogenic carbon cycle: renewable energy-driven CO_2 conversion technologies allows the production of value-added chemicals and fuels which are used in mobility, household and industrial purposes. The as-emitted CO_2 in the process of utilizing the fuels and chemicals is feedback to the CO_2 conversion technologies.

1.1. Electrochemical CO_2 reduction

CO_2 is a very stable chemical that imposes significant energy demands for its conversion into the targeted chemicals. The inertness of CO_2 is due to the fact that it is in the most oxidized state of carbon. Although different pathways exist for activation and conversion of CO_2, it is still a challenge to overcome the thermodynamic and kinetic barriers to effectively and optimally design efficient and cost-effective CO_2 reduction (CO_2R) technology [5].

In a broad sense, the pathways for CO_2 utilization can be divided into two: chemical and physical (Fig. 2). The chemical methods for CO_2 conversion involve radiochemical [6], biochemical [7], photochemical [8], chemical [9] as well as (photo)electrochemical routes [10, 11]. The advantage of the later is that it opens the possibility to store the renewable energy in line with renewable electricity costs which are impressively dropping down in recent years. These processes allow for the conversion of CO_2 into other energy storage chemicals, such as ethylene, syngas, formic acid, methanol, methane and dimethyl ether [12-14]: The global market procises for some of these products are shown in Table 1. CO_2 can also be used as a source material or building block for chemical production replacing the large majority of feedstocks used in fossil-based industries. For example, the insertion of CO_2 into epoxides can be used for the production of various polymeric materials, which also has an advantage in terms of avoiding the use of fossil feedstock and hence CO_2 emissions [15, 16]. The CO_2 consumption in the various chemical conversion pathways is estimated to be 0.3 - 0.7 Gt of CO_2 per year [17]. CO_2 can also be converted in large volumes into inorganic minerals that can be used in building materials. Moreover, physical methods allow for the utilization of CO_2 directly without conversion. A good example of this is the use of CO_2 as a beneficial working medium to replace N_2 which increases the generating efficiency of gas turbines [12].

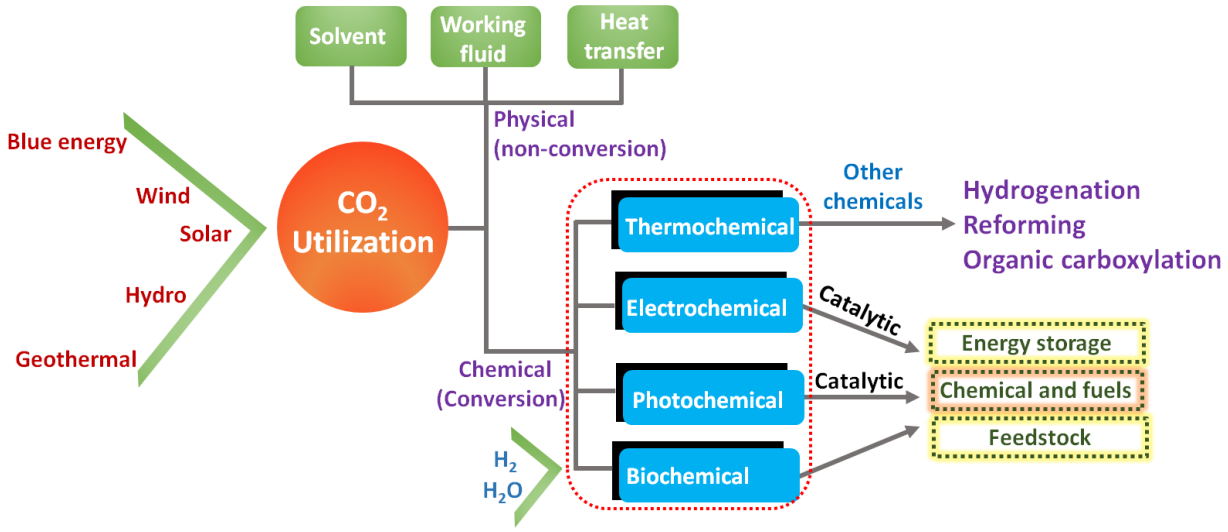

Fig. 2. The different pathways for CO_2 utilization/conversion. CO_2 can be converted directly into useful chemicals and fuels, or it can be utilized directly through physical methods which allow for the utilization of CO_2 without any conversion.

Electrochemical CO_2R (eCO_2R) is considered as one of the most useful techniques for the decarbonization process. Such a process is controllable by means of electrode potential and operating temperature and allows for the possibility to exploit the power of renewables to convert CO_2 and water into value-added fuels and chemicals. The electrochemical CO_2R occurs at the interface of electrode/electrolyte, which involves three main steps: (i) absorption of the CO_2 on the surface of the catalysts; (ii) transfer of at least two protons and electrons to break one of the oxygen-carbon bonds forming a water molecule in the case of CO or subsequent further protonation; (iii) desorption of the final products from the electrode surface. The employed electrocatalysts, local electrode potential, the type and composition of electrolytes are crucial to the efficiency and selectivity of a CO_2 reduction process. Up to now, a lot of work has been done for developing the catalysts towards high selectivity and low CO_2 reduction overpotential. During the process, the surface binding energy of CO_2R reduction intermediates can control the selectivity of the products as well as the rate-limiting step the CO_2 reduction mechanism [18, 19]. Typically, the first electron transfer to form the anionic $CO_2^{\bullet -}$ radical has a large reduction potential (-1.9 V vs SHE) and is often considered as the rate-determining step [17, 18]. As stated earlier, the CO_2R reduction reaction also involves proton-assisted electron transfer processes which are more favorable. Therefore, kinetic dependence of CO_2R reduction reaction on the concentration of

available protons in solution, type of catalysts utilized, etc, is also essential in addition to the thermodynamic barrier, which limits a straight forward comparison of operating potentials for the different CO_2R reactions.

Table 1. The estimated global market prices (in USD/kg) and sizes (USD/year) of major CO_2 reduction products [20, 21]. USD: United States Dollars.

Product	**Market price($/kg)**	**Estimated market size (billion $/year)**	**Global production (Mtonne/year)**
Carbon monoxide (syngas)	0.06	2.7-3.2	-
Formic acid	0.74	0.62	0.6
Ethylene	1.30	155-248	140.0
Methanol	0.58	54	110.0
Ethanol	1.00	-	77.0
Methane	0.18		250.0
Carbon monoxide	0.6	-	-
n-propanol	1.43	-	0.2

Overall, poor understanding of the complex reaction mechanisms and kinetics involved in CO_2R for the different products, along with large overpotential for the formation of $CO_2^{\bullet-}$ intermediate poses several challenges including lack of efficiency, poor product selectivity, and fast degradation of electrocatalytic activity all compromising the final economics of a potential application [22]. Therefore the state-of-the-art techniques are unable to meet the requirements for their industrial application.

The electrochemical CO_2R reaction is a series of electron transfer process, which creates significant thermodynamic and kinetic barriers, due to the stable nature of CO_2 as discussed earlier. Overall, 16 eCO_2R products have been detected, such as carbon monoxide (CO), formic acid (HCOOH), methane (CH_4), ethylene (C_2H_4), ethanol (C_2H_5OH), ethane (C_2H_6), *n*-propanol

(C_3H_7OH), methanol (CH_3OH), oxalic acid ($H_2C_2O_4$), and formaldehyde (HCHO). The standard cell potential ($\Delta E°$) of a redox reaction is related to the standard Gibb's free energy change ($\Delta G°$), as expressed in Eq. 1 below:

$$\Delta E^o = -\frac{\Delta G^o}{nF} \tag{1}$$

where n is the number of electron transfer for the balanced redox couple and F is the Faraday constant. The standard cell potential can be obtained from the difference between the standard potentials of the two half cells. For each half-reaction, the standard electrode potential (E^o) is defined at room temperature for gases at 1 atm and solutes at an activity of 1. For the half-reactions involving H^+ or OH^-, increasing the pH from 0, leads to a decrease of the reduction potential by 0.059 *ΔpH (V). Table 2 presents the standard electrode potentials (vs. the standard hydrogen electrode, SHE) of the different CO_2 reduction reaction (CO_2RR). In the eCO_2R reaction process, it is the catalytic and kinetic issues that are decisive to the types of products. It is likely, at the typically applied potentials, that a mixture of products is being formed composed of gaseous (CO, CH_4, C_2H_4, C_2H_6) and liquid solutes (HCOOH, CH_3OH, C_2H_5OH, etc.). Because of the required overpotential to form the first intermediate for subsequent reduction, the hydrogen evolution reaction (HER) is inevitably competing in aqueous solutions and needs to be suppressed by tailoring the electrocatalyst for the desired eCO_2R product.

Table 2. Electrode potentials *(E)* of selected CO_2 reduction reactions in aqueous solutions at pH = 7 and 25 °C.

Half-reaction of CO_2 reduction	***E* (V vs. SHE)**
$CO_2(g) + 6H_2O(l) + 8e^- = CH_4(g) + 8OH^-$	−0.240
$2CO_2(g) + 10H_2O(l) + 14e^- = C_2H_6(g) + 14OH^-$	−0.270
$3CO_2(g) + 13H_2O(l) + 18e^- = C_3H_7OH(l) + 18OH^-$	−0.320
$2CO_2(g) + 9H_2O(l) + 12e^- = C_2H_5OH(l) + 12OH^-$	−0.33
$2CO_2(g) + 8H_2O(l) + 12e^- = C_2H_4(g) + 12OH^-$	−0.34
$CO_2(g) + 5H_2O(l) + 6e^- = CH_3OH(l) + 6OH^-$	−0.380
$CO_2(g) + 3H_2O(l) + 4e^- = CH_2O(l) + 4OH^-$	−0.480
$CO_2(g) + H_2O(l) + 2e^- = CO(g) + 2OH^-$	−0.520
$CO_2(g) + 2H_2O(l) + 2e^- = HCOOH(l) + 2OH^-$	−0.610

1.2. Scope of the review

This review is mainly focused on the electrochemical CO_2 conversion for the production of useful chemicals and fuels, system design optimization, as well as assessment of design criteria for the key components. Nowadays, the electrochemical eCO_2R driven by renewable energy, in the logic of "power-to-X", is gaining significant attention beyond the scientific community. Most of the research on CO_2R has been focused on the fundamental studies on the catalysts and reaction mechanisms using lab-scale flow cells [20, 23-33]. The eCO_2R reactions involve different pathways resulting in a number of possible product outcomes. Each of these products differs in market prices and sizes (Table 1) depending on the demand and technology utilized in the production process [21, 34]. Several review and perspective papers do exist on CO_2 reduction dedicated to cell design and engineering aspects [23, 26-28, 33, 35-37], electrocatalytic materials and product selectivity [27, 28, 30, 31, 38-41], mechanistic insight on reaction pathways [24, 27], and gas-diffusion electrodes and design of membrane electrode assembly [42-44]. However, a comprehensive type assessment of eCO_2R from system components and design to fundamental applications are few [20, 25, 32]. Herein, we provide a broader look into the thermodynamics of CO_2RR for different cell configurations and compare the performance of the different types of

membranes/electrolytes/electrodes along with the thorough assessment of the operating requirements for the CO_2 reduction. Insights on the membrane and catalyst requirements were used to evaluate the optimal design of membrane electrode assemblies and the proper choice of optimal process conditions. We support these analyses by computational approaches for heterogeneous and homogenous catalysis. Moreover, the electrolyte chemistry in aqueous and non-aqueous media is briefly revised along with a systematic analysis of the chemical phenomenon at the membrane-electrolyte-electrode interface, ultimately putting forward the necessary research directions required for the design and development of CO_2 electrolyzers towards industrial-scale implementation.

2. Cell configurations

Electrochemical studies of CO_2R has been performed in different designs of cells. For catalyst and electrolyte evaluation, a simple half-cell (H-cell) in H-form is most often used where the dissolved CO_2 is reduced to the desired product. When the investigation is extended to evaluate materials such as porous catalyst layers and gas diffusion electrodes (GDE), a cell with a microlayer of flowing liquid electrolyte where the gaseous CO_2 is supplied from the backside of the electrode is typically used, i.e a microfluidic cell. The practical study of the CO_2 reduction is better-performed by using a cathode and an anode with an electrolyte layer in between separated by a membrane, i.e. divided cells, often with forced convection (flow cells).

2.1. Material evaluation cells

2.1.1. H-Cell

Most of the material research on eCO_2R has been carried out using an H-cell, in which a diaphragm separates the two-compartment of the electrochemical cell [25, 33, 45-48]. In a typical H-cell, the working electrode and reference electrode are located in the cathode chamber whereas the counter electrode is located in the anode chamber (Fig. 3a).

The separator between the compartments supports ion conductivity but limits the diffusion of reaction products to the anode side, where they otherwise would be oxidized. The majority of research using an H-cell is reported for evaluation of catalytic materials [49-52] and studies of fundamental issues e.g. catalyst-electrolyte interactions [53], an experimental-computational mechanistic study [54-56], reaction conditions and eCO_2R efficiency [57], product cross-over [58], etc. To achieve an accurate measurement of the cathode potential versus the reference electrode,

the design and location of the reference electrode is critical, which is, however, a general issue for basic electrochemistry and will not be discussed further.

2.1.2. Microfluidic reactors

Microfluidic reactors (MFR) for CO_2R were first reported by Kevin in 2010 [59] based on a previously devised hydrogen fuel cell [60]. In a microfluidic reactor, the anode and cathode are separated by a very thin spacer (<1 mm), creating a channel of flowing liquid electrolyte (Fig. 3b), thus forming a membrane-free cell. The cell is featured by a supply of gaseous CO_2 to the cathode and hence eliminating the solubility restriction to the CO_2R. The gas-phase diffusion through a porous gas diffusion layer is fast and the CO_2R at the electrode/electrolyte interface is not limited by the mass transport of dissolved CO_2. The MFR is, therefore, suitable for the evaluation of catalyst layers and GDEs. A reference electrode is often inserted in the electrolyte flow stream. As a membrane-less device, MFR is prone to product re-oxidation.

2.2. Membrane-based flow reactors

Membrane-based flow reactors (MR) provide a device for practical CO_2R. MR is a design based on the conventional low-temperature water electrolysis or fuel cells either with a spacer-filled flow channel between the electrode and membrane (Fig. 3c) or in a zero-gap arrangement with the fluid flow on the backside of both electrodes (in zero gap) (Fig. 3d). In a typical MRs, an ion exchange membrane is used to prevent the product crossover between the cathode and anode. The CO_2 is supplied to the cathode either dissolved in a liquid solution (liquid-phase) [61-63] or in the gas (pure or partly humidified) phase [62-65] while the anode is fed with a liquid electrolyte. In some cases, both electrodes can be fed with humidified CO_2 [66-69]. Thus, the technological advances in such systems can be systematically adopted to design a highly efficient CO_2 electrolyzer [26]. The research development on MRs in flow cell is in its early stage with technological gaps to be addressed that will be discussed in the next sections.

2.3. Other configurations

Solid oxide electrolyzers (SOEs) are also used for CO_2R at high temperatures (> 600 °C), which has attracted strong attention among the scientific community recently. In a typical SOE, the anode and cathode are separated by a solid electrolyte, which can be either an oxygen ion conductor or protonic conductors. The electrochemical reduction of CO_2 at the interface of the electrodes, solid electrolyte and the reactant gases at high temperature leaves more efficient mass

transport of CO_2 and lower activation energy barrier. This phenomenon derives a higher current density for SOE compared to the classical, low-temperature CO_2R in aqueous electrolytes. Despite these advantages, the SOE is highly limited by the complex electrocatalytic chemistry and significant degradation of electrodes, electrolytes and the electrode-electrolyte interface at high temperatures [70-75].

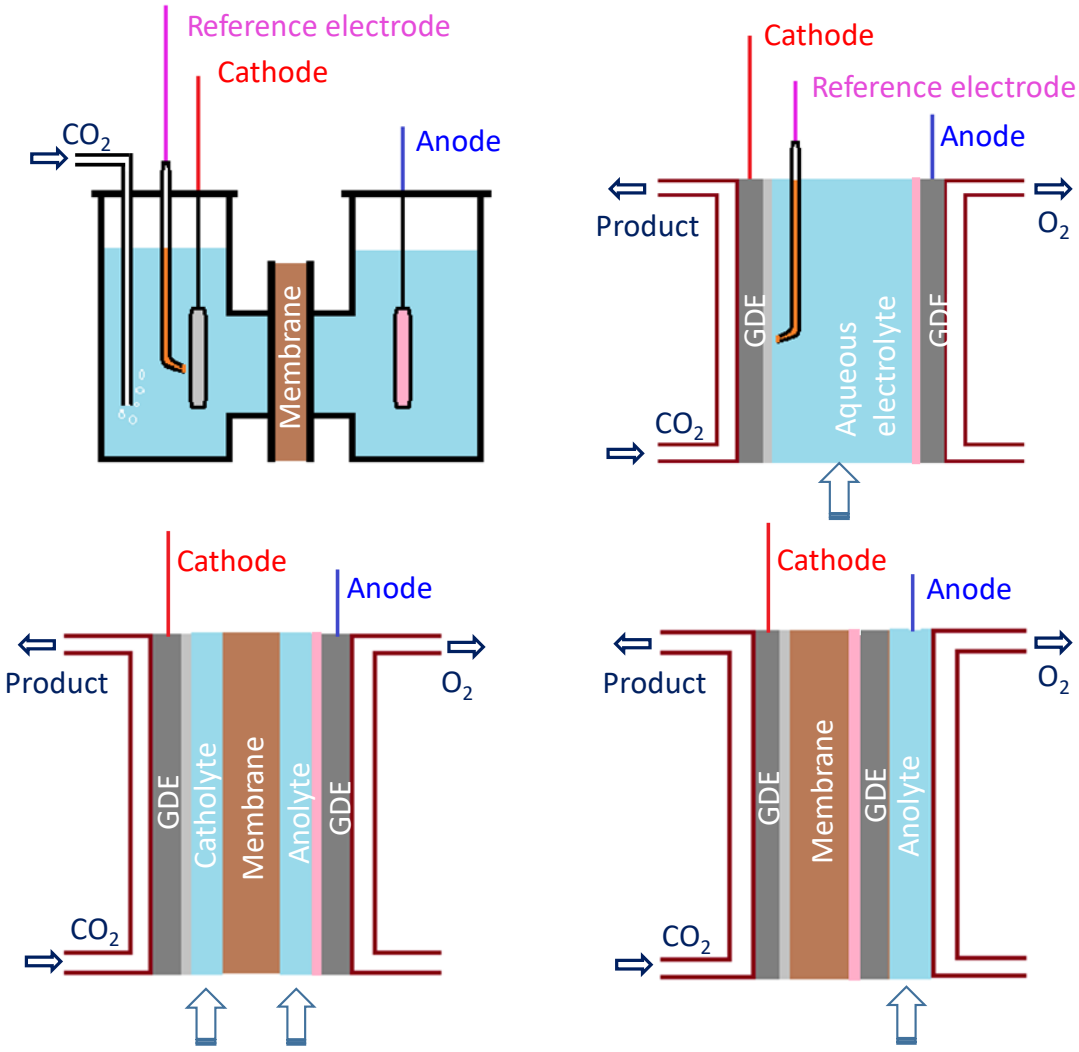

Fig. 3. Schematic illustration of half-cell designs of a) H-cell and b) microfluidic cell, and cell designs of electrolyzers with c) liquid-phase CO_2 supply and d) gas-phase CO_2 supply. A diaphragm can also replace the membranes.

3. Materials

3.1. Electrolytes

In principle, the cathode reactions in eCO_2R may involve protons or hydroxide ions depending on the pH range at the catalyst-electrolyte interface:

$$CO_2 + 2H^+ + 2e^- \rightarrow CO + H_2O \quad \text{(R1)}$$

$$CO_2 + H_2O + 2e^- \rightarrow CO + 2OH^- \quad \text{(R2)}$$

The anodic reaction involves the evolution of oxygen which occurs by the consumption of OH^-:

$$2OH^- + 2e^- \rightarrow \tfrac{1}{2}O_2 + H_2O \quad \text{(R3)}$$

Therefore, understanding the chemistry of CO_2 in aqueous/non-aqueous media in relation to local pH, and the effects of the available anions and cations is highly crucial for the optimal CO_2R to desired products.

3.1.1. Chemistry of CO_2 in aqueous media

Carbon dioxide physically dissolves in pure water. The hydration of dissolved CO_2 leads to the formation of carbonic acid with the equilibrium constant (K_h) [76]:

$$CO_2 + H_2O \rightleftarrows H_2CO_3 \qquad K_h = \frac{[H_2CO_3]}{[CO_2]} = 1.7x10^{-3} \quad \text{(R4)}$$

Here, the carbon dioxide speciation towards bicarbonate (HCO_3^-) and carbonate (CO_3^{-2}) is notable, which is related to the 1st and 2nd acid dissociation constants, respectively:

$$H_2CO_3 \rightleftarrows HCO_3^- + H^+ \qquad pK_a^1 = 3.6 \quad \text{(R5)}$$

$$HCO_3^- \rightleftarrows CO_3^{2-} + H^+ \qquad pK_a^2 = 10.3 \quad \text{(R6)}$$

Combination of (R5) and (R6) with the dissociation equilibrium of water (R7) and a charge-neutral restraint (R8) leads to:

$$H_2O \rightleftarrows OH^- + H^+ \qquad pK_a = 14 \quad \text{(R7)}$$

$[H^+] = [OH^-] + [HCO_3^-] + ½ [CO_3^{2-}]$ (R8)

One can obtain the equilibrium concentration of these species in the CO_2-H_2O mixture as a function of the partial pressure of CO_2 (P_{CO2}) and the pH. The variations in equilibrium concentration ratios of the carbonate species as a function of pH can be presented in a Bjerrum plot as shown in Fig. 4. It is interesting to note that the H_2CO_3 is always in equilibrium with CO_2 while the concentration of H_2CO_3 is much lower than that of CO_2. In practice, the sum of concentrations of H_2CO_3 and dissolved $CO_{2(aq)}$, denoted as $H_2CO_3^*$, is used in the consideration of the solution equilibrium:

$H_2CO_3^* \rightleftharpoons HCO_3^- + H^+ \qquad pK_a^* = 6.35$ (R9)

As shown in Fig. 4, the curves for $CO_{2(aq)}/H_2CO_3$ and HCO_3^- intersect at $\text{pH} = pK_a^* = 6.35$ while the curves for HCO_3^- and CO_3^{2-} intersect at $\text{pH} = pK_a^2 = 10.3$, indicating the dominance of HCO_3^- in the respective pH range i.e. 6.35-10.3.

Under ambient atmosphere with $P_{CO2} = 4 \times 10^{-4}$ atm, the saturation of CO_2 in pure water reaches a solubility of 0.012 mmol L^{-1}, which makes water slightly acidic having pH = 5.7. At P_{CO2} = 1 atm, the solubility of gaseous CO_2 in water is about 34 mmol L^{-1}, equilibrated with 0.12 mmol/L HCO_3^-, which means that it ends up at an aqueous solution of pH = 3.9. In solutions of elevated pH values, the acid dissociation is promoted and dissolved CO_2 will manifest as bicarbonate HCO_3^-. In even more alkaline solutions of pH > 10.3, it will be present as CO_3^{2-} and no molecular dissolved CO_2 is present.

The CO_2 solubility is substantially affected by the presence of other salt species, as for example, it is significantly lower in seawater. For the CO_2R studies, however, the gaseous CO_2 is usually continuously bubbled through the electrolyte, which makes a big difference, for example, the partial pressure of CO_2 is increased from the atmospheric value (4×10^{-4} atm) to 1 atm and hence the dissolved amount, as shown by work of Zhong *et al.* [77]. Other approaches to increase the solubility involved the use of high-pressure CO_2 flow or the use of non-aqueous solvent [78].

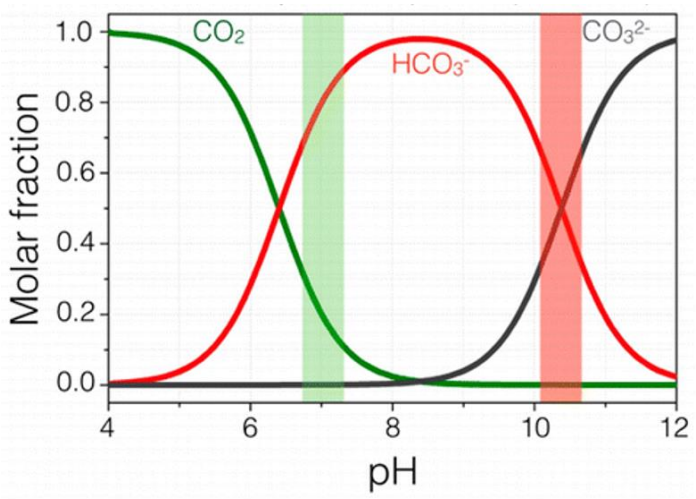

Fig. 4. Bjerrum plot of carbonate speciation as a function of pH. Reproduced with permission from ref [79]. Copyright 2015, American Chemical Society.

3.1.2. Aqueous Supporting electrolytes

The most commonly used electrolytes in CO_2R are aqueous solutions in which the dissolved CO_2 exists in equilibrium with bicarbonate at a bulk pH range between 6 to 8. Salts of halides, sulfates, carbonates, bicarbonates as well as hydroxides have been used for investigation of CO_2R. As Zhong *et al*. [77] reported, as CO_2 is bubbled through liquid electrolyte solutions, high pH solutions such as KOH and KCO_3 reach a carbonate equilibrium by conversion of OH^- and CO_3^{2-} into HCO_3^- anions as well as molecular CO_2 and H_2CO_3, thereby stabilizing the solution pH in the neutral regions.

The CO_2R, as seen from Table 2, involves either the formation of OH^- or consumption of H^+. As the reaction proceeds, particularly at higher current densities, the activity of protons and/or hydroxyl anions changes, affecting the thermodynamics as well as the kinetics of the cathodic reaction. The solubility of CO_2 as well as the electrode reaction intermediates [80] is affected as well. Solutions with buffering capacities such as bicarbonates and phosphates are preferred, which further dissociate when the electrolyte pH in the vicinity of the cathode increases and reaches their pK_a values and therefore stabilizes the pH of the electrolyte.

Bicarbonate solutions are commonly used for the CO_2RR. It is unique in several ways, as for instance, the HCO_3^- exhibiting a good buffering capability serves as a CO_2 reservoir. It has long been known that the dissolved CO_2, rather than ionic HCO_3^- or CO_3^{2-}, are the active species for

the CO_2RR [81, 82]. On the other hand, it has also been reported that the CO_2RR activity is enhanced in HCO_3^- electrolyte compared to other electrolytes under similar operating conditions [83, 84]. It is hence suggested that the HCO_3^- is actively involved in the reduction, probably via the formation of bicarbonate-CO_2 complex, which increases the CO_2 concentration in the vicinity of the electrode [85].

In aqueous media, water molecules play a role either as donating, generating hydroxyl anions, or receiving protons, forming the hydronium structure. Bicarbonate serves also as a better proton donor than e.g. water [86, 87]. Moreover, other ionic species, both cations and anions, have been proved to have a significant impact on the activity and selectivity of the CO_2RR. This will be discussed in section 4.3.1.

3.1.3. Non-aqueous electrolytes

The electrocatalytic CO_2R has also been carried out in non-aqueous solvents mainly due to the high solubility of CO_2 in organic solvents compared to aqueous solutions. For example, the solubility of CO_2 in acetonitrile is about ~0.28 M, which is almost 8-fold higher than in water at 1 atm and ambient temperature [88]. Non-aqueous solvents, for example, aprotic organic solvents, allows circumventing the competing HER compared to aqueous solvents. Depending on the type of catalyst employed, the choice of aprotic solvents is also favored as some catalysts based on metal complexes might undergo hydrolysis in aqueous solvents.

Organic solvents such as acetonitrile [88-97], dimethylformamide [93, 95, 98, 99] and methanol [100-105] are among the most widely reported electrolytes for CO_2R. When working with organic solvents, the water content (mole fraction of 0.15-0.45) was shown to influence the performance and product distribution of a CO_2RR. A study conducted using a nanostructured Cu electrode for CO_2R in different mixtures of H_2O/acetonitrile resulted in the highest reduction currents for a mixture with 0.25 mole fraction of H_2O [90]. Owing to the high solubility at low temperatures, methanol is considered the best solvent for hydrocarbon production compared to other organic solvents [104, 105]. An eCO_2R to methane performed on a Cu-based electrode in various sodium-based supporting salts solutions resulted in the best Faradaic efficiency of 70.5% when using $NaClO_4$/methanol as the electrolyte solution [103].

Aqueous and non-aqueous solutions of ionic liquids have also been investigated because of their CO_2 absorption capacity, chemical, and thermal stability, wide electrochemical window, and

because they can act as mediators for redox catalysis [106-108]. In CO_2RRs, ILs play a key role in absorbing CO_2 and stabilizing the $CO_2^{\bullet-}$ anionic radical which is ascribed to the electronic properties of its cationic and anionic components.

Despite some advantages over aqueous ones, wide spread use of non-aqueous solutions is limited by additional factors like safety, cost and toxicity issues. Moreover, the formation of $CO_2^{\bullet-}$ as the first anionic radical demands larger overpotentials than in aqueous-based electrolytes solutions.

3.2. Membrane separator

In CO_2R electrochemical cells, a membrane separates the two electrodes in order to prevent the crossover of CO_2R products, which would cause poor current efficiency of CO_2RR. The employed materials are ion-exchange membranes, which, ideally, are selectively permeable for certain types of ions, while blocking other ions or neutral molecules. The most commonly used membranes are monopolar membranes which can be a cation exchange membrane (CEM) [66, 109-135], also called "proton exchange membrane" (PEM), and anion exchange membrane (AEM) [68, 124, 129, 130, 133, 136-147]. Bipolar membranes, which are composed of a cation exchange layer on one side and an anion exchange layer on the other, have also emerged as a promising material for CO_2R [62, 63, 113, 148-152]. The following sections are devoted to a brief discussion focusing on the conducting species and conductivity issues, whereas the CO_2R cell performance is reviewed later in section 4.4.

3.2.1. Cation exchange membrane

A CEM allows for the passage of cations, while retaining the anions. A cation exchange membrane is exemplified by proton conduction, and so-termed as a proton exchange membrane (PEM), which is widely used in fuel cells and water electrolyzers. The most commonly used PEM is perfluorosulfonic acid (PFSA)-based membranes, e.g. Nafion®, with sulfonic acid groups immobilized on the polymer backbones. For PEM membranes in contact with e.g., NaOH solution, a cation exchange takes place via the sulfonic acid groups of the membrane:

$$R\text{-}SO_3H + NaOH \rightleftarrows R\text{-}SO_3Na + H_2O \quad (R10)$$

The neutralization has a drastic effect on the physical properties of the PEM membrane. The glass transition temperature of the membrane increases from 125 °C for Nafion to as high as over

200 °C. With an excess of NaOH in the solutions, the ionic species existing in the PFSA-NaOH system are primarily Na^+ and OH^-.

Under these conditions, the ionic conductivity is via transport of alkali metal cations (Na^+), which is well known from the chlor-alkali cells where a PEM is used to separate chlorine gas from hydrogen and sodium hydroxide formed at the cathode. In alkaline conditions, a continuous feed of gaseous CO_2 on the cathode side will be converted into carbonate and eventually bicarbonate, gradually lowering the pH:

$$CO_2 + 2OH^- \rightleftarrows CO_3^{2-} + H_2O \quad \text{(R11)}$$

$$CO_2 + OH^- \rightleftarrows HCO_3^- + H_2O \quad \text{(R12)}$$

The transport mechanism of a variety of anions through a CEM is well known. In low pH region, where protons are available, anions like Cl^-, SO_4^{2-} and NO_3^- are in fully dissociated form. These ionic species are blocked due to the Donnan exclusion effect and hence their permeability through a CEM is very low. On the contrary, weak acid anions like F^- and NO_2^- occur in their associated form, minimizing the Donnan effect and therefore exhibiting higher permeation rates driven by activity gradients [153]. Though no permeation data are reported, the HCO_3^- ion is believed to belong to the second group of anions with the transport depending on the partial pressure of CO_2 under the CO_2R conditions.

3.2.2. Anion exchange membranes

An AEM allows for the passage of anions while retaining the cations. An anion exchange membrane (AEM) is exemplified by the hydroxide conducting membrane, allowing for conduction of hydroxide (OH^-) anions while minimizing the crossover of gas molecules (oxygen or hydrogen) in fuel cells and water electrolyzers. The typical alkaline anion exchange membrane is composed of a polymer backbone coupled with anion exchange functional groups. For example, poly(arylene ethers) of varied structures e.g. polysulfones, poly(ether ketones) or carbon backbones can be functionalized with quaternary ammonium anion exchange sites to form AEMs [154].

In AEM-based CO_2R cells, a common practice is to circulate a strongly alkaline solution at the anode side, which significantly promotes the membrane conductivity and enables the use of non-noble catalysts for the oxygen evolution reaction.

The HCO_3^- and CO_3^{2-} ions are apparently conducting species through an AEM separator in CO_2R cells, although little information is available on the transference numbers of the OH^- and HCO_3^-/CO_3^{2-} ions. Electrochemical formation of HCO_3^- and CO_3^{2-} are also possible at the cathode for, e.g., during the production of CO as:

$$3CO_2 + H_2O + 2e^- \rightleftarrows CO + 2\,HCO_3^- \quad \text{(R13)}$$

$$2CO_2 + 2e^- \rightleftarrows CO + CO_3^{2-} \quad \text{(R14)}$$

As a result of transport from the cathode to the anode, the HCO_3^-/CO_3^{2-} ions will be consumed at the anode as:

$$2HCO_3^- \rightleftarrows \tfrac{1}{2}O_2 + 2\,CO_2 + H_2O + 2e^- \quad \text{(R15)}$$

$$CO_3^{2-} \rightleftarrows \tfrac{1}{2}O_2 + CO_2 + 2e^- \quad \text{(R16)}$$

The overall cell reaction for the reduction of CO_2 to CO is accompanied by parasitic transport of CO_2 molecules. This phenomenon is termed as "CO_2 pumping", which is detailed in section 4.4.2. Larrazábal *et al*. [142] reported that the CO_2 crossover through an anion-exchange membrane exceeds the amount of electrochemically reduced CO_2. Details on CO_2 cross-over and/or CO_2 pumping effects are presented later (section 4.4.2).

3.2.3. Bipolar membranes

A BPM is formed by lamination or close contact of AEM and CEM, creating two ion-exchange membrane layers: a cation exchange layer (CEL) and an anion exchange layer (AEL). An interfacial layer (IL) is formed at the junction between the CEL and AEL.

In electrochemical cells, BPM can operate in either forward bias mode or reverse bias mode. In the former case, the CEM faces the anode side and the AEM the cathode side (Fig. 5a). The anode reaction is the oxygen evolution with proton formation and therefore needs noble metal oxide e.g. IrO_2 as the catalyst. The cathode reaction is CO_2 reduction with the formation of hydroxide ions as well as bicarbonate. In the absence of the Donnan effect of co-ion exclusion, the AEM exhibits significant conductivity of OH^- and HCO_3^-. At the IL between the CEM and AEM, water is formed from proton and hydroxide recombination. The bicarbonate reacts with a proton at the IL and releases CO_2, i.e., the CO_2 pumping remains an issue as that of AEM monolayer membranes.

The application of BPM in reverse bias is more interesting than the forward bias, pertinent to the water dissociation phenomenon occurring at the interface between AEM and CEM, which is essential for its functioning. Under reverse bias, the AEM faces the anode, often with a circulation of alkaline supporting electrolyte, and CEM faces the cathode with CO_2 feeding (Fig. 5b). The dissociation of water at the AEM/CEM interface leads to the separation of H^+ toward the highly acidic CEM side (e.g. 1 M H^+) and hydroxide ions toward the highly alkaline AEM side (e.g. 1 M OH^-) [148, 155, 156]. Catalysts can be used to facilitate water dissociation, and such materials can be based-on weak acids (HA) or weak bases (B) such as phosphoric acid [157] or pyridines [158], heavy metal ion complexes like those of iron, chromium, zirconium [159, 160], metal hydroxides [161-163] or graphene oxides [164, 165]. The mechanism in which water dissociation occurs at the BPM interface is believed to be due to the catalytic proton transfer reaction between the water and the fixed groups at the IL and the enhanced electric field effect defined by Onsager's theory of the second Wien effect [159, 160, 166-175]. The assumed catalysis of water dissociation by a weak acid (HA) or base (B) proceeds in two consecutive steps of reversible deprotonation or protonation [176]:

$$A^- + H_2O \rightleftarrows AH + OH^- \rightleftarrows A^- + H^+ + OH^- \quad \text{(R17)}$$

$$B + H_2O \rightleftarrows BH^+ + OH^- \rightleftarrows B + H^+ + OH^- \quad \text{(R18)}$$

The overall water dissociation is presented as:

$$H_2O \rightleftarrows H^+ + OH^- \quad \text{(R19)}$$

The transport of protons and hydroxides ions from the IL of the BPM to the cathode and anode, respectively, allows for balancing the consumed protons and hydroxides at the electrode reactions leading to a stable pH, which is one of their unique advantages of BPMs over the monopolar membranes. This stabilization of the local change in pH potentially allows for better design and optimization of low-cost CO_2 electrolyzers as reported in many publications utilizing BPM [58, 62, 63, 113, 148, 177-179]. For instance, the BPM enables the use of abundant and cheap catalyst materials that are only stable in basic conditions such as Ni, $FeNiO_x$ and highly active acid-stable electrocatalysts for CO_2R [62, 63, 148].

When performing CO_2R using electrolytes based on aqueous HCO_3^- salts, the supply of protons to the cathode side under reverse bias occurs as stated earlier which is a unique

phenomenon of BPM. The acid-base equilibrium between the protons and HCO_3^-, yields the formation of CO_2 and H_2O at the membrane-solution interface, which has been shown to influence the efficiency of CO_2R reactions at the cathode [180]. Meanwhile, the transport of HCO_3^- to the anode side is highly restricted due to Donnan exclusion effect whereas the transport of proton prevails in the CEM. In this way, the CO_2 pumping issue, which is associated with the HCO_3^- /CO_3^{2-} transport to the anode side (severe in the case of AEMs) is sufficiently reduced [68]. Overall, in BPM-based cells, the HCO_3^- functioning as a source of CO_2 leads to a higher local concentration of CO_2 over the cathode than the solubility limits of CO_2 in aqueous media, presenting as alternative pathway towards high current density in liquid-phase CO_2 electrolysis [180].

Under both the forward and reverse bias, the BPM layers should have a sufficient swelling property to allow for a water flux into the interface to replenish the water consumed by the water dissociation.

Overall, the special function of BPMs in the aspect of water dissociation at IL between the monopolar junctions offers an advantage of better restriction of product crossover, among others, compared to the monopolar membranes which exhibit a low capability of maintaining a pH balance and hence a reduction of product crossover. The dominant ionic species existing in an electrolyte and hence in the functional sites of the membrane highly depends on the local pH. For example, a crossover of anionic products in AEM-based configurations has been shown to be a major problem occurring as a result of pH change between anodic and cathodic compartments under continuous (electrolytic) operation, both at low high and high current densities [58, 181]. As the flux of protons occurs in an opposite direction to the product crossover from the cathode to the anode, it is anticipated that the electromigration of anionic products and the transport of neutral molecules by electroosmotic drag are minimized in the BPM-based CO_2 electrolyzers [58]. However, this is not really assured as there is a risk of cross-contamination between electrodes when using BPM in CO_2 electrolyzers, and it's uncertain, if BPM effectively prevents an ion or product from the cross over at nearly-neutral CO_2R conditions [148, 156, 182], depending on the composition and concentration of electrolyte [148, 183-185]. A rigorous experimental study on BPMs under a broad range of properties related to membranes and electrolytes is essential. Details on the BPM testing and crossover properties is discussed in section 4.4.2.3.

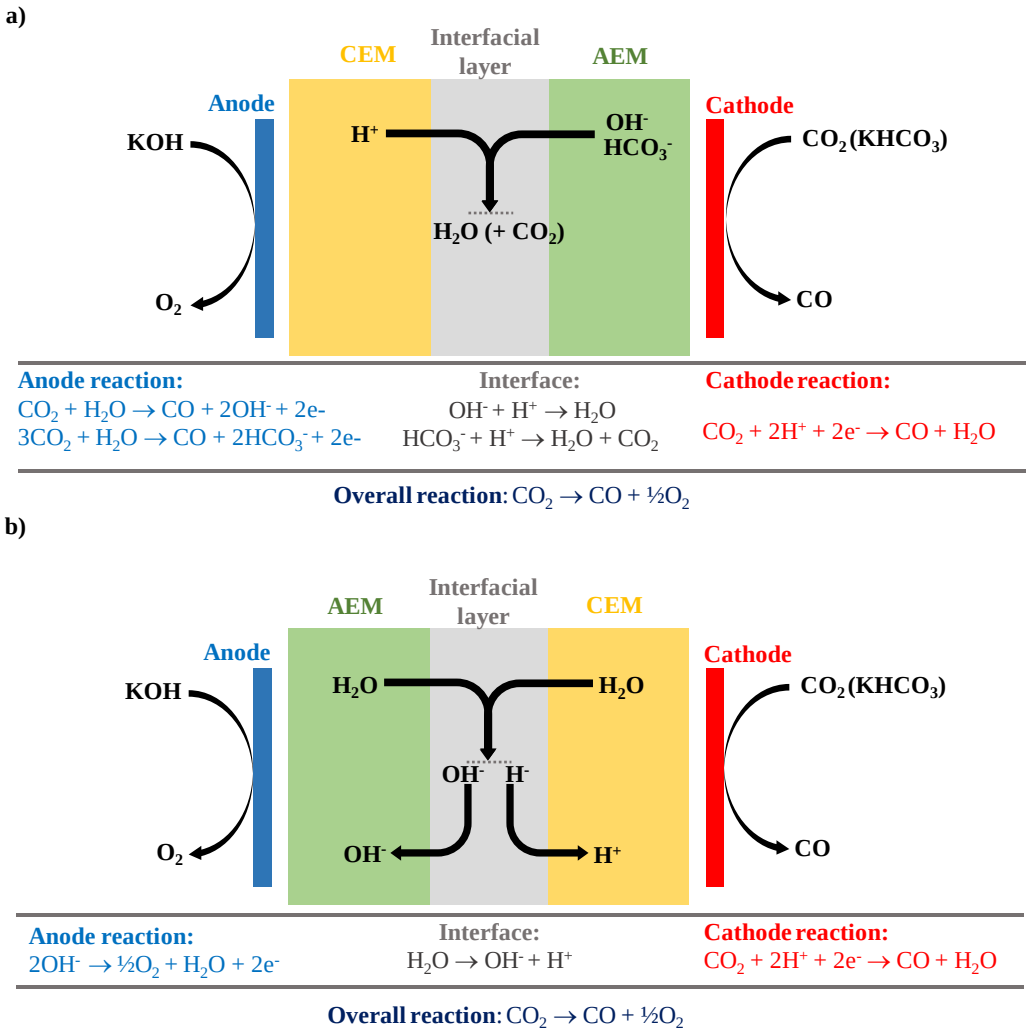

Fig 5. Configurations of BPM-based CO_2 electrolyzer. a) The forward bias mode where the AEM faces the cathode with CO_2 feeding and CEM faces the anode. Water and possible CO_2 formation takes place in the interfacial layer. b) The reverse bias mode where the AEM faces the anode and often with alkaline supporting electrolyte and CEM faces the cathode with CO_2 feeding. Water dissociation takes place in the interfacial layer.

3.3.Electrocatalyst

3.3.1. Metals (noble and non-noble)

In the past few decades, the electrochemical CO_2R has been extensively explored on various transition metal surfaces in CO_2-saturated aqueous solutions [186-193]. Based on the product selectivity, Hori *et al.* [186] categorized these metals into four different groups. In the first group, Pb, In, Sn and Bi could selectively reduce CO_2 into formate in aqueous solutions. Au, Ag and Zn

surfaces, as the second group, produce CO as a major product in electroreduction of CO_2. The third group only contains Cu, which has the capability of uniquely catalyzing CO_2 to significant amounts of hydrocarbons (CH_4 and C_2H_4) and alcohols with relatively high catalytic selectivity. In the fourth group, metals such as Pt, Ni, Fe, and Ti do not produce obvious carbon products, but tend to favor H_2 formation. In this review, we categorized all the CO_2R metals into two groups, noble metals (such as Au and Ag) and non-noble metals (such as Zn and Cu), since the large-scale applications require catalyst materials with low cost and earth abundance (in addition to high catalytic activity and selectivity).

Catalytic performance is not only dependent on the materials, but also correlated with surface morphology. It has been demonstrated that nanostructured metal surface could provide a large amount of low-coordinated sites (edge or corner sites), which are more active for CO_2R in comparison with that of a bulk meal (planar metal surface). The nanostructured metal electrocatalysts with controllable size and shape are the focus of the most CO_2R research and are also the main focus of this section.

3.3.1.1. Noble metals (Au and Ag) for CO formation

While Au is the most active metal surface for electrochemical conversion of CO_2 into CO, the CO formation on Au is still limited by the CO_2 activation (COOH intermediate formation) [194]. The nanostructured morphology offers a platform for further improving this CO_2 activation step, which may dramatically reduce the required overpotential for final CO formation in CO_2R. Sun *et al.* [195] has explored that the electrochemical CO_2R on Au nanoparticles (NPs) with a series of controllable sizes (4, 6, 8 and 10 nm) in CO_2 saturated-0.5 M $KHCO_3$, discovering that the highest selectivity for the reduction of CO_2 to CO over the 8 nm NPs (FE= 90% at -0.67 V vs. Reversible Hydrogen Electrode (RHE)). Authors found that edge sites on Au NPs are active for CO formation, while corner sites favored the competitive HER. Thus, the stabilization of $COOH^{\bullet}$ intermediate is facilitated by the presence of more edge sites than corner sites on the Au NP surface, leading to the enhancement in a reduction of CO_2 to CO while suppressing H_2 evolution [195]. Based on this finding of that the edge sites of Au favor CO_2 conversion into CO while corner sites are preferred for H_2 evolution, a one-dimensional Au morphology (nanowires) with an abundance of edge sites was designed [196]. These Au nanowires electrocatalytically converted CO_2 into CO with FE of 94% at -0.35 V vs. RHE in CO_2 saturated-0.5 M $KHCO_3$, which is ascribed to the favorable CO_2

activation via a high edge-to-corner ratio in ultrathin Au NWs and the facile CO release via the weak CO binding energy on the reactive edge sites [196].

Metallic Ag is the focus of the most CO_2R to CO research, owing to its relatively low cost compared to Au surface and high catalytic selectivity. Jaramillo *et al*. [197] have systematically studied CO_2R performance of Ag foils as a function of potential, demonstrating that catalytic selectivity (CO and H_2 formation) was dependent on the applied potentials. Besides, the optimal selectivity of CO production on the Ag electrodes was detected at the range from -1.0 to -1.2 V vs. RHE, to a range of overpotential from ~0.9 V to ~1.1V. The overpotential of > 0.9 V required for driving selective and efficient CO_2R with suppressed H_2 evolution remains high, which limits the practical applications. This large overpotential needed for selective CO_2R is due to the high activation energy barrier of initial electron transfer for the stabilization of $COOH^{\bullet}$ intermediate [198-200]. In this context, the theoretical study has demonstrated that nanostructured Ag has low-coordinated sites, which can facilitate CO_2 activation or COOH stabilization via the decrease of the activation energy barrier of the initial electron transfer [200].

Experimentally, many attempts have concentrated on developing nanostructured Ag surface to overcome the limitations of Ag catalysts. Lu *et al*. [199] developed a dealloying process to prepare a nanoporous Ag (np-Ag) catalyst via an Ag-Al precursor (Fig. 6a and b show the SEM and TEM images). The np-Ag catalyst has been demonstrated to be able to electrochemically convert CO_2 into CO with a very high FE of more than 90% at a potential of -0.6 V vs. RHE in CO_2-saturated solutions, which corresponds to a moderate overpotential of 0.49 V relative to the CO_2/CO equilibrium potential of -0.11 V vs. RHE. Tafel analysis for the np-Ag catalysts and the polycrystalline Ag electrodes was performed (Fig. 6c). A Tafel slope of 132 Mv dec^{-1} was found for the untreated planar Ag, revealing that the initial electron transfer to CO_2 for the $CO_2^{\bullet-}$ formation is the rate-determining step. In contrast, a low Tafel slope of 58 mV/dec for the nanoporous Ag indicates a fast initial electron-transfer step for CO_2 activation, which corresponds to a better stabilization of $CO_2^{\bullet-}$ intermediate on np-Ag in comparison with that of planar Ag, leading to the improvement of CO_2R to CO.

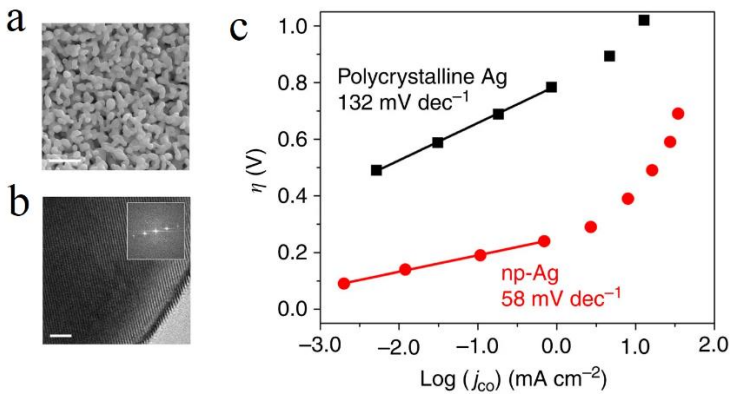

Fig. 6. (a) Scanning electron micrograph of np-Ag dealloyed in 5 wt% HCl for 15 min and further in 1 wt% HCl for 30 min (scale bar, 500 nm). (b) The respective high-resolution transmission electron micrograph with visible lattice fringes. Inset: the Fourier transform indicates that the np-Ag consists of an extended crystalline network (scale bar, 2 nm). (c) Overpotential vs. CO production partial current density on np-Ag and polycrystalline silver [199].

Hsieh *et al*. [201] reported that a high-surface-area Ag nanocoral catalyst synthesized by an oxidation-reduction process using chloride anions (Cl^-) with the scheme and SEM images of the prepared catalysts and related Ag nanocorals indicated in Fig 7a and Fig. 7b, respectively. These catalysts exhibited a Faradaic efficiency of 95% for CO formation in the electroreduction of CO_2 at the low overpotential of 0.37 V, as shown in Fig. 7c. By electrochemical surface area measurement, authors discovered that the specific activity for the Ag nanocorals was 32 times higher than that of unmodified Ag electrodes. In addition to nano morphology effect, the authors believed that Cl^- adsorbed on the Ag surface played an important role in the improved intrinsic activity of CO_2R. Synchrotron X-ray photoelectron spectroscopy (XPS) was performed, finding that Cl^- was adsorbed on the Ag nanocoral surface during the electrocatalytic reduction of CO_2. Thus, the authors postulated that the chloride anions not only facilitated the synthesis process for achieving a high surface area nanostructured Ag, but also adsorbed on the Ag surface to suppress H_2 evolution while enhancing the catalytic performance of CO_2R.

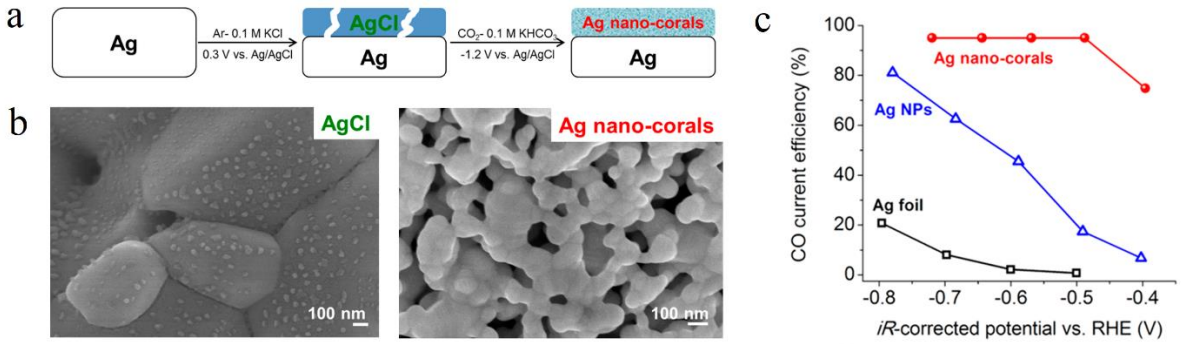

Fig. 7. (a) Schematic illustration of the fabrication of as-prepared AgCl and Ag nanocorals. (b) SEM images of the prepared AgCl after 12 h oxidation and related Ag nanocorals. (c) comparison of CO selectivity for different Ag catalysts measured in CO_2-saturated 0.1 M $KHCO_3$ at different potentials (iR-corrected). Reproduced with permission from ref [201]. Copyright 2015, American Chemical Society.

While the studies mentioned above on the nanostructured Ag catalysts show a significantly improved selectivity for electroreduction of CO_2 to CO at reduced overpotentials [199, 201], the fabrication methods of this nanostructured Ag remain complex and time-consuming. Recently, the group of Smith developed a very simple, fast, scalable and low-cost method for synthesizing high-performance nanostructured Ag catalysts [202]. Specifically, a Ag_2CO_3 layer (Fig. 8a) was formed by in situ anodic-etching of an Ag foil for 3 min in CO_2-statured $KHCO_3$ electrolyte. The formed Ag_2CO_3 electrodes were thereafter directly used for CO_2R in CO_2-statured $KHCO_3$, reducing to nanostructured metallic Ag (Fig. 8b) within the initial 2 min electrolysis. A high FE of > 92% for CO production was achieved on the Ag_2CO_3-derived Ag at an overpotential as low as 0.29 V, as shown in Fig. 8c. In addition, this Ag_2CO_3-derived Ag maintained about 90% CO catalytic selectivity for more than 100 h. The improved catalytic performance is ascribed to the increased intrinsic CO_2R activity via reduced energy barrier for CO_2 activation and the enhanced number of active sites for CO_2R by nanostructuring Ag surface. Later, Sargent *et al.* [203] combined Ag_2CO_3-derived Ag with polytetrafluoroethylene GDEs for electrocatalytic CO_2R in flow-electrolyzers, achieving a CO Faradaic efficiency of > 90% at 150 mA/cm^2 for long-term electrolysis of 100 h.

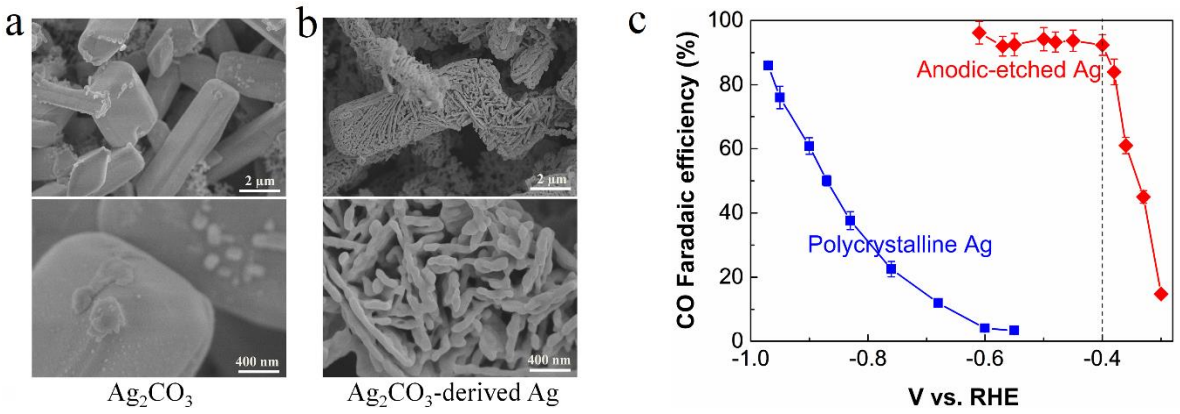

Fig. 8. SEM images of anodic-etched Ag before (a) and after (b) CO_2 electroreduction electrolysis. (c) Comparison of CO selectivity of polycrystalline Ag and AE-Ag in CO_2- saturated 0.1 M $KHCO_3$. Reproduced with permission from ref [202]. Copyright 2018, American Chemical Society.

In addition to the nanostructure strategy, Ag facets also play a critical role in CO_2R selectivity. Hori *et al.* [189] have demonstrated that the electrochemical CO_2 conversion into CO is favorable on Ag(110) compared to Ag(111) or Ag(100). A DFT simulation study further explained the Ag facet effect, finding that a lower free energy change for the initial proton-coupled electron transfer on Ag (110) or Ag (211) surface provides better $COOH^{\bullet}$ stabilization in comparison with Ag(111) or Ag(100), which correspondingly lead to the improved reduction of CO_2 to CO on Ag(110) or Ag (211) [200].

3.3.1.2. Non-noble metals for CO formation

Au, Ag and Zn are capable of electrochemically reducing CO_2 to CO with relatively high selectivity in CO_2-saturated electrolytes [186]. Among these identified metallic materials, Zn is the most earth-abundant material. Hori *et al*. [186] has demonstrated that polycrystalline Zn electrodes exhibited the catalytic reduction of CO_2 to CO with a Faradaic efficiency of 79.4%, however, planar Zn electrodes require a high overpotential for achieving selective CO_2R, which limits its practical utilization of CO_2 reduction. Nanostructured Zn dendrite electrodes were synthesized on Zn foil, resulting in a CO faradaic efficiency of around 3 times higher than that of bulk Zn counterparts under similar conditions [204]. Recently, Luo *et al*. [51] prepared highly porous Zn electrocatalysts via a facile electrodeposition method, and found that this porous Zn was capable of achieving > 55% CO Faradaic efficiency at an overpotential of ~0.5V, which is a

positive shift by 0.4 V than that of untreated Zn foil in CO_2-saturated 0.1 M $KHCO_3$ [51]. To overcome the mass-transport limitations, the porous Zn based GDE was synthesized, demonstrating 84% CO selectivity at a commercially-relevant current density of 200 mA/cm^2 in a flow-cell reactor. Of particular note, while Zn is an earth-abundant and low-cost material, there is only limited research on the development of selective and stable Zn catalyst at reduced overpotentials [51, 204-207]. Therefore, future studies should pay more attention on earth-abundant Zn catalysts for practical utilization of CO_2R to CO.

3.3.1.3. Non-noble metals for hydrocarbon and oxygenate products (Cu)

The electrochemical conversion of CO_2 and H_2O into hydrocarbons and oxygenates has gained significant attention due to their high energy density and the ease of consumption as fuels in the energy infrastructure. Until now, copper is the only known material that can electrochemically reduce CO_2 to high amounts of chemicals like C_2H_4, CH_4 and alcohols in aqueous electrolytes under ambient pressure and temperature conditions. This is mainly due to the suitable binding strength of intermediates like CO, COH and CHO on its surface during CO_2R [208-210]. With moderate binding energy, 16 different CO_2R products, including many hydrocarbons and oxygenates, have been discovered on Cu catalysts [211]. In addition, the product distribution is potential-dependent, and high-value multi-carbon product formation ($\geq C_2$) requires high overpotentials [211]. Thus, many works have been focused on finding a selective and efficient Cu catalyst at low overpotentials.

The surface morphology and roughness of copper catalysts could significantly influence the catalytic activity and selectivity in the CO_2 electroreduction [210, 212-216]. For instance, Cu nanoparticles covered Cu electrodes showed an improved selectivity for CO and C_2H_4 production compared to an argon gas sputtered Cu electrode and an electropolished Cu electrode, which was described by the roughened Cu surface which provides greater abundance of undercoordinated sites [210]. In addition, the particle size effect for the electrocatalytic CO_2R has been explored via Cu nanoparticles with the size range from 2 to 15 nm [213]. As shown in Fig. 9, an increase in the catalytic selectivity for CO and H_2 was found upon decreasing Cu particle size, and hydrocarbon selectivity (CH_4 and C_2H_4 formation) was inhibited on the nanoscale Cu surface than that of the bulk Cu counterparts. Authors believed these findings could be ascribed to the more

undercoordinated sites provided by smaller Cu NPs, which could have strong binding strength for key intermediates such as H and COOH.

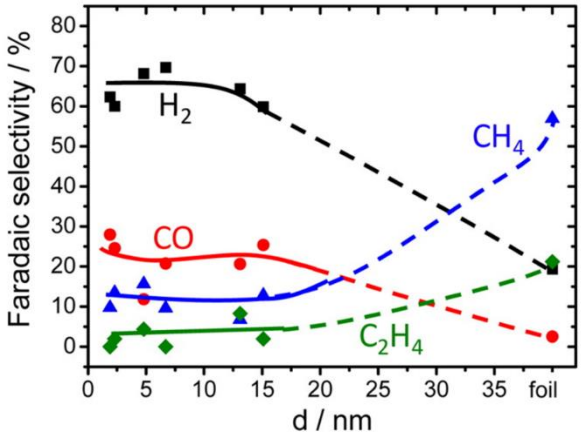

Fig. 9. Catalytic selectivity of CO_2R products on Cu nanoparticles in CO_2-saturated 0.1 M $KHCO_3$ at -1.1 V vs. RHE under 25 °C. Reproduced with permission from ref [213]. Copyright 2014, American Chemical Society.

Smith *et al*. [217] reported that the selectivity of hydrocarbon products could be tuned on Cu nanowire arrays by a systematic variation of the length and density of the nanowires. As the nanowire length and density increased, an enhanced catalytic selectivity for C_2H_4 formation was detected on Cu nanowire arrays, which is due to an improved CO dimerization caused by an increased local pH within the Cu nanowire arrays. Interestingly, on longer Cu nanowires ($\geq 7.3 \pm 1.3$ µm), C_2H_6 formation was observed, along with the ethanol formation, and the authors proposed a reaction pathway towards C_2H_6 from the intermediate (CH_3CH_2O) or -CH_3 dimerization. Later, Yeo *et al.* [218] performed a detailed mechanistic investigation for the reaction path toward C_2H_6 formation via the reduction of potential intermediate molecules, indicating that C_2H_6 is likely to be produced from the dimerization of -CH_3, instead of the hydrogenation of C_2H_4 or CH_3CH_2O intermediates.

Sen *et al.* [216] have demonstrated that the electrocatalytic reduction of CO_2 over copper foams, showing that HCOOH, H_2, and CO were formed as major products along with small amounts of C_2H_4, C_2H_6, CH_4, and C_3H_6, which meant a distinct product distribution compared to that on planar copper counterparts. This distinct CO_2R performance was explained by the high surface roughness, confinement and hierarchical porosity of reactive species. In addition, the catalytic selectivity for

HCOOH formation enhanced upon gradually increasing the thickness of the copper nanofoams, via suppressing the electroreduction of adsorbed $H^{\bullet}$ to H_2.

In addition to the surface morphology effect, the crystal orientation of Cu surface is closely correlated with the binding strength of the intermediates that determine the final product formation. The eCO_2R on Cu single crystal electrodes (100), (110), and (111) in aqueous electrolytes has been done by Hori, demonstrating that favorable C_2H_4 formation over Cu (100) and preferred CH_4 selectivity on Cu (111) [219]. Koper *et. al* studied CO_2R mechanism toward CH_4 and C_2H_4 on single-crystal Cu electrodes, demonstrating that two possible different mechanisms: (i) an -CHO intermediate for both CH_4 and C_2H_4 formation on Cu(111), (ii) CO is selectively reduced to C_2H_4 via CO dimer adsorbed on surface, which favorably occurs on Cu (100) [220, 221]. Thus, controllable hydrocarbon formation could be achieved by engineering the Cu facets. Buonsanti *et. al* prepared single Cu nanocube (100) with tunable edge lengths, showing that the highest selectivity for electrochemically reducing CO_2 to C_2H_4 was achieved on 44 nm nanocube (100) in comparison with those of nanocube (100) of 63 nm and 24 nm edge lengths, as shown in Fig. 10a [222]. Based on a simple model, the statistics of surface atoms for Cu nanocubes was plotted as a function of edge length in Fig. 10b. The tendency of the active sites with the different size indicates that the highest catalytic selectivity for the 44 nm Cu nanocube (100) originates from a proper balance between plane sites and edge sites. The authors believed that an optimal ratio of edge sites to (100) plane-sites (N_{edge}/N_{100} =0.025 for d=44 nm) is crucial to maximizing ethylene selectivity.

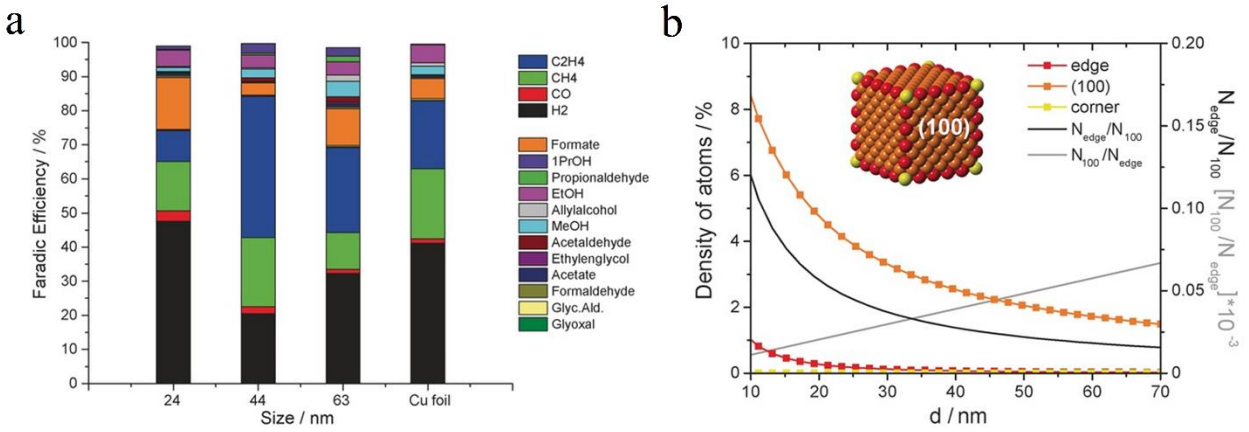

Fig. 10. (a) Faradaic efficiencies for products on Cu nanocubes (100) with the different size and Cu foil at -1.1 V vs. RHE. (b) On the left axis: Density of adsorption sites in Cu NC cubes versus the edge length. On the right axis: the trend of N_{edge}/N_{100} and N_{100}/N_{edge} versus edge length,

where N_{edge} is the number of atoms at the edge and N_{100} is the number of atoms on the (100) plane. Reproduced with permission from ref [222]. Copyright 2016, Wiley.

3.1.1.4. Oxide-derived metal

3.1.1.4.1. Oxide–derived Cu

Kanan *et al.* [214] reported the electrochemical reduction of CO_2 on a metallic Cu catalyst prepared from the reduction of thick Cu_2O films made by annealing Cu foil in the air. The Cu foil was annealed in air at 500 ºC for 12 hours to give a thick Cu_2O layer, which layer was thereafter reduced electrochemically to a nanostructured Cu (Fig. 11a) during CO_2R electrolysis. This oxide-derived Cu (OD-Cu) was capable of producing CO with ~ 40% FE and HCCOH with ~ 33% FE at -0.5 V vs. RHE (Fig. 11b). A slope of ~116 mV dec^{-1} was obtained by a Tafel analysis for OD-Cu in the low overpotential range (Fig. 11c) indicating a favorable formation of the $CO_2^{\bullet-}$ intermediate on the oxide-derived Cu, and hence an improved catalytic activity for CO_2R. To further uncover the link between a unique structural feature of oxide-derived Cu and the related catalytic activity, the authors proposed that the Cu catalysts derived from copper oxide may have a high density of grain boundary surfaces, which likely provides a highly active site for CO_2R [223]. Using temperature-programmed desorption (TPD) of CO, it has been demonstrated that the enhanced CO reduction activity on OD-Cu is correlated with the active sites that bond CO more strongly as compared to the low-index and stepped Cu facets [224]. The authors believed that the strong binding sites with CO could be provided by grain boundaries on the OD-Cu, that are only available in this nanostructured platform.

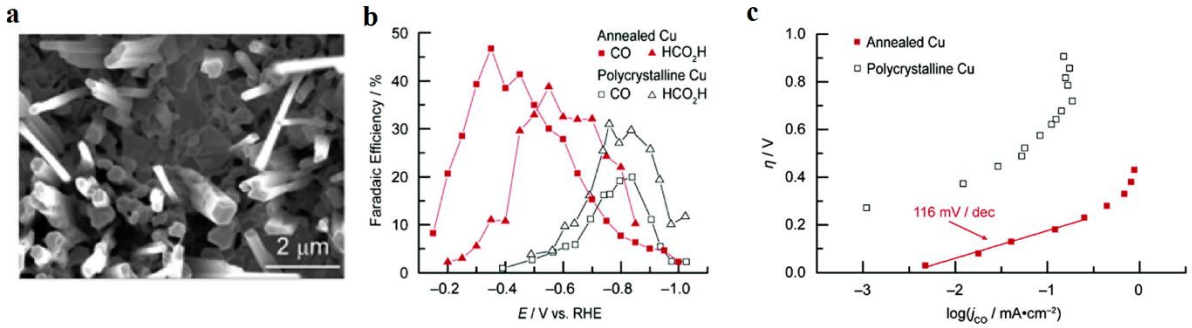

Fig. 11. (a) SEM image of OD-Cu (annealed at 500 °C for 12 h). (b) Faradaic Efficiencies for CO and HCOOH vs. potential, and (c) CO partial current density Tafel plots for polycrystalline Cu and OD-Cu (annealed at 500 °C for 12 h). All the catalytic performance was tested in CO_2-

saturated 0.5 M $NaHCO_3$. Reproduced with permission from ref [214]. Copyright 2012, American Chemical Society

3.1.1.4.2. Oxide–derived Au

Oxide-derived Au (OD-Au) nanocatalysts were also studied for CO_2R [225]. Firstly, the Au oxide layers were synthesized on Au electrodes by periodic square-wave pulsed potentials in 0.5 M H_2SO_4 solutions. The Au oxide layers coated Au electrodes were directly used for CO_2R in CO_2-saturated electrolytes, and were electrochemically reduced to metallic Au at the start of electrolysis (SEM image of OD-Au is shown Fig. 12a). At a low overpotential of 0.24 V, ~96% Faradaic efficiency for CO formation was achieved on the OD-Au, which was much better than that (1-4%) of polycrystalline Au foils (Fig. 12b). A Tafel slope of 114 mV dec^{-1} on polycrystalline Au revealed that the rate-determining step is the first electron transfer for stabilization of $CO_2^{\bullet-}$ intermediate, thus the poor stabilization of $CO_2^{\bullet-}$ intermediate was linked to the high overpotential required on polycrystalline Au (Fig. 12c). In contrast, OD-Au offered the fast initial electron transfer, which meant the enhanced stabilization of $CO_2^{\bullet-}$ intermediate. Later, a mechanistic study showed that the OD-Au may provide a high density of grain boundaries which was thought to be associated with its enhanced catalytic performance [226].

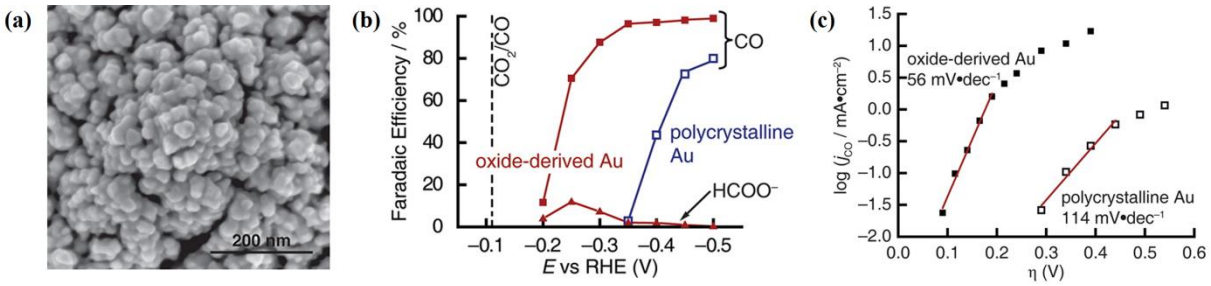

Fig. 12. (a) SEM image of oxide-derived Au NPs. (b) Faradaic Efficiencies for CO and HCOOH, and (c) CO partial current density Tafel plots of oxide-derived Au NPs and polycrystalline Au. All the catalytic performance was tested in CO_2-saturated 0.5 M $NaHCO_3$. Reproduced with permission from ref [225]. Copyright 2012, American Chemical Society.

4.1.1.4.3. Oxide–Derived Ag

A nanoporous Ag catalyst (Fig. 13a) was fabricated via electrochemical reduction of Ag_2O, which was synthesized by anodization of a Ag foil in alkaline solution [227]. The Ag_2O-derived metallic Ag (OD-Ag) showed an increase in the catalytic activity for CO_2R and a shift of > 400 mV towards a lower overpotential (for the related high CO selectivity) than that of untreated polycrystalline Ag. The OD-Ag was able to reduce CO_2 to CO with ~80% EF at an overpotential of 0.49 V, which is significantly higher compared to that (~4%) of untreated Ag foils at identical conditions (Fig. 13b). The enhanced catalytic performance for CO_2R to CO was attributed to the preferred stabilization of ⁎COOHintermediate (a low Tafel slope of OD-Ag in Fig. 13c), which was likely linked to highly active sites provided by the nanostructured surfaces. In addition, a local pH effect was also proposed in this work, demonstrating that a porous-like nanostructured Ag catalyst likely created a high local pH near the catalyst surface, which may also contribute to the improved CO_2R while suppressing H_2 evolution.

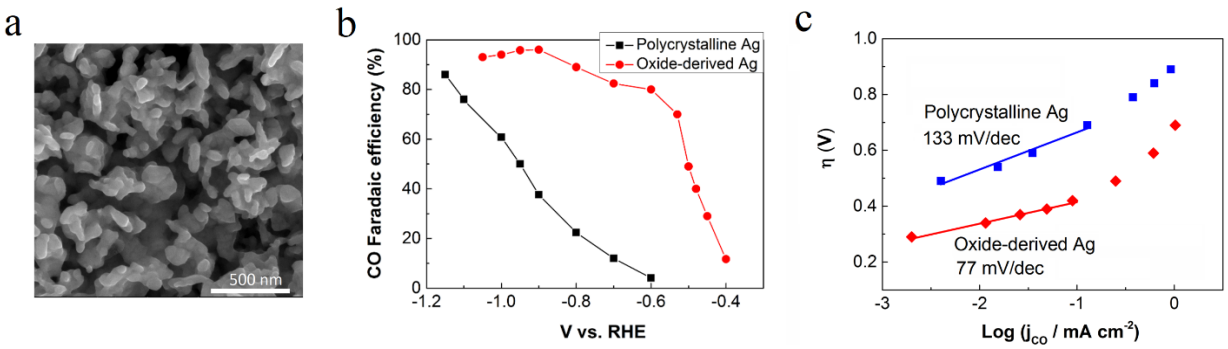

Fig. 13. (a) SEM image of oxide-derived Ag. (b) Faradaic Efficiencies for CO, and (c) CO partial current density Tafel plots for the oxide-derived Ag and polycrystalline Ag. All data for CO_2R were obtained in CO_2-saturated 0.1 M $KHCO_3$. Reproduced with permission from ref [227]. Copyright 2012, Wiley.

3.3.2. Bimetallic catalysts

3.3.2.1. Cu based binary catalysts

The process of CO_2R on metal surfaces is a complex multistep reaction with many adsorbed intermediates, and the binding energies of related intermediates adsorbed on the electrodes play a key role in the final product formation. In addition to the method of nanostructuring metal surfaces, alloying two different metals could also enable the tuning of the binding energies of intermediates

because of geometric and electronic effects. Thus, bimetallic catalysts have recently gained significant interest as an alternative strategy for improving the catalytic selectivity and activity of CO_2R.

Yang *et al.* [228] reported the electroreduction of CO_2 on monodisperse Au-Cu bimetallic nanoparticles with different compositions, demonstrating the different product formation with an increase in the Cu content and the largest number in product distribution on pure Cu nanoparticles. The authors believed that with tuning the composition of Au-Cu bimetallic nanoparticles, the degree of stabilization of the intermediates on the binary surfaces could be changed, resulting in the formation of the different products. The catalytic performance of these bimetallic catalysts was influenced by two factors: (i) the electronic effect on the binding energies of intermediates, which is correlated with the variation of electronic structure that is tuned with the Au-Cu surface composition, and (ii) the geometric effect, influenced by the atomic arrangement, is also closely corrected with the binding energies of intermediates [228, 229].

Nanostructured Cu-In bimetallic catalysts were prepared by in-situ electrochemical reduction of Cu_2O in $InSO_4$ electrolytes, and the Cu catalysts incorporated with In have showed a dramatic improvement in the catalytic selectivity for CO_2R to CO with high catalytic stability [230]. Faradaic efficiency of ~ 90% for CO formation was achieved on the Cu-In bimetallic surfaces at an overpotential of 0.39 V. A density functional theory investigation showed that the incorporation of In may lead to both local electronic effect and local geometric effect, which plays a significant role in the binding energies of the related intermediates adsorbed on binary surfaces. In addition to Cu-In, Cu-Sn and Cu-Pd bimetallic electrocatalysts were also synthesized, exhibiting a dramatically enhanced catalytic selectivity for the conversion of CO_2 into CO at decreased overpotentials [231, 232].

Yeo *et al*. [233] prepared CuZn catalyst by introducing different amounts of Zn dopants, demonstrating that the catalytic selectivity of ethanol versus ethylene production could be tuned by varying the amount of Zn in the bimetallic catalysts. A remarkable Faradaic efficiency of 29.1% for ethanol formation was achieved on Cu_4Zn at −1.05 V vs RHE. The spillover effect for transferring CO produced on Zn to Cu sites was proposed to be responsible for the selectivity trend in the C_2 product selectivity with tuning binary composition [233]. Recently, Gratzel *et al*. [234] reported that Cu nanowires decorated with Ag islands, formed by the reduction of Ag-covered

Cu_2O, was able to achieve a total of 76% faradaic efficiency for ethylene and other C_{2+} products in CO_2R. With Operando Raman spectroscopy, intermediate formation of CO at Ag sites was found to undergo spillover process and further reduction on Cu surfaces.

Using bimetallic CuPd nanoparticles with ordered, disordered and phase-separated atomic-arrangement for CO_2R, Kenis *et al*. [235] demonstrated that phase-separated CuPd favored C_2 formation (> 60%) while ordered CuPd had the highest C_1 selectivity (Fig. 14). The authors believed that phase-separated CuPd could facilitate C_1 dimerization with neighboring Cu atom, which caused enhanced C_2 products. With different elemental mixing patterns and composition as well as the related surface valence band spectra, geometric effects (the mixing patterns of elements, atomic arrangement) rather than electronic effect was found to be the key for determining the catalytic selectivity of bimetallic catalysts.

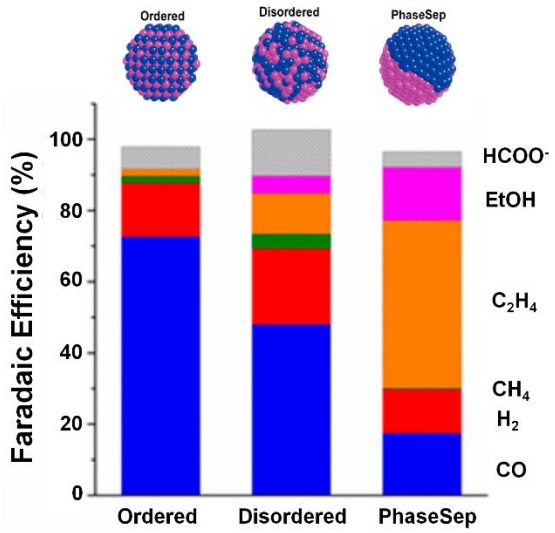

Fig 14. Faradaic efficiencies of CO_2 reduction products for Cu-Pd nanoparticles with different mixing patterns. Reproduced with permission from ref [235]. Copyright 2017, American Chemical Society.

3.3.2.2. Non-Cu binary catalysts

To explore the electronic effect on catalytic selectivity in bimetallic catalysts for CO_2R, AuPt bimetallic planar thin films with controllable compositions were prepared by sputtering co-deposition [236]. The planar AuPt exhibited a gradually increased catalytic selectivity and activity

for CO formation with increasing Au content, due to electronic effect. However, authors found that the binding strength of intermediates of AuPt still followed the scaling relation with varying binary compositions, indicating that the electronic effect alone was likely unable to tune the binding strength of certain intermediates without influencing others for CO_2R to CO. Atomic arrangement needs to be considered for designing bimetallic catalysts for driving highly selective CO_2R to CO.

Jaramillo group has demonstrated that AuPd thin films synthesized using an electron-beam co-deposition method were more active and selective for producing formate while both pure Au and Pd metals had negligible amounts of fomate [237]. The authors believed that Au and Pd could act synergistically in AuPd alloys to obtain new electrocatalytic properties. In addition, Koper *et al.* [238] reported bimetallic Pd-Pt nanoparticles, showing that Pd-Pt nanoparticles had a low onset potential for the reduction of CO_2 to formate which started at 0 V vs. RHE. While this potential for formate formation is close to the theoretical equilibrium potential of producing formate, the selectivity toward formate is very low. In addition, the catalytic selectivity for formate production was influenced by the composition of the nanoparticles and a Pd_{70}-Pt_{30} experienced a HCOOH Faradaic efficiency of as high as 88% at -0.4 V vs. RHE.

3.3.3. Metal chalcogenides

Nowadays, transition metal chalcogenides (TMDs) are investigated as electrochemical CO_2 reduction reaction (eCO_2RR) catalysts, due to their abundance as well as facile and reproducible synthesis method. The performance of the TMDs catalysts is strongly correlated with the active edge sites compared to the exposed basal plane. Moreover, the eCO_2RR intermediates can be attached to the different active edges of the TMDs catalysts and has a specific relationship of bonding energy to break the metal-intermediate. Interestingly, different edge sites of TMDs can control the selectivity of the specific eCO_2RR products. For example, three-dimensional bulk MoS_2 showed excellent activity towards CO_2R in ionic liquids with the FE of CO (90 %) at -0.764 V vs. RHE [239]. The surface activity of the MoS_2 catalysts strongly depends on the terminal edges where d electrons are present with higher energy density. Vertically aligned WSe_2, $MoSe_2$, WS_2, and MoS_2 NFs exhibited more than 90% CO selectivity with current densities above 130 mA cm^{-2}, and the decreasing trend of the current density follows $WSe_2 > MoSe_2 > WS_2 > MoS_2$, indicating a different electron transfer processes for each [240]. Furthermore, doping of transition

metal (Ta, Nb etc) on MoS_2 edges can increase the edge sites, which facilitates the eCO_2R reaction [241]. Abbasi *et al*. [241] have introduced Nb-doped vertically aligned MoS_2 for electrochemical CO_2R process, where the presence of Nb near Mo can increase the active edge sites as well as reduced the binding energy of intermediates for enhancing the CO formation activity.

3.3.4. Non-metals

Mostly, metal-based catalysts have been used as an electrocatalyst for eCO_2R reaction. However, recent studies also focused on the metal-free catalysts as this class of materials exhibit low cost and can be easily modified structurally for better activity and selectivity [242, 243]. Pure carbon materials are not promisingly catalysts for the eCO_2RR process because of the very poor ability to absorb the $CO_2^{\bullet-}$ intermediates. The doping of the heteroatoms such as nitrogen (N), fluorine (F), sulfur (S), and boron (B) in carbon materials could improve eCO_2RR process, due to the delocalization of π-orbital electrons in the conjugation of sp^2–sp^2 linkages. It is well known that the nitrogen-doped carbon materials efficiently catalyze eCO_2RR process in which the amount of nitrogen and pyridinic N can influence the activity and selectivity of the eCO_2RR process. For example, N defects in three dimensional (3D) graphene foam can act as a promising eCO_2RR candidate, resulting in up to 85 % at -0.47 V vs. RHE FE for CO that was stable up to 5 h [244]. The DFT calculation suggests that the eCO_2R to CO strongly depends on the pyridinic N active sites compared to the other active sites, where pyridinic N creates lower energy for *COOH intermediates, which is more favorable for CO formation. In addition, heteroatom doped carbon has been investigated for eCO_2R [245, 246]. Sreekanth *et al*. [245] have reported boron-doped graphene for electrocatalytic reduction of CO_2 to formic acid with a FE of 66 % at an overpotential of -1.4 V vs. RHE. DFT calculation indicates that the graphene has an asymmetric spin density, which is suitable for absorbing the eCO_2RR process intermediates rather than pristine graphene, which could promote the CO_2R to formate. Also, B and N doped nanodiamond was investigated as a selective catalyst for electrocatalytic reduction of CO_2 to ethanol. The FE of C_2H_5OH is 93.2 % at -1 V vs. RHE and DFT calculation indicates the activity and selectivity of ethanol production are mainly attributed to the synergistic effect of N and B co-doping [246]. Li *et al*. [247] have reported S-doped and S,N-doped nanoporous carbon (NPC) materials for electroreduction of CO_2 in aqueous solution, which showed better catalytic activity towards the formation of CO (FE =11.3 %) and CH4 (FE = 0.18%) at potential −0.99 V (*vs.* RHE). The activity of the catalysts depends on pyridinic N based active sites and positive sites of the carbon and adjacent pyridinic N sites that stabilize the

$CO_2^{\bullet-}$ and *COOH intermediates that can facilitate better CO formation activity. In another work, N-C layers and N,S-doped carbon layers (NS-C) have been shown to efficiently catalyze the CO_2 to CO process, where N, S contents/configurations were prepared based on carbon nitride-templated pyrolysis strategy (Fig. 15a) [248]. The doping of N and S is identified by elemental mapping images (Fig. 15b), and indicates that the N and S elements are homogeneously distributed on the carbon frameworks. Linear sweep voltammetry (LSV) of NS-C was measured in 0.1 M $KHCO_3$ and the obtained current density was higher in CO_2-saturated solution as compared to the Ar-saturated solution, indicating that the CO_2R happens along with the hydrogen evolution (Fig. 15c). In Fig. 15d, a sudden drop of current is observed in the first 2 h of electrolysis, after a which the CO production efficiency was found to be around 91 % with stable current density of 2 mA/cm^2. Some other recently published metal-free catalysts are summarized in Table 3.

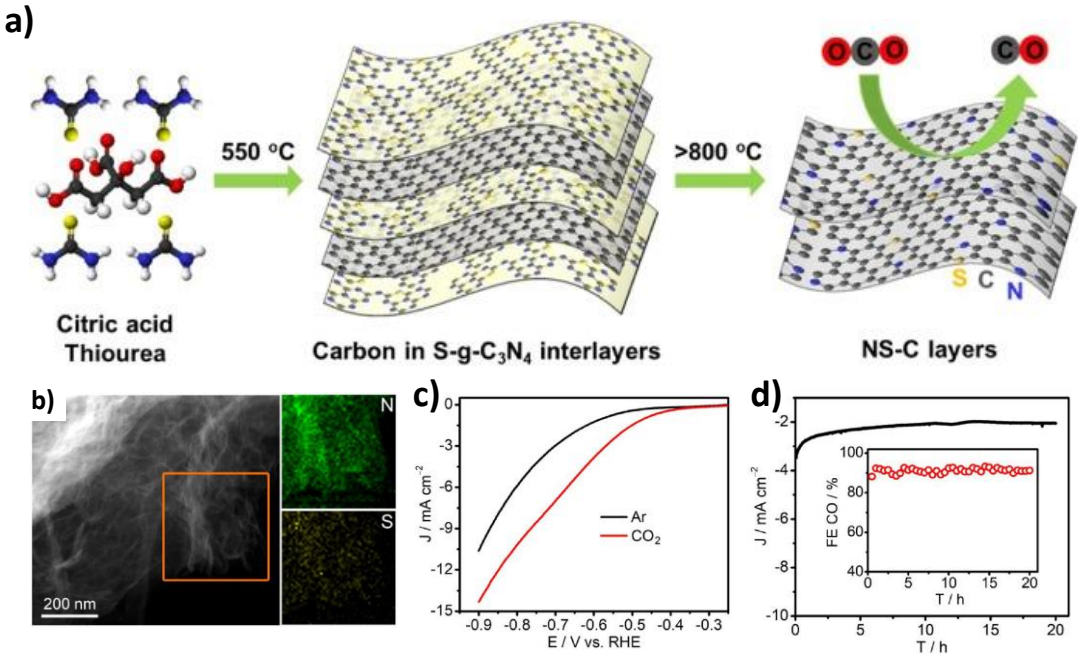

Fig 15. a) Schematic diagram of the synthesis processes of NS-C layers; b) TEM and N,S elemental mapping; c) LSV curves recorded on NS-C in the Ar- and CO_2-saturated 0.1 M $KHCO_3$ solution at a scan rate of 5 mVs^{-1}; d) Chronoamperometric responses and FE (CO) at -0.6 V on NS-C catalysts for stability tests. Reproduced with permission from the ref [248]. Copyright 2019, Elsevier.

Table 3. Summaries of metal-free catalysts for electrocatalytic CO_2 reduction.

Catalysts	**Electrolyte**	**Applied potential V vs. RHE**	**Products efficiency**
CNTs	0.1 M $KHCO_3$	-1.05	83% （CO）[249]
CNPs	0.1 M $KHCO_3$	-0.6	92% （CO）[250]
F doped C	0.1 M $NaClO_4$	-0.62	89.6% （CO）[251]
B doped graphene	0.1 M $KHCO_3$	-0.99	11.3% (CO), 0.18 % (CH_4) [247]
S doped C	0.1 M $KHCO_3$	-1.4	66% (HCOOH) [245]
N porous carbon	0.1 M $KHCO_3$	-0.93	78% （CO）[252]
C-NF	0.1 M $KHCO_3$	-0.6	90% （CO）[253]
NGQD	1 M KOH	-0.75	45% （C_2H_5OH），45%（C_2H_4）[254]
N-diamond	0.5 M $NaHCO_3$	-1	77.6% (CH_3COOH), 14.6 (HCOOH)[255]
N,B diamond	0.1 M $NaHCO_3$	-1	90% （ C_2H_5OH ）[246]
B-diamond	0.1 M MeOH	-0.65	74% (HCHO), 14 % (HCOOH)[256]
N doped graphene	0.5 M $KHCO_3$	-0.84	14% (HCOOH) [243]
CN-MWCNT	0.1 M $KHCO_3$	-0.82	70% （CO）[257]
g-C_3N_4/MWCNTs	0.1 M $KHCO_3$	-0.75	70% （CO）[258]

3.3.5. Molecular catalysts

Molecular catalysts are another promising alternative for the electroreduction of CO_2, with the main advantage being that it can be easily tailored for better performance by tuning the ligand position with advanced organic synthesis methods [259, 260]. The active sites can be generated due to the reduction of metal center or ligand scaffold that can facilitate the multiple proton-

coupled electron transfer process for better electroreduction of CO_2 and consequently deep understanding the eCO_2RR mechanism [261, 262]. The broad area of molecular catalysts that has been largely investigated includes bipyridine, porphyrin, phthalocyanine, aza-macrocycles, and phosphine ligands. Nichols *et al*. [263] synthesized a series of amide pendants tetraphenylporphyrin complexes, where amide pendants occupied the various positions of the peripheral metalcore. The position of the amide pendants could affect the electroreduction of CO_2 to CO. Specifically, proximal and distal amide pendants bearing ortho-derivatives exhibited higher CO_2R efficiency compared to the para-position bearing amide isomers or bare complex. The heterogenization of the molecular catalyst has been developed through non-covalent and covalent immobilization and periodic conjugation method. For non-covalent immobilization, the molecular complex attaches with the substrate through π-π interactions. Importantly, the molecular complexes are mostly aromatic and delocalized electrons enhance the interaction of substrate as well as facilitate the electron transfer process. Porphyrin and phthalocyanine ligand-based complex can be directly immobilized onto a substrate through strong π-π conjugation. For example, cobalt phthalocyanine (Co(Pc)) immobilized onto pyrolytic graphite or carbon cloth shows eCO_2RR activity to the formation of CO in a citrate buffer solution (pH = 5.0) with a high turnover frequency of 100 s^{-1} and ratio of CO/H_2 is 1.5/1 [264]. Carbon nanotubes (CNT) substrate bearing Cobalt(II) phthalocyanine (CoPc) efficiently catalyzed the reduction of CO_2 to CO with FE of 92% at -0.63 V vs. RHE and a high current density of 10 mA cm^{-2} [265]. Choi *et al*. [266] developed a 3D Fe-porphyrin graphene hydrogel (FePGH) for efficient catalysis of the electroreduction of CO_2 to CO. The detailed fabrication process of FePGH is shown in Fig. 16a. The FePGH electrodes were decorated on the reticulated vitreous carbon (RVC) by hydrothermal method (Photographical image of FePGH/RVC electrode is shown in Fig. 16b). Different amounts of FeTMAP was taken (0.6 and 1.1 mg, marked as FePGH-L and -H, respectively) and analyzed in 0.1 M $KHCO_3$ electrolyte under an Ar or CO_2 atmosphere. As shown in Fig. 16c, the FePGH-H exhibited a promising current density of ~2.7 mA/cm^2 at -0.69 V vs. RHE while FePGH-L reached ~1.8 mA cm^{-2} at similar applied potential. As confirmed by the results obtain from GC analysis (Fig. 16d), FePGH-H showed a maximum FE of up to 95% for CO at 0.39 V vs. RHE at a current density of 2.3 mA cm^{-2}.

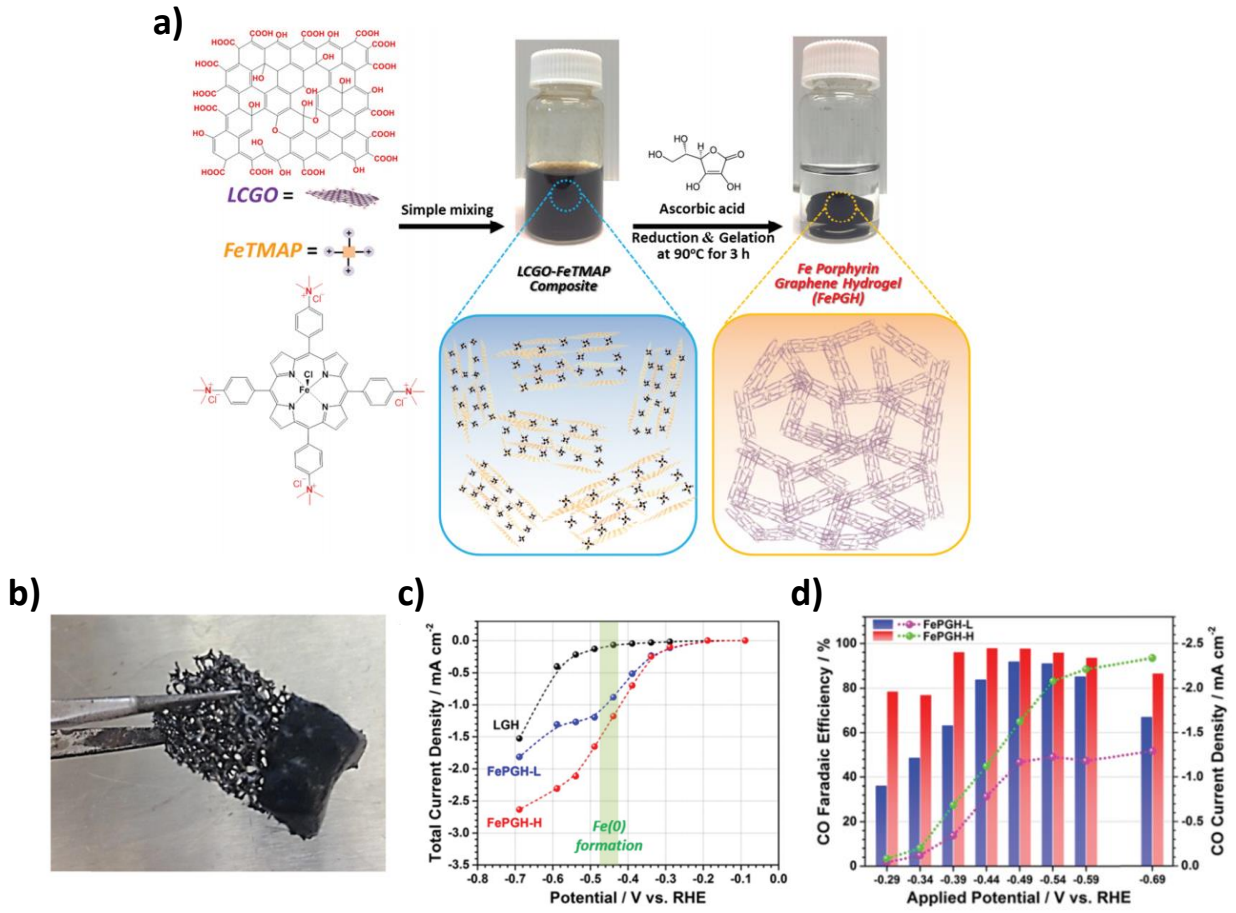

Fig. 16. a) Schematic representation of 3D Fe-porphyrin graphene hydrogel (FePGH) synthesis method; (b) Photographical image of FePGH/RVC electrode; c) Total current densities of LGH (black), FePGH-L (blue) and FePGH-H (red) at different applied potentials with metallic Fe formation highlighted; d) CO faradaic efficiencies (bar graph) and CO partial current densities (line graph) obtained by FePGH-L (blue bar and magenta line) and FePGH-H (red bar and green line) [266].

For covalent immobilization of e.g. porphyrin, phthalocyanine or bipyridine derived complexes, polymerization and grafting were used for attachment to the substrate. For such purpose, chemical and electrochemical methods have been widely used. For example, cobalt porphyrin bearing alkyne groups can react with an azide-functionalized diamond surface via a copper catalyzed alkyne-azide cycloaddition (CuAAC) reaction to form a monolayer heterogeneous molecular catalyst. This catalyst exhibits a promising CO production activity with a turnover frequency of 0.8 s^{-1} at -1.6 V vs. RHE [267]. Furthermore, electrochemical method adopted FTO containing M-tetrakis aminophthalocyanines (M = Co, Ni, Fe) exhibits diverse selectivity towards CO_2 conversion with the presence of metal

complex precursors [268]. More importantly, the Co-based film was highly selective towards formic acid, and both formic acid and formaldehyde were found when using Ni-based film as an electrode, while formaldehyde and H_2 were detected when using Fe-based film. Zhu *et al*. [269] have developed new strategy to synthesize cobalt porphyrin/carbon nanotubes molecular electrocatalysts for selective conversion of CO_2 to CO. Protoporphyrin IX cobalt chloride with the structure shown in Fig. 17a was used as a precursor. The molecular electrocatalysts were well-dispersed onto the CNT, which were directly grafted onto the metal centers through covalent bonding, which leads to improved performance compared to the traditional non-covalent method. TEM images indicated that the prepared molecular catalyst designated as CoPP@CNT and CNT-OH have similar surface morphologies, without presence of aggregated species (Fig. 17b), and the corresponding EDX mapping showing the distributions of C, N, and Co onto the CNT (Fig. 17c) indicated that the overlap of N or Co signals that can further confirm the homogeneous distribution of CoPP. In cyclic voltammetry analysis, the catalyst exhibits a sufficient current density at potential of -0.4 V vs. RHE (Fig. 17d). During long-term electrolysis, the obtained current densities were stable at all applied potentials and the catalyst showed high CO selectivity (Fig. 17e), and the obtained FE efficiency of CO varied from 90 % to 80 % between -0.65 V and -0.5 V vs. RHE (Fig. 17f).

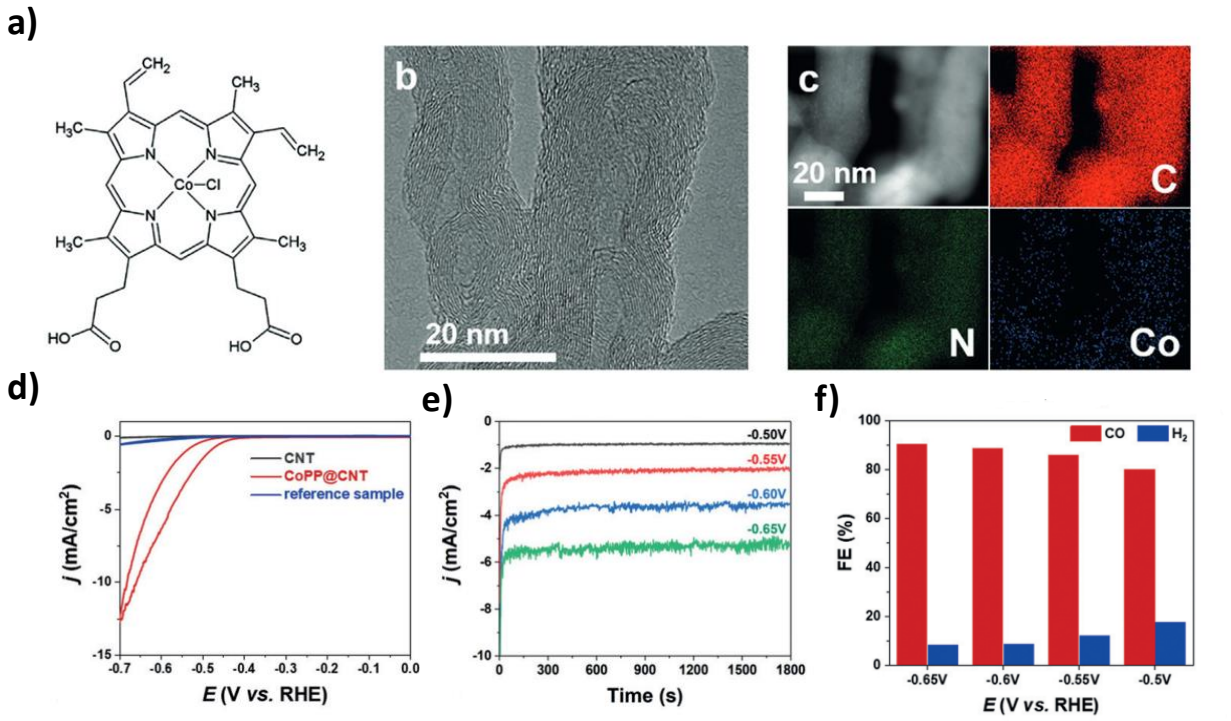

Fig. 17. a) Structure of protoporphyrin IX cobalt chloride. b) TEM images of CoPP@CNT. c) STEM image of CoPP@CNT and the corresponding EDX maps of C, N, and Co. d) Cyclic voltammograms at a sweep rate of 5 mV s^1 for CNT-OH, CoPP@CNT and a control sample. e) Current densities vs. time and f) Faradaic efficiencies vs. potential for CoPP@CNT. Reproduced with permission from the ref [269]. Copyright 2019, Wiley.

Periodic porous crystalline materials (metal-organic frameworks (MOFs)) have gained a huge attention for electrochemical conversion and storage due to their topology, and possibility of tuning the structure at molecular level, etc. This catalysts have inorganic or organic secondary building blocks that can create active sites, and tunable secondary building blocks as well as high surface area which could improve the selectivity, activity and durability for eCO_2RR. For example, the copper rubeanate MOF (CR-MOF) showed an excellent eCO_2RR activity with an onset potential of 0.2 V in 0.5 M $KHCO_3$ and exhibited a high selectivity of HCOOH (90%) at -1.6 V vs. RHE. The organic secondary building blocks can create active sites and linked with MOF as active catalytic centers. Kornienko *et al*. [270] have introduced conductive Al/FTO coated Co-TCPP (TCPP = 4,4′,4″,4‴-(porphyrin-5,10,15,20-tetrayl)-tetra benzoate) for conversion of CO_2 to CO, which exhibited the selectivity of 76% with a current density of about -1 mA cm^{-2} at around -0.70 V vs. RHE in 0.5 M $KHCO_3$ aqueous media (Fig. 18a-c). On the other hand, the covalent

organic framework (COF) can be a porous organic polymer which is widely used for storage and separation of gases. COF is highly crystalline materials and stable in an acidic and basic medium. Amine linkage covalent organic frameworks (COFs) can potentially catalyze the eCO_2R reaction process and the CO conversion efficiency increased from 13% to 53% at -0.70 V and from 43% to 80% at -0.85 V in comparison with bare Ag electrode (Fig. 18d-f) [271]. One of the last example, 3D metal atoms (Co, Ni or Cu) modified covalent triazine frameworks efficiently catalyze the electroreduction of CO_2 and achieves the maximum FE of 90% (CO) at -0.8 V versus RHE for Ni-CTF [272] . Some more examples of molecular complexes are summarized in Table 4.

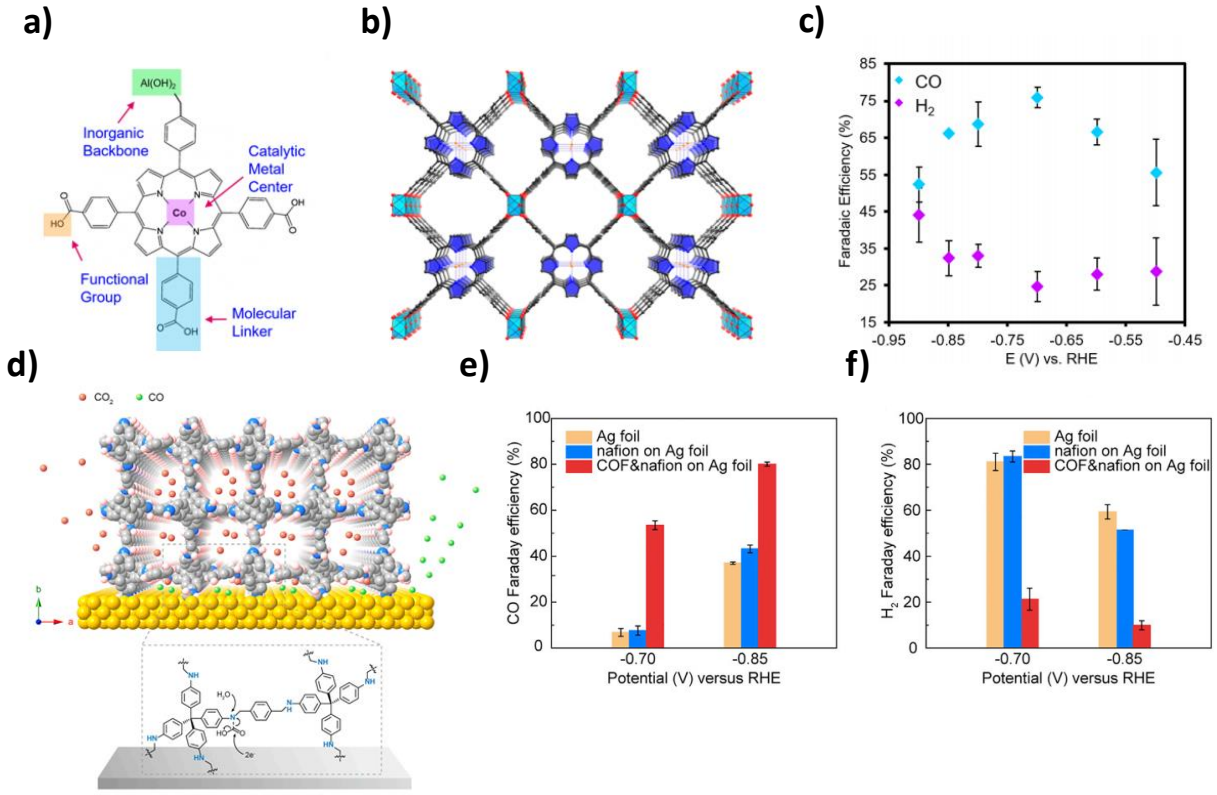

Fig. 18. a) MOF allowing for modulation of metal centers, molecular linkers, and functional groups at the molecular level; b) cobalt-metalated TCPP as an organic building units assembled into a 3D MOF, $Al_2(OH)_2$TCPP-Co with variable inorganic building blocks; c) the selectivity for products determined over a potential range of -0.5 to -0.9 vs RHE. Reproduced with permission from ref [270]. Copyright 2015, American Chemical Society. d) Molecularly Defined Interface formed by combining the catalytic surface of Ag electrode with COF-300-AR; e and f) FE of CO and

H_2 production on the COF-300-AR and Ag electrocatalysts at various potentials. Reproduced with permission from the ref [271]. Copyright 2018, Elsevier.

Table 4. Summary of molecular catalyst for electrocatalytic CO_2 reduction.

Catalysts	**Electrolyte**	**Applied potential (V vs. RHE)**	**Products efficiency**
Co protoporphyrin/pyrolytic graphite	$NaClO_4/HClO_4$	-0.6	CO (60%) [273]
Ru(II) Polypyridyl Carbene	0.5 M $NaHCO_3$	−0.53 to −0.63	H_2/CO: 1.5−5.6 [274]
Co-phthalocyanine	0.1 M $KHCO_3$	-0.59	CO (70%) [265]
Fe triphenyl porphyrin	0.5 M $KHCO_3$	-0.59	CO (93%) [275]
Ir Pincer	0.5 M $LiClO_4$/0.1 M $NaHCO_3$, 1% v/v MeCN	-1.4	Formate (93%) [276]
Perfluorinated cobalt phthalocyanine	0.5 M $NaHCO_3$	0.8	CO (93%) [277]
PorCu	0.5 M $KHCO_3$	-0.976	CH_4 (27%); C_2H_4 (17%) ; CO (10%) [278]
ZnPor	0.1 M $TBAPF_6$/DMF/H_2O	-1.7	CO (93%) [279]
CoPc-py/CNT	0.2 M $NaHCO_3$	-0.63	CO (93%) [280]
Fe-PB	0.5 M $KHCO_3$	-0.63	CO (100%) [281]
ZIF-A-LD	0.1 M $KHCO_3$	-1	CO (75%) [282]

3.4. Ionomer and binder

The performance of the gas diffusion electrode (GDL) is strongly dependent on the binders. In most cases, catalysts are attached to the electrode layer with a binder by using different techniques (spray, drop-casting, etc). An ideal binder not only binds the catalyst in the catalytic layer but also facilitates the transport of ions (e.g., H^+ and OH^-) at the membrane-electrode interface. Nafion is the most commonly used binder for eCO_2RR process, due to its commercial availability and high activity. The drawback of using Nafion is that in alkaline medium, it exhibits a reduced transport property for OH^- ions. On the other hand, PTFE (polytetrafluoroethylene) is considered as a highly stable binder, but the high hydrophobicity of PTFE tend to result in mass transfer limitations. In the case of eCO_2RR process, the functional group of the binder can play an

important role for suppressing the HER process and enhance the eCO_2RR, because the eCO_2RR process are strongly dependent on *COOH and *CO intermediates with *H (HER) that can correlate with the activity and selectivity of the catalysts. Specifically, the binder behaves like a surfactant, where one end stabilizes the catalyst in the electrode surface and another end functionalizes the catalyst surface for controlling the selectivity of the products. Lee *et al*. [283] have investigated the Au catalysts with different binders for a selective approach of eCO_2RR process for the formation of CO. Five different binders were used including PVA (polyvinyl alcohol), PAA (polyacrylic acid), PVDF (polyvinylidene difluoride), and PTFE (Fig. 19a). Among all binders containing Au-catalysts, Au-PTFE exhibited better CO formation performance than those of other binders containing Au NPs (Au-Nafion, Au-PVA, Au-PAA, Au-PVDF), resulting in the highest FE of CO is 94.7 % at -0.7 V vs. RHE (Fig. 19b). A similar trend has been observed for the partial current density of the CO formation (J_{CO}), and Au-PTFE showed the maximum current density close to 10 mA cm^{-2} (Fig. 19c). Furthermore, a DFT study indicated that the PTFE binder containing Au showed the highest FE for CO evolution (up to 94.7 %) due to the reduction of hydrogen adsorption (*H) activity on the PTFE decorated Au surface, and simultaneously allows more active sites for eCO_2RR intermediates (*COOH and *CO) (Fig. 19d). On the other hand, the oxygen-containing binder (-OH and -COOH) stabilizes the intermediates and reduces the activity of CO production (Fig. 19d). Also, it was reported that the Sustainion ionomer has been used for eCO_2RR [284].

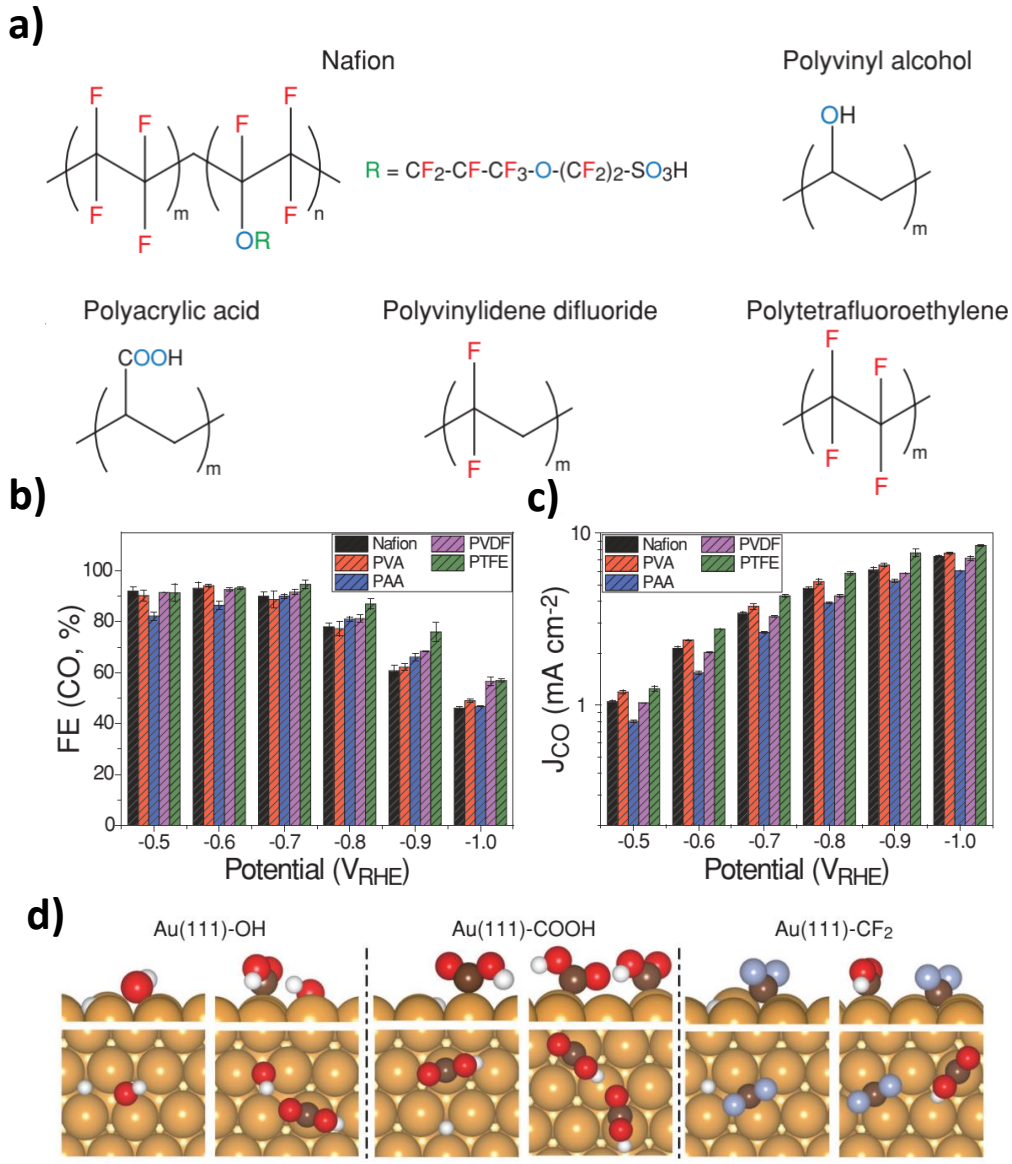

Fig. 19. a) The chemical structure of the investigated binders; b) FE_{CO} and c) J_{CO} for CO production over the Au NPs using different binders; d) DFT (PBE-vdW) optimized geometries of *H and *COOH in the presence of co-adsorbed -OH (left), -COOH (center) and -CF_2 (right) groups on Au(111). Reproduced with permission from the ref [283]. Copyright 2018, Wiley.

4. Cell optimization and testing

4.1. Internal losses

In membrane-based CO_2 electrolyzers, a certain amount of energy is required to overcome the different energy barriers and carry out the electrochemical CO_2R into the products of interest, which proportional to the cell voltage (E_{cell}) expressed as:

$$E_{cell} = E_{\mathrm{Rev}} + \eta_{Ohmic} + \eta_{Act} \tag{2}$$

where E_{Rev} the reversible cell voltage, η_{Ohmic} is the ohmic losses in the cell and η_{Act} is the activation overpotential at the electrodes. In this regard, Fig. 20a shows the different resistances contributing to the total cell resistances in typical liquid-phase CO_2 electrolyzers along with the electrical circuit analogy representation. Ohmic losses occur as a result of resistance to the flow of ions and to the flow of electrons through the electrically conductive electrolyzer components (wiring and connections) for cathode ($R_{e,c}$) and anode ($R_{e,a}$). The resistance to the flow or transport of ions in CO_2 electrolyzers includes physical resistances due to ionic transport in the electrolytes (R_s) and in the membranes (R_m) as well as resistances due to gas bubbling and/or flooding that influence the active surface area of the cathodes ($R_{g,c}$) and anodes ($R_{g,a}$). Therefore, this can be summed up to present the total Ohmic loss which is linearly dependent on the current (i) flowing through the cell:

$$\eta_{Ohmic} = i(R_{e,a} + R_{g,a} + R_s + R_m + R_{g,c} + R_{e,c}) \tag{3}$$

The activation overpotential is the potential required to overcome the activation energy for the electrochemical reactions occurring at anode (R_a) and cathode (R_c) in CO_2 electrolyzers. Conventionally, the kinetic effect of typical electrolytic reactions are expressed with the Butler-Volmer equation which shows a logarithmic dependence of activation overpotential on current [285-287]:

$$\eta_{Ohmic} = \frac{RT}{F} \ln\left[\frac{J}{2J_o} + \sqrt{\left(\frac{J}{2J_o} \right)^2 + 1} \right] \tag{4}$$

where R is the ideal gas constant (8.3145 J mol^{-1} K^{-1}), T is the temperature, F is the Faraday constant (96, 485 C/mol^{-1}), J is the operating current density and J_o is the exchange current density.

From a thermodynamic point of view, the activation overpotentials at electrodes vary depending on the catalytic activities but the ratio of electrochemical reaction rate at the cathode to anode is determined by the stoichiometric ratio rather than by their catalytic activities since the electric current passing through the cathode is the same as the current passing through the anode [286]. Further details on thermodynamics and electrochemical CO_2 reactions and kinetics over a broad range of product spectrum are beyond the scope of this review, which is a point of future analysis."

The potential required to overcome the activation energies for the reaction at the electrodes highly influence the kinetics of CO_2R reaction. The resistances related to ion transport as well as reaction kinetics highly depend on the nature of the electrocatalytic materials, membranes and electrolyzer design itself. Similar to the typical water electrolyzers, the solution and membrane resistances, as well as the resistances due to the gas bubble, also contribute to the ohmic losses inside membrane-based CO_2R electrolyzers [288]. These losses also vary depending on the cell designs. For instance, in the zero-gap configuration where the distance between the CL over the electrode and membrane is kept minimal, the ohmic drops due to the liquid electrolytes significantly decrease. Therefore, a careful investigation of all these resistances is generally essential to the design of energy-efficient CO_2 electrolyzers. Vennekoetter *et al*. (2019) [23] did a thorough investigation of CO_2R electrolyzers through a comparison of different configurations of CO_2R electrolyzers, including the conventional liquid-phase electrolysis as well as the zero-gap systems, to identify the best design for enhanced energy efficiency. It was found out that the use GDEs of the zero-gap assembly (Fig. 20b) significantly reduces the ohmic losses and maximizes energy efficiency compared to the liquid-phase CO_2R electrolyzers (Fig. 20c). Here, the choice of membrane for a different environment is also crucial. For instance, the use of CEM results in an acidic environment that impedes the CO_2R and calls for precious electrocatalysts. Therefore, some of the drawbacks and advantages of both the monopolar and bipolar membrane should also be considered as design criteria for optimal CO_2R set-ups.

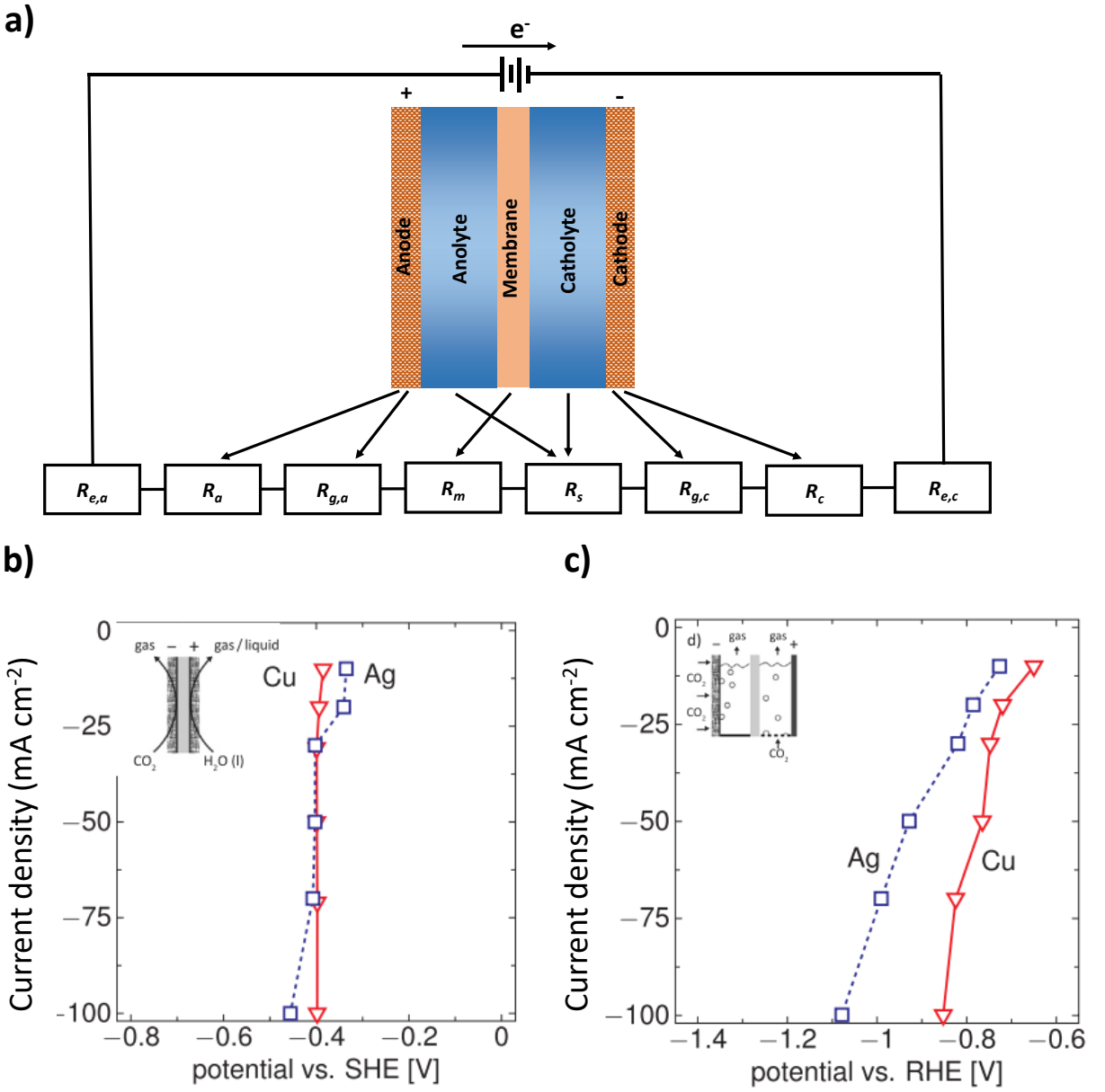

Fig. 20. a) Break down of the total cell resistances in liquid-phase (symmetrical) CO_2 electrolyzers: an electrical circuit analogy representation. Polarization curves for b) zero-gap CO_2R electrolyzers and c) liquid-phase CO_2R electrolyzers using Nafion membrane; cathodes: Ag or Cu-based GDE, anode: platinized titanium, catholyte and anolyte: 0.5 M H_2SO_4. Reproduced with permission from ref [23]. Copyright 2019, Elsevier.

4.2. MEA design

The inherent design of membrane electrode assemblies (MEA)s for CO_2R is related to several factors determining the performance of CO_2 electrolyzers. For instance, in CO_2R electrolyzers with a buffered layer, the thickness of the layer affects the internal ohmic losses. Weng *et al*. [44] performed model studies on the different MEA designs for CO_2R to investigate the advantages and limitations in terms of ohmic losses, temperature changes, local ion concentration and flooding issues. It was found out that a mesh-like structure or GDE better reduces the deterioration caused by the evolution of the oxygen bubbles at the anode. A reduced inter-electrode distance, which partially minimizes the internal losses was also shown to be associated with increased cross-over. Operations in liquid and gaseous phase also affect the membrane swelling, which is linked to membrane conductivity and hence the ohmic drops inside the cell. At high current densities, the membrane swelling slowly decreases due to the reduced concentration of water in the gas channel, which is restrained by the water vapor, and in turn, consumed during the CO_2RR. Therefore, increasing the relative humidity of the gas-phase CO_2 electrolyzers would help prevent the membranes from drying.

Electrode structure influences the kinetics of the CO_2RR at the interface between the electrode and the membrane. In CO_2R electrolyzers, planar (dimensionally stable) or porous electrodes, are mostly used for fundamental research purposes, for instance, electrocatalytic screening, as well as the impact of process conditions [38, 40, 289-292]. Planar or porous electrodes are simple to construct and integrate with reference electrodes. The kinetics of CO_2RR over such electrodes is mainly governed by the rate of CO_2 transfer to and from the electrolyte, which calls for the use of selected electrolytes and operations under optimal process conditions and hence added costs [35, 293]. On the other hand, the use of GDE in 3D structures could also increase the active electrode area facilitating the transport of gaseous and/or liquid reactants and products to and from the catalytic layer. As shown in Fig. 21, a typical GDE consists of a macro/microporous layer (differing in size of pores), a catalytic layer, and a current collector, which can be of a single-layer and dual-layer of porous materials with different properties like porosities and wettabilities. The type and nature of GDE have a direct impact on mass transfer and the kinetics of CO_2RR and hence a careful design of GDE plays a crucial role in CO_2 electrolyzers for enhanced current efficiency and product selectivity. In general, GDL should consist of a hydrophobic material to prevent the flow of liquid electrolytes to gas compartment, which limits the effective concentration of CO_2 at

the triple-phase boundary. For instance, a hydrophobic macroporous layer can be derived from a carbon-based GDE material coated with polytetrafluoroethylene (PTFE). Recently, different works on the use of GDE has been reported focusing on the design perspective and surface chemistry in relation to the CO_2R kinetics [35], the interdependence of high current density, catalytic testing and operating conditions [42], interplay between catalytic activity and gas-phase CO_2 electrolyzer performance towards practical implementation [43], modeling approaches on mass transport and redox reaction kinetics for different MEA designs [293]. In general, the optimal design of GDE-based MEAs considering the employed operating conditions such as the pressure and temperature, amount and composition of the electrolyte, and pH, etc., is crucial for the selective and energy-efficient conversion of CO_2 into the desired product.

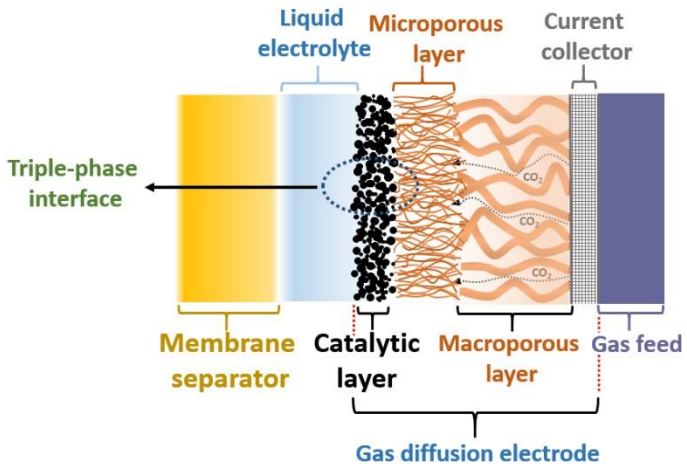

Fig. 21. Schematics of a gas diffusion electrode along with the membrane separator in liquid-phase CO_2 electrolyzer; the three-phase interface is mainly constituted by the liquid electrolyte, catalytic layer and the CO_2 gas molecules; the macro/microporous layer presents the diffusion medium for both the gas/liquid reactants and products.

4.3. Process parameters

4.3.1. pH/electrolyte effect

One important parameter in CO_2R is the pH value of electrolytes. The formation of certain intermediates was thought to be correlated with the pH value, which could influence the formation of the final product [220, 221, 294, 295]. For instance, the pH effect of electrolyte on product selectivity in the reduction of CO_2 over Cu electrodes was investigated by Hori, demonstrating that the selectivity of C_2H_4 prevails over that of CH_4 in high pH solutions, and the increased

formations of alcohols are accompanied with the high selectivity for C_2H_4 [295]. Koper *et al*. [220, 221] also studied the product selectivity in electrolyte with various pH for the reduction of CO to C_2H_4. The authors proposed that one pH-dependent pathway to ethylene has a common intermediate (CHO) with the formation of methane and takes place on both the (111) and (100) surfaces of Cu. Recently, the Sargent group has demonstrated that hydroxide ions near the Cu surface could reduce the activation energy barriers for CO_2R and C-C coupling which facilitates C_2H_4 formation [296].

The pH increases locally at the interface between the electrode and the electrolyte, which is due to OH^- production at the cathodic reactions. The effect of local pH on product selectivity in the electroreduction of CO_2 was initially proposed by Y. Hori [81, 186]. It has been shown that electrolytes like $KHCO_3$, $KClO_4$, K_2SO_4 and KCl solutions could favor the CO_2R on Cu surfaces. In contrast, K_2HPO_4 solutions highly facilitate H_2 evolution rather than CO_2R. Specifically, the FE for H_2 in the same concentration of electrolytes decreased as $K_2HPO_4 > KHCO_3 > K_2SO_4 > KClO_4 >$ KCl. While the pH would rise locally at the interface between the electrolyte and the cathode, these electrolytes have different buffer capabilities via neutralization reaction with OH^- produced locally near the electrode surface. For example, K_2HPO_4 has a strong buffer ability and could easily neutralize OH^- and maintain the local pH at relatively low value. On the other hand, K_2SO_4, $KClO_4$ and KCl electrolytes do not have obvious buffer ability for OH^- generated near cathode surface at CO_2-saturated neutral solutions, therefore, all these electrolytes will lead to relatively high pH. It is known that low pH favors H_2 evolution. Thus, the enhanced catalytic activity of H_2 evolution is attributed to lower pH value at the interface between electrode and electrolyte. It was also found that K_2SO_4, $KClO_4$ and KCl electrolytes facilitated selectivity toward C_2H_4 and alcohol formation, and Hori believed that a high local pH contributed to the reduction of CO intermediate to C_2H_4 and alcohols. Thus, the electrolytes with different buffer abilities provide different product distributions due to local pH effect. Recently, a local pH was systematically tuned via varying Cu nanowire morphology, demonstrating a controllable hydrocarbon formation under identical conditions [217].

The pH of the electrolyte solutions needs to be effectively controlled for efficient utilization of the selected catalyst, which in turn influences product efficiency and selectivity. The pH of the CO_2R medium highly influences the predominant dissolved species of CO_2 in aqueous solutions as a function of pH and potentials, which is described by the Pourbaix (E-pH) diagram (Fig. 22)

[35, 79, 297]. H_2CO_3 is the predominat species in strongly acidic and closely neutral pH medium (below ~6), HCO_3^- in a neutral and mildly basic pH medium (between 6 and 10.3) and CO_2^{2-} in a strongly basic medium. It is worth noting that the pH near the catalytic layer of the cathode and the bulk electrolyte is quite different due to the mechanistic variations in CO_2RRs for the different products, which either produce H^+ or consume OH^- ions. In general, as the pH change affects the rate of CO_2RR, product selectivity of CO_2RR and rate of HER, it is very complicated to relate the dynamics of such reaction to better control the efficiency of CO_2RR [35]. For instance, the rise of pH shifts the product selectivity at the surface of Cu from H_2 and CH_4 to higher hydrocarbons products like C_2H_4 and C_2H_6. Superimposing the Pourbaix diagrams of aqueous phase CO_2R (involving bicarbonate and carbonate species) and a molecular or extended material catalyst, it is shown that the proximity of the boundaries between different Pourbaix diagrams helps to identify the optimal conditions that would be appropriate for electrocatalysis with low overpotentials. Li *et al*. [79] explored the optimum E-pH conditions for the production of $HCOO^-$ using SnO_2 catalysts at a high selectivity, FE and electrode stability. As can be seen from the combined Pourbaix diagram for the different phases of Sn-SnO_2, the SnO_2 catalyst was shown to be stable with in the pH range of 8.42 - 11.72 (identified as an optimal region), whereas it´s reduction to metallic Sn was found to be limited in the same region. An optimal pH of about 10.2 (within the overlay region of Fig 22) was reported for a stable SnO_2 activity considering the balanced effect of $HCOO^-$ depletion from the electrode surface and CO_2 bubbling of the electrolyte.

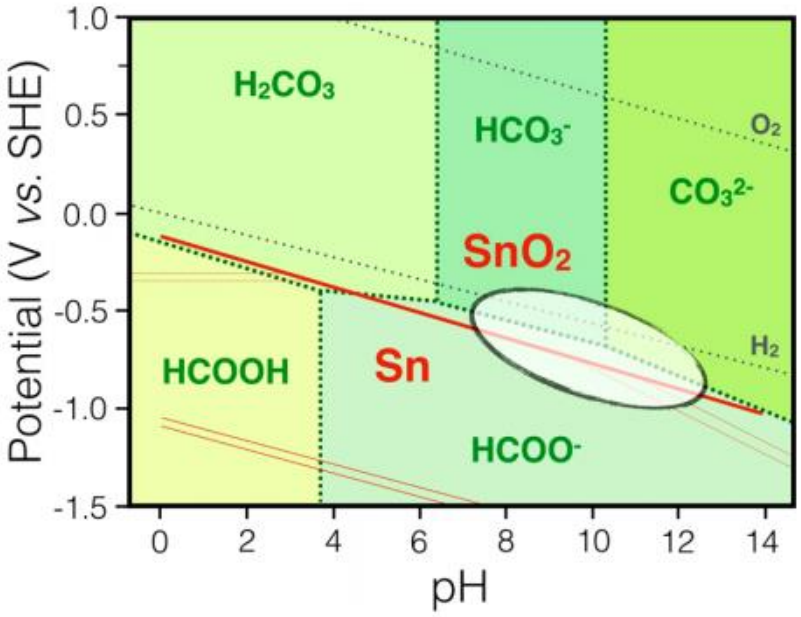

Fig 22. Combined Pourbaix diagram showing the overlay region between the phases of Sn-SnO_2 in aqueous solutions and the dissolved species of CO_2 and for different pH and potentials. A stable SnO_2 phase was observed within the overlay (encircled) region. Reprinted with permission from [79]. Copyright 2015, American Chemical Society.

4.3.1.1. Effect of cation and anion

The type of the cation and anion present in the electrolyte has been shown to have a considerable impact on the activity and selectivity of the electrochemical CO_2R [298, 299]. A strong dependence of the selectivity on size of cationic species has been demonstrated for the reduction of CO_2 and CO on Cu, indicating that the formation of multiple carbon products at a limited HER is better achieved by using larger cations [298]. It was reported that H_2 evolution could be obviously favorable over CO_2R in Li^+ electrolyte (when using Li^+, Na^+ and K^+, FE of H_2 had 60.5%, 25.1% and 14.5%, respectively), and the enhanced formation of alcohol and C_2H_4 was observed with increasing the cation size (in the order of $Li^+ < Na^+ < K^+ < Cs^+$) [186]. Recently, Bell *et al.* [300] also demonstrated that the size of the electrolyte cation affects the rate of C−C bond formation by electrostatic interaction between solvated cation and adsorbed species, and this rate increases with increasing cation size, which influenced the catalytic activity (Fig. 23). Koper at al. has performed CO reduction in electrolytes with different cation size and demonstrated that the alkaline cations on Cu catalysts could decrease the energy barrier of CO coupling, affecting the product formation [301]. It should be noted that smaller cations are more hydrated due to their more intense electric field, thus leading to larger hydrated radii than larger ions. In this review, the size of cations is stated without considering hydrated water molecules.

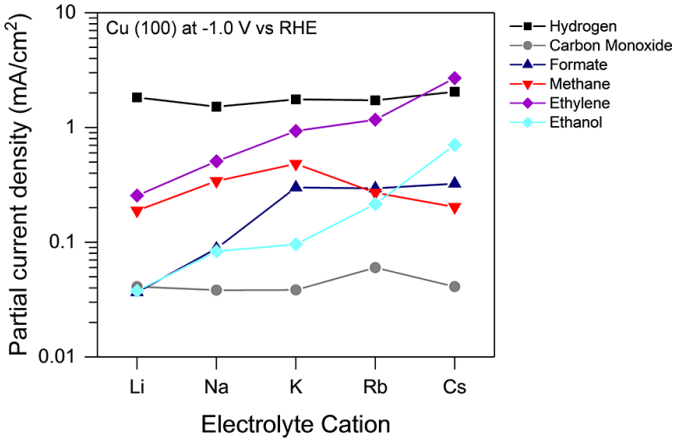

Fig. 23. Partial current densities of products as a function of cation size. Reproduced with permission from ref [300]. Copyright 2017, American Chemical Society.

The type of anions in the electrolyte have been shown to have an impact on the product distribution in CO_2R. Non-buffering anions (Cl^-,ClO_4^-, SO_4^{2-}) were observed to enhance the selectivity for C_2H_4 and CH_3CH_2OH compared to buffering HCO_3^- anion [81]. The HCO_3^- anion based salt solutions are widely used for CO_2RR due to its buffering effect, which is able to keep a neutral bulk pH. However, the change in concentration of HCO_3^- have been shown to affect the product selectivity. It was reported that the use of high concentrations of HCO_3^- (> 0.2 M) improves the overall Faradaic efficiency for H_2 and CH_4 whereas the low concentrations (< 0.05 M) result in high selectivity towards ethylene [302]. In addition to maintaining the bulk pH, HCO_3^- have also been shown to serve as a source of C [85, 86, 303, 304] as well as proton [87] in CO_2R. Beside HCO_3^-, other ions, for instance, halides, could also impact the CO_2R performance metrics but the mechanism is not well understood in such a case so far [305-307].

4.3.2. Temperature and pressure

High temperature generally offers an advantage of more efficient mass transport of CO_2 and better kinetics towards a high-rate CO_2 reduction. Although higher current densities can be achieved at higher temperatures, this is associated with the loss of cell performance in terms of selectivity and the reduction in the solubility of CO_2 at elevated temperatures [35]. Elevated temperatures generally increase the availability of water (enhancing the water vapor) in the electrolyzer thereby preventing the MEA from dehydration and flooding issues with a positive impact on high current densities. However, excessive temperature may also result in drying and damage of the MEA which could generally lead to performance losses due to increased cell resistance, among others. A particulalr damange on a membrane with opened pores may also result in crossover issues. Summary of the research works focusing on/related to the impact of the temperature on CO_2R, mostly performed on H-cell, has been well documented recently [28, 35].

Pressure is another process parameter with a profound impact on the performance of CO_2 electrolyzers. High pressure has been shown to enhance the mass transfer to the catalytic layer due to the increase of CO_2 solubility in aqueous electrolytes [113]. However, high-pressure CO_2R also requires a balanced pressure between the anode and cathode compartments, which otherwise may lead to the mechanical stress on the separator and enhanced crossover. For instance, a state of

delamination in BPM has been reported for applications in CO_2R under the high-pressure condition of up to 50 bar [113]. This calls for separators with good mechanical strength, perhaps a thicker and reinforced membrane materials carefully optimized to keep the resistance as low as possible. The impact of pressure on CO_2R has been widely investigated from the perspective of mass transfer and reaction kinetics using various cell designs but there is still a gap in extensive studies focused on the mechanical and crossover properties of membrane separators in pressurized CO_2 electrolyzers [113, 308-321].

4.4. Cell testing

4.4.1. Membrane-less (microfluidic) cells

Early investigations on microfluidic devices were focused on the electrocatalysts and CO_2RR conditions. Practical assessment of different metallic/bimetallic catalysts (Ru-Pd and Sn) for CO_2R to formic acid was carried out under different operating conditions (including pH), and up to 89% faradaic efficiencies along with ~100 $mAcm^{-2}$ current density was reported [59]. Moreover, catalyst layer preparation methods [322] and the composition of electrolytes [323, 324] have also been reported to have a considerable impact on the microfluidic CO_2 electrolysis system. Jhong *et al*. [322] investigated the impact of different deposition methods on the catalyst layer structure and hence the performance of CO_2R. Surface SEM images indicated a more uniform distribution of the catalyst particles in the catalyst layer deposited over Ag-based electrodes by air-brush method (Fig. 24a) than the hand-painted method (Fig. 24b), which was associated with an agglomeration and unevenness of the catalyst particles. In the MRF cell test, the air-brushing catalyst layers resulted in a FE of up to 95% for CO, which was much higher than the hand-painted catalyst layers displaying FE of up to 83% at -1.56 V vs Ag/AgCl (Fig. 24c) [322]. With the aim to understand the dynamics of GDE flooding, Leonard *et al*. [325]carried out an investigation on electrode stability at different current densities in MFR. The electrolyte penetration into the GDE during electrolysis was evaluated by determining the electrochemical double-layer capacitance (EDLC), and it was observed that the operations at high current densities increased the flooding of the electrodes. Although most of the MFR has have been investigated using aqueous salt solutions as liquid electrolytes, ionic liquid has also been investigated for CO_2R. Rosen *et al*. [326] demonstrated the possibility of lowering the free energy of formation of $CO_2^{\bullet-}$ intermediate and hence the CO_2R overpotential by using an ionic liquid electrolyte in MFRs. A faradaic efficiency (FE) above 96% was reported for CO production at low overpotentials (< 0.2 V) by CO_2RR

mediated using 1-ethyl-3-methylimidazolium and Ag catalysts. Validation of modeling approaches have also been a fundamental issue which has been attempted using MFRs [327-329]. Recently, a mathematical model was also developed and validated for quantification of electrical resistance losses from electrode and electrolytes losses in a pH differential microfluidic electrolytic cell for the reduction of CO_2 to formic acid [327].

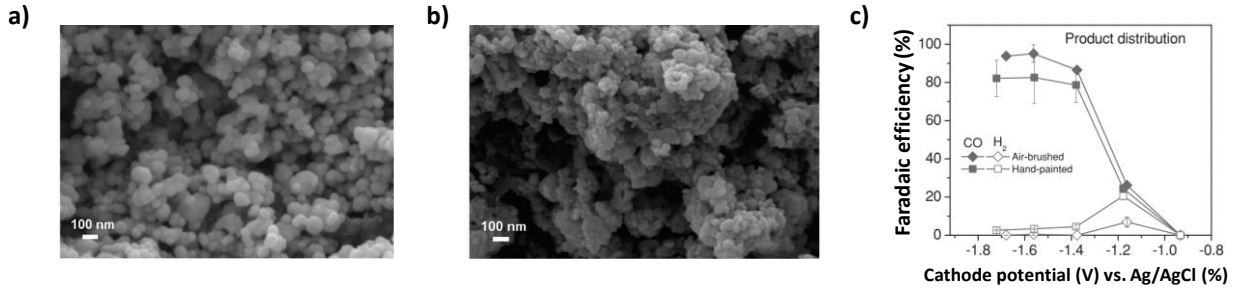

Fig. 24. Surface SEM images of a) hand-painted and b) air-brushed Ag-based cathode for CO_2 reduction in MFR. c) The variation of FE for CO and H_2 as a function of cathode potential (V) vs. Ag/AgCl. Cathode catalyst: unsupported Ag nanoparticles with 0.75 mg cm^{-2}; anode catalyst: 4.25 mg cm^{-2} unsupported Pt black; CO_2 flow rate: 7 sccm; Electrolyte: 1.0 M KCl at a flow rate of 0.5 mL min^{-1}. Reprinted with permission from ref [322]. Copyright 2013, Wiley-VCH.

4.4.2. Membrane-based flow cells

Table 5 summarizes some of the works reported on each type of ion exchange membranes (Table 5a: AEM, Table 5b: CEM, Table 5c: BPM) applied for CO_2R during the past decades. Most of these studies employed neutral, anion buffering electrolyte such as $KHCO_3$ with concentrations in the range of 0.25-1 M when working with CO_2 electrolyzers based on monopolar membranes and the cathode electrode/catalysts of interest. The anodic reactions were also performed in similar solutions but also possibly employing earth-abundant anodes in basic solutions (e.g. 1 M KOH) when using BPM-based CO_2 electrolyzers.

4.4.2.1. Anion exchange membrane

The key issue when working with AEMs using anion buffering electrolytes is the effect of CO_2 pumping. Ma *et al*. [181] performed a systematic investigation of the CO_2 utilization in AEM-based-CO_2 electrolyzers to figure out the apparent consumption for product formation and parasitic CO_2 pumping to the anode side. Based on a separate analysis of the outflow streams from cathode

and anode sides, it was found out that most of the consumed CO_2 (70%) was parasitically pumped out to anode side. Only about 30% of the CO_2 consumption was utilized for CO_2R product formation (Fig. 25a). The key implication was that in basic solutions, there is a huge discrepancy in the inlet and outlet flow rates of gas streams depending on the current densities, which leads to an overestimation of the performance metrics, for instance, up to 12% discrepancy in FE estimation for C_2H_4 in 5 M KOH solution without consideration of the effect of CO_2 pumping. Similarly, a poor CO_2 utilization (< 50 % consumed for product formation) was reported using a gas-fed MEA-type electrolyzer with zero-gap cathode configuration, although a good cathodic activity and selectivity was achieved [142]. In another work, Schmidt group have performed an experimental study on the formation of CO_2 on anode side due to CO_2 pumping effect in the alkaline CO_2 electrolyzer. The amount of produced CO_2 on the anode side was found to be proportional to the increasing cell current density (Fig. 25b) [68], but it is also believed to be produced at large fractions even when working at low current densities due to other side reactions like catalyst oxidation which leads to the CO_2 formation instead of O_2. The use of alkaline AEMs is also associated with large Ohmic losses compared to the cation exchange membranes, which limits the energy efficiency of the system. Thus, while tuning membrane microstructure and properties are required to design highly conductive AEMs, this is counteractive to CO_2 pumping phenomenon, which might be aggravated by the improved HCO_3^-/CO_3^{2-} conductivity [136, 137, 141].

Several attempts have been performed to explore the materials and properties of AEMs for the optimal design of CO_2R cells [127, 136, 137, 141, 145, 330]. Early investigators were focused on the use of catalyst coated AEMs to optimize the CO_2R cells for specific products. Komatsu *et al*. [129] prepared Cu-coated Selemion AEMs by electroless plating and found out CO and HCOOH as a major product with a maximum of 27% total current efficiencies. The performance of different membranes materials and functionalities have also been tested for CO_2R. The use of AEM based on alkali doped polyvinyl alcohol (PVA) along with Cu-based cathodes favored the formation of CO at an FE of 12 % [127], whereas the use of AEM based on polystyrene polymer functionalized with quaternary ammonium (QA) groups coupled with Cu_2O-based cathodes favored the production of CH_4 at FE of 32% [330]. Proper choice of AEM functional groups have a direct impact on the mass transfer of CO_2 within the reaction zone, and hence the kinetics of the CO_2RR [136, 137, 141, 145]. Two different types of AEM with different functionalities were prepared and

tested for CO_2R: i) AEM by a direct blending of polyethylenimine (PEI) with poly(vinyl alcohol) (PVA) and doped with KOH (PEI-PVA_{OH}), ii) AEM by blending of quaternized PEI with PVA and doped with KOH ($_Q$PEI-PVA_{OH}) [136]. For $_Q$PEI-PVA_{OH}, the bulky alkyl groups hampered the water association (limits H_2 production) and facilitated the adsorption of CO_2 to the reaction zone by the formation of an ion pair (QA^+-$CO_2^{\bullet-}$) [136]. Although the membrane performances were too low for industrial implementation, the works mentioned above remark that the optimal design of membranes is one strategy to enhance the performance of CO_2 electrolyzers.

Imidazolium-functionalized AEMs have been applied in a variety of systems, including fuel cells, driven by their relatively high chemical stability due to the structure consisting of the π-conjugated imidazole ring, and the environmentally-friendly nature [331-341]. In particular, alkaline stability is related to the π conjugated structure with the delocalized positive charges which restrict the nucleophilic attack by OH^-, i.e., the Hofmann or S_N2 elimination. Dioxide Materials (DM, USA) has developed a group of novel imidazole-functionalized AEMs which exhibit strong stability in alkaline medium, that are now available commercially (Sustanion membranes) for applications in water and/or CO_2 electrolyzers [139]. The synthesis of such membranes can be carried out by a two-step process involving copolymerization followed by subsequent functionalization [137, 139, 141]. Kutz *et al*. [137] attempted recently to extend the applicability of Imidazolium-functionalized AEMs for CO_2R. Imidazolium-functionalized styrene and vinylbenzyl chloride (VBC)-based (PSMIM) polymers were prepared by the solution casting and evaporation method, with the structure depicted in Fig. 25d. A stability test was performed by recirculation of 10 mM $KHCO_3$ on the anode side and humidified CO_2 on the cathode side of a cell equipped with Ag cathodes and IrO_2 anodes. The good stability of the membranes over an extended period (up to 6 months) was recorded at 50 mA cm^{-2}. For the selectivity study, a cell with both anolyte-free (anode left open to atmosphere) and catholyte-free (humidified CO_2) configuration was run at 3 V for about 30 min, with dominant products being H_2 and CO. Up to 98% FE for CO was recorded at a current density >100 mA/cm^2 [137]. The observed FE and current density of the new imidazolium-functionalized AEMs were up to 4-fold and 14-fold higher, respectively, when compared to any of the other membranes tested in the experiment. It is worth noting that the imidazolium functional group acts as a co-catalyst for the CO_2R and reduces the activation barrier for the formation of the CO_2 radical, ultimately leading to the high selectivity for the products of interest [326]. The scope of *N*-heterocycles as co-catalysts was further explored by

Zhao *et al*. [342], and was shown to extend beyond the imidazolium cations. In another study, a 3-compartment electrochemical cell equipped with a proprietary Sustanion™ anion exchange membrane [137, 343] on the cathode side (with imidazole-Sn nanoparticle catalyst-based GDE), stable performance for >500 h was observed at a current density of 140 mA/cm^{-2} and 3.5 V with a FE of up to 94% for formic acid. Further improvement in the performance of Sustanion-based electrochemical cells for eCO_2R to CO was demonstrated by optimizing the GDE for the cathode. A FE above 95% was recorded for CO at 600 mA/cm^2 and 3.3V under the optimal conditions (i.e. Ag/2/2, implying to 2 wt% of the porous carbon and 2 wt% of Sustainion XA-7 ionomer based on the weight of the Ag, with a loading of 2 mg cm^{-2} for an active area of 5 cm^2) [141]. To demonstrate operational development towards industrial-scale systems, Sustanion membranes were also tested over a larger active area of 250 cm^2, and a stable voltage in the range of 2.9 - 3.0 V was recorded for about 90 h [139].

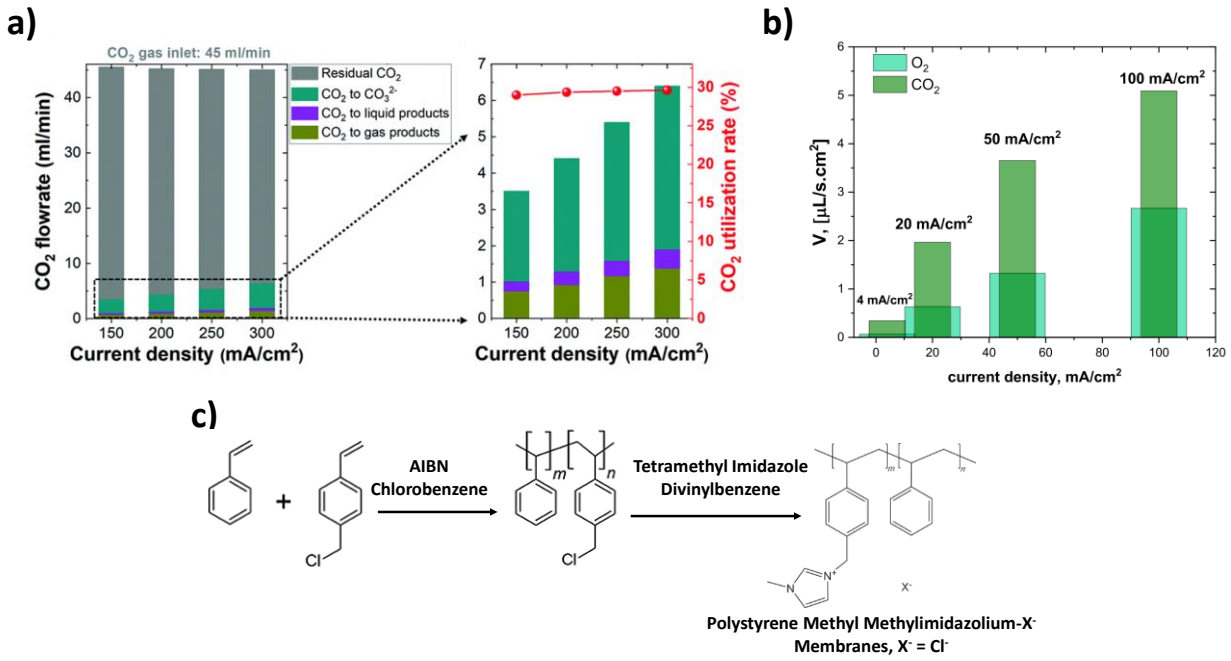

Fig. 25. (a) Fraction of the CO_2 flow utilized for carbonate formation, CO_2R product formation, and residual CO_2 flow [181]. b) Volume flows of O_2 and CO_2 formed at the anode side in AEM-based CO_2 electrolyzer equipped with Au-based cathode and IrO_2-TiO_2 anode; The catholyte was pure, humidified CO_2 and the anolyte was Ar (100% RH) [68]. Presentation of c) steps for the preparation of the pre-polymer for the synthesis of Sustainion AEMs. Illustration of (humidified

CO_2 fed at a temperature of 50 ^oC and rate of 5 sccm) and anolyte-free (anode in an open-air) conditions. Reprinted with permission from ref [137]. Copyright 2017, Wiley-VCH.

4.4.2.2. Cation exchange membranes

Earlier studies on CO_2 conversion technologies demonstrate the possibility of using CEMs coated with electrocatalysts (i.e., catalyst coated membranes - CCMs). The use of the CCM approach allows the implementation of a solvent-free, gas-phase eCO_2R, which enables better mass transfer as well as reduces the risk of the catalyst poisoning by the solvent or electrolyte impurities. Dewulf and Bard investigated Cu-coated Nafion membranes for the gas-phase eCO_2R and reached up to 20% FE for CH_4 and C_2H_4 at a potential of -2.00 V vs. SCE [131]. Several other researchers in the past have used CEMs extensively along with the other metal catalysts such as Au and Sn for the eCO_2R (both in the gas-phase and liquid-phase) to various products, including HCOOH and CO mostly using the designs based on H-cells [126, 128, 344].

Delacourt *et al*. [124] developed and compared, for the first time, the performance of different designs of gas-phase CO_2R flow cells based on Nafion separators for simultaneous CO_2 and H_2O reduction at ambient temperature. Flow cell designs similar to the typical polymer electrolyte membrane (PEM) water electrolyzers fuel cells (zero-gap configuration), and modified system utilizing a pH-buffer layer of aqueous $KHCO_3$ placed between the CEM and the Ag cathode (buffered configuration) (Fig. 26a) were considered, among others. A 100% FE for H_2 at a current density of 20 mA/cm^2 was recorded when using the zero-gap configuration utilizing only Nafion, implying no observation of gaseous CO_2R products (Fig. 26b). On the other hand, the production of CO was prominent with up to 82% FE at 20 mA/cm^2 (Fig. 26b) when operating with the buffered system; however, with poor stability as CO FE reduced at a rate of ~3%/h. This change in FE with time was related to the variations in the composition of the buffer medium due to the formation of other CO_2R products like $HCOO^-$ and $C_2O_4^{2-}$, as well as the electrode poisoning. Similarly, a zero-gap configuration flow cell equipped with a Nafion membrane in alkaline medium was tested for liquid-phase ($NaHCO_3$ as catholyte) eCO_2R [130]. Up to 80% FE was recorded for formate (using In-Pb bimetallic catalysts), which reduced over the course of 1 h due to the formation of diffusion barriers at the membrane-electrode interface. In zero-gap CEM-based CO_2 electrolyzers, the importance of electrolyte composition for stability has been demonstrated: acidic anolytes with only protons as cations prove good stability [134].

As mentioned above, one of the problems of using aqueous solvents for PEM-based CO_2 electrolyzers is the presence of competitive HER due to the low solubility of CO_2 in the water (~35 mM) and the low diffusion coefficient of CO_2 in water (0.0016 mm^2 s^{-1}) at standard conditions [345]. These mass transport limitations can be mitigated, by working with gas-phase CO_2 electrolyzers and/or operating at high CO_2 pressures, and one example is work by Dufek *et al*. [135] who investigated a pressurized electrolysis system (up to 20 bar) at varying temperatures (up to 90 °C)) for a continuous reduction of CO_2 to CO and syngas mixtures. The FE was observed to increase with the rise of gas pressure (> 18 bar), reaching up to 92% observed at 350 mA cm^{-2}, which was about a five times higher compared to operations at ambient pressure. However, no significant impact of temperature was observed on CO selectivity. Recently, Ramdin *et al*. [113] developed CO_2 electrolyzers equipped with CEMs for a comparative assessment with BPM, through operations at high pressures of up to 50 bar in flowcells for the first time. A high-pressure CO_2 gas was supplied to the cathodic compartment and the impact of different process conditions (like electrolyte concentrations and flow rates, cell potentials, and CO_2 pressures) on the efficiency of the production of formate was investigated. FE reaching 90% was reached (Fig. 26c) for formate at CO_2 pressure of 40 bar, which slightly reduced with time due to formate crossover through the CEM leading to pH variations between compartments, which is one of the limitations of using CEM. This issue can be overcome by using BPM as discussed earlier in section 3.2.4. Moreover, CEM-based CO_2 electrolyzers with a large active area (up to 100 cm^2) were also investigated to demonstrate the potential for upscaling and longtime operation of these technologies [110]. The drawback of such a system was the penetration of some electrolyte through the pores of the Ag-based GDE observed initially (about 5 min after turning on the power supply) (Fig. 26d) which was related to the reduction in rigidity of the GDE caused by the buildup of pressure inside the pores from the accumulation of the gaseous products. This penetration effect was controlled through different strategies such as the installation of turbulence facilities in the gas compartment and the control of differential pressures at GDE. The FE for CO was observed to increase with an increase of CO_2 utilization efficiency but a plateau was reached at about 75% (for 100 cm^2 CO_2 electrolyzer) corresponding to ~3.5 of λ, which is a parameter representing the ratio of the amount of the CO_2 feed gas to the theoretically amount of CO_2 convertible by the actual electrolysis (Fig. 26e): This implies that the concentration of CO_2 gas no more limits the reaction kinetics. A long-term CO_2-electrolysis with a FE for CO in the range of 60-80% (at λ-value of about 3.1 and current

density of 150 mA cm^{-2}) was demonstrated (Fig. 26f) by using the 100 cm^2 CO_2 electrolyzer optimized mainly in terms of electrolyte penetration into the GDE. This study lays a conceptual groundwork for assessing process requirements and optimization protocol when advancing the lab-scale CEM-based CO_2 electrolyzers to industrial-scale implementations, in particular, focusing on the flooding issues of the GDEs. Various other studies on CEM-based CO_2R systems have also been recently reported with a focus on analysis and testing new catalytic materials either in an H-cell or flow cell [109, 116-118, 121]. There is a research gap in a specific study reported in tailoring CEM base materials and functionalities for a better understanding of mechanistic relevance to efficiency and selectivity of eCO_2RRs. A wide range of high performance, low-cost CEMs are required, which could be either based on new materials or modification of the existing ones used in other relevant technologies such as low-temperature water electrolyzers and fuel cells [346-351].

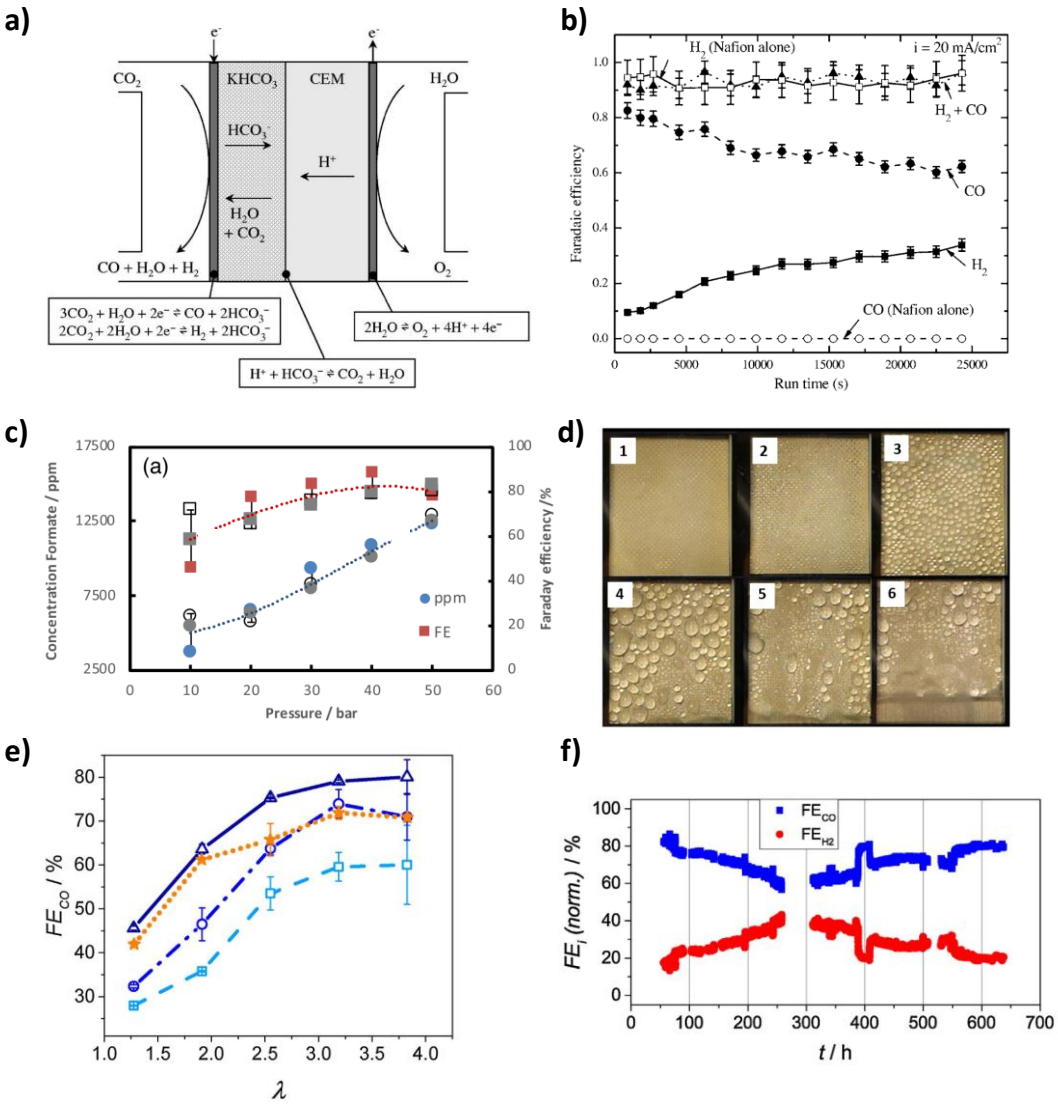

Fig 26. CEM-based eCO_2R flow cell: a) schematic illustration of the cell with a buffer layer of aqueous $KHCO_3$ between the CEM and cathode. b) FE of CO and H_2 obtained at 20 mA cm^{-2} with the fuel-cell-type (zero-gap) configuration (open symbols) and the modified configuration with a buffer layer of aqueous $KHCO_3$ (filled symbols). Cathode: 10 mg/cm^2 unsupported Ag; Anode: 7.7 mg cm^{-2} unsupported Pt/Ir alloy; CO_2 flow rate 20 mL min^{-1}. Reproduced with permission from ref [124]. Copyright 2003, The Electrochemical Society. Pressurized CEM-based eCO_2R flow cell: (c) concentration (circles) and Faraday efficiency (squares) of formate at 3.5 V. Anolyte (0.5 M H_2SO_4) and catholyte (1 M $KHCO_3$) flow rate: 10 $Lmin^{-1}$; electrolysis time: 20 min. Data are presented for three different runs, with the dotted lines showing the arithmetic mean of the results. Reproduced with permission from ref [113]. Copyright 2019, American Chemical Society. CEM-

based eCO_2R flow cell: d) electrolyte droplets on the gas-side of the GDE after about 5 min of electrolysis (1-3), merging (4), flowing downwards (5), and flooding the GDE (6). e) FE for CO vs. the utilization efficiency of CO_2 (λ). Star: 10 cm^2 CO_2 electrolyzer; square: 100 cm^2 electrolyzer, low turbulence; circle: 100 cm^2 CO_2 electrolyzer, high turbulence; triangle: setup 2, high turbulence and circulating pump. f) Stability test on 100 cm^2 CO_2 electrolyzer at a current density of 150 mA cm^{-2}; Anolyte and catholyte: 0.5 M K_2SO_4. Reproduced with permission from ref [110]. Copyright 2018, Elsevier.

4.4.2.3. Bipolar membranes

A BPM-based CO_2 electrolyzer in flow cell was first demonstrated by Li *et al*. [68], who used a commercial BPM (Fumasep FBM) with non-precious electrocatalyst (NiFeOx) as the anode (for OER) and Ag or BiOx as the cathode (for CO_2RR). A maximum FE for CO of about 60% at a current density of 30 mA cm^{-2} was initially recorded, which reduced with time over 8 h run. This performance was further enhanced by operating the BPM in gas-phase to overcome the intrinsic CO_2 solubility limitations in liquid-phase [62]. A solid-supported aqueous $NaHCO_3$ layer was also used between the BPM and Ag-based cathode to prevent the over-acidification of the GDE (Fig. 27a). Up to 67% FE for CO was recorded at a current density of 100 mA/cm^2 which was more than two times higher than the case with no support layer (Fig. 27b). Such a system even displayed up to 200 mA cm^{-2}, and a stable FE over 24 h recorded when adequate hydration of the support layer, i.e. using high humidity (>90 %) CO_2 was kept. Vermaas *et al.* [148] used a non-precious electrocatalyst based on $NiFeO_x$ for the OER and Ag catalysts for CO_2RR in a BPM-based CO_2 electrolyzer. A maximum FE for CO of >78% was recorded at an applied potential of -1.1 V vs RHE, which remained quite stable at more negative potentials (up to -1.3 V vs RHE) (Fig. 27c). The advantage in terms of stable FE when using a BMP compared to the monopolar membranes (Nafion) has also been demonstrated for CO_2 electrolyzers (Fig. 27c), which is mainly the reduction of crossover as discussed in earlier section 3.2.3. However, there is a possibility of water and CO_2 formation at the BPM interface under forward bias, as shown in the following reactions:

$$HCO_3^- + H^+ \rightarrow H_2O + CO_2 \quad [R20]$$

$$CO_3^{2-} + 2H^+ \rightarrow H_2O + CO_2 \quad [R21]$$

This phenomenon may lead to delamination of the BPM or blistering. Also, considering similar thicknesses of the CEM and AEM layer of the bipolar membrane, the CO_2 formed at the BPM

interface will diffuse at equal proportion both to the anode (50%) and the cathode (50%) side [68]. This could lead to CO_2 pumping which reduces the CO_2RR efficiency like the case of using AEMs. To mitigate this effect, the Schmidt group has demonstrated an approach of using a unique alkaline-acidic interface created by close contact of a thin film of alkaline ionomer layer coated over the GDE catalyst layer and CEM layer in a CO_2 electrolyzer [68]. This type of design was observed to increase the active catalytic area with a simultaneous reduction of the parasitic CO_2 pumping as shown in Fig. 27d, represented as a novel configuration CO_2 electrolyzer. The thin film alkaline ionomer formed over the rough surface of the cathode catalyst layer allows for in-plane diffusion of the resulting CO_2 and H_2O through ionomer to the cathode electrode pore volume while the CEM prevent the passage to the anode side. Other researchers have also demonstrated the utility of BPM for CO_2R [68, 113, 151].

Other applications of BPM have also been demonstrated in solar-driven CO_2R cells [149], mainly used reverse bias mode, and also in cells coupled with a CO_2 capture electrolyte towards a more advanced CO_2 conversion systems. For instance, a BPM-based capture-electrolysis system maintained a stable conversion throughout 145 h at a current density of about 180 mA/cm^2, consistent with the anticipated benefits of BPM in reducing ion or product crossover by keeping a stable local pH [151].

Unlike the research mentioned above, which were works that are performed under ambient temperature and pressures, investigations at elevated pressure and temperature are scarce. As mentioned before, elevated pressures alleviate the solubility limitations of CO_2 in aqueous electrolytes, which enhances system performance. A BPM-based CO_2 electrolyzer operated at a pressure of about 40 bar attained FE for the formate reaching up to 90 % [113].

In membrane-based CO_2 electrolyzers, understanding the impact of pH difference over the membrane allows for better control of the overpotential for CO_2RR/HER and the oxygen evolution reaction (OER), thereby allowing for the reduction of the total cell voltage [352]. Hence, pH is also strongly linked to both the energy efficiency and the FE of the cell. As mentioned previously, when using BPMs, a minimum voltage of about 0.83 V is required to maintain a pH gradient at the interface where water dissociation occurs [183, 352]. Vermaas *et al*. [352] performed a series of experiments to investigate the behavior of BPM in a flow cell by determining the membrane voltage as a function of 16 pH differences. Under low current density (CD) conditions

($\leq$1 mA cm^{-2}) (Fig. 27e), the experimental membrane potential becomes closer to or lower than the theoretical potentials obtained by the Nernst equation (0.0591ΔpH), implying that the membrane potentials is exclusively dependent on the bulk pH. The charge at low CDs dominantly carried out by water dissociation (>70 %), and the co-ion exclusion and ohmic losses mainly explain the membrane voltage deviations from the theoretical ones. At high CDs (10 mA cm^{-2}) (Fig. 27f), most of the membrane voltages over the different pH ranges are close to 0.8 V, which is thought to be associated with water dissociation at membrane-solution interface under extreme pH. Clarification of this phenomenon is useful, particularly under the CO_2R conditions, in which the local pH varies depending on the composition of the electrolyte (with dissolved CO_2) and the rate of H^+/OH^- ion pumping or consumption during CO_2RRs. For instance, some of the recent research works demonstrate the water-splitting behavior of the BPM under the reverse bias enhances the stability of local pH and concentration of the electrolyte, which allows for efficient utilization of non-platinum electrocatalysts for OER (anode side) and better control of product selectivity during CO_2R [62, 63, 148].

Despite some of the general benefits from BPM operations, it is worth noting the drawbacks as well. The large membrane potential that develops when operating BPMs under reverse bias mode in electrolytes having similar pH levels increases the required voltage for the electrolysis, thereby reducing the overall energy efficiency [155]. This calls for a prospective research direction in advancing BPM-based electrolyzers, among others, through the design of high performance polymeric materials towards practical applications.

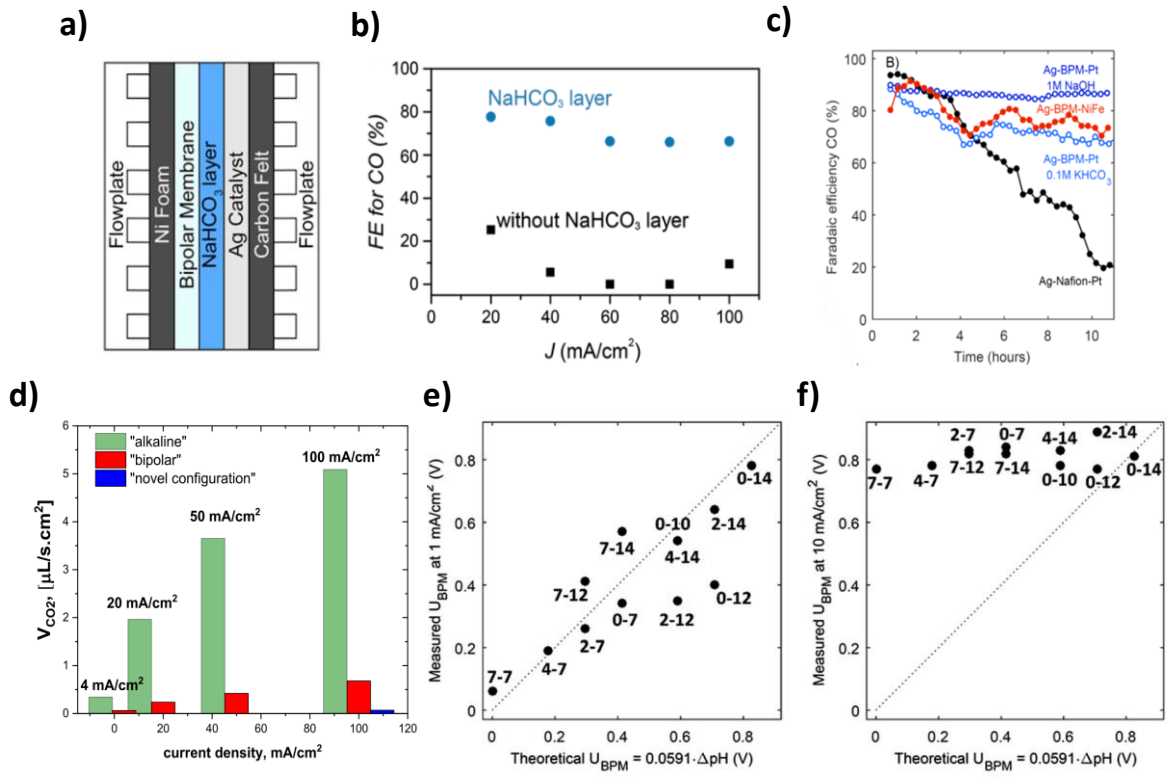

Fig. 27. a) Illustration of the gas-phase electrolyzer with the solid-supported aqueous $NaHCO_3$ layer, functioning as a buffer layer between the Ag-based cathode and BPM; b) The variation of FE for CO with current densities (20 - 100 mA cm^{-2}); cathode: silver on carbon GDE; Anode: nickel foam; anolyte: 1 M NaOH at flow rate of 10 mL/min; catholyte: humidified CO_2 at flow rate of 100 sccm. Reproduced with permission from ref [62]. Copyright 2018, American Chemical Society. c) FE for CO as a function of time for different cell configurations at an applied voltage of -1.1 V vs RHE: Ag-BPM-NiFe with anolyte of 1 M NaOH, Ag-Nafion-Pt with anolyte of 0.1 M $KHCO_3$ and Ag-BPM-Pt with anolyte of 0.1 M $KHCO_3$; catholyte of 0.1 M $KHCO_3$ in all cases. Reproduced with permission from ref [148]. Copyright 2016, American Chemical Society. d) Volume flows of CO_2 formed at the anode side for CO_2 electrolyzer with different membrane configurations; the catholyte was pure, humidified CO_2 and the anolyte was highly humidified Ar [68]. The variation of the experimental potential as a function of thermodynamic potential (determined as 0.0591ΔpH) for 12 different cases at a current density of e) 1 mA cm^{-2} and f) 10 mA cm^{-2}; measured voltages are determined by chronopotentiometry series of 300 s; the numbers show the pH in the catholyte-anolyte. The salt concentration of all electrolytes was set to 1 M except for the case of pH 10 with 0.5 M salt concentrations. The flow rate of the electrolytes was fixed at 0.63 cm s^{-1} [352].

4.5. Stability

While most studies on electrochemical CO_2 reduction have focused on assessing the catalytic activity, investigations on the structural stability have been given poor attention with leaving room for the requirement of highly stable materials for commercial implementation of CO_2R devices [353, 354]. In CO_2 electrolyzers, a deeper understanding of the interdependence of the GDE performance and stability, along with the possible degradation mechanisms under different cell design and operating conditions is highly essential.

One of the key factors leading to poor stability of the catalytic layer is the catalyst deactivation, which is mainly caused by the poisoning and contamination of the electrode surface [355-360]. In particular, for Cu electrodes, deactivation was shown to occur as a result of electrode contamination by heavy metal such as Fe and Zn [361], or trace organic impurities coming from electrolytes or water solutions, as well as contaminations due to some intermediate products formed during the CO_2R [356]. Such a phenomenon has been shown to result in a quick decay of FE of formation of CH_4 and C_2H_4 on Cu from 65 % at 20 min to 0% within 2 h [362]. Preelectrolysis, among others, has been suggested as a procedure for effective purification of electrolyte solutions to mitigate electrode deactivation [361].

The use of well-engineered catalysts and GDE in general [43, 354], for instance, by attaching a catalyst to an appropriate cathode material [363] or combination of micro-and nanostructured electrodes with selected electrocatalysts [364] could also be an interesting approach to improve the stability of CO_2R reaction. Recent work by Sargent group focusing on CO_2R to ethylene in highly alkaline medium (10 M KOH) demonstrates the possibility of enhancing stability by designing a unique electrode configuration that can operate in a highly alkaline environment [354]. The employed configuration, shown in Fig. 28a, consisted of polytetrafluoroethylene (PTFE), acting as a stable, hydrophobic gas diffusion layer to prevent flooding, and graphite/carbon nanoparticles (NPs), that stabilizes the surface of Cu catalyst surface. The PTFE was introduced at the reaction interface between separate hydrophobic and conductive supports [354]. These electrode design based on graphite/carbon NPs/Cu/PTFE electrode resulted in the stable operation for up to 150 h (Fig. 28b) without any loss in ethylene selectivity (~70% FE) at current densities in the range of 75-100 mA cm^{-2} in 7 M KOH, which was a significant (300-fold) improvement compared to the classical configuration (Cu/based gas layer). In practice, a careful design of the

reactor is highly essential for the operability of CO_2R under highly alkaline conditions as the neutralization of the electrolyte by CO_2 could lead to regeneration of the KOH which adds extra cost for downstream product separation. Moreover, the chemical transformation of the catalyst for multiple functionalities can also ben used as a strategy to design stable material. Examples are the modification of Ag nanoparticles with an aluminum-based metal organic framework [365] and N-heterocycliccarbenes (NHC) [366] to enhance the morphological stability of the catalyst under CO_2R conditions.

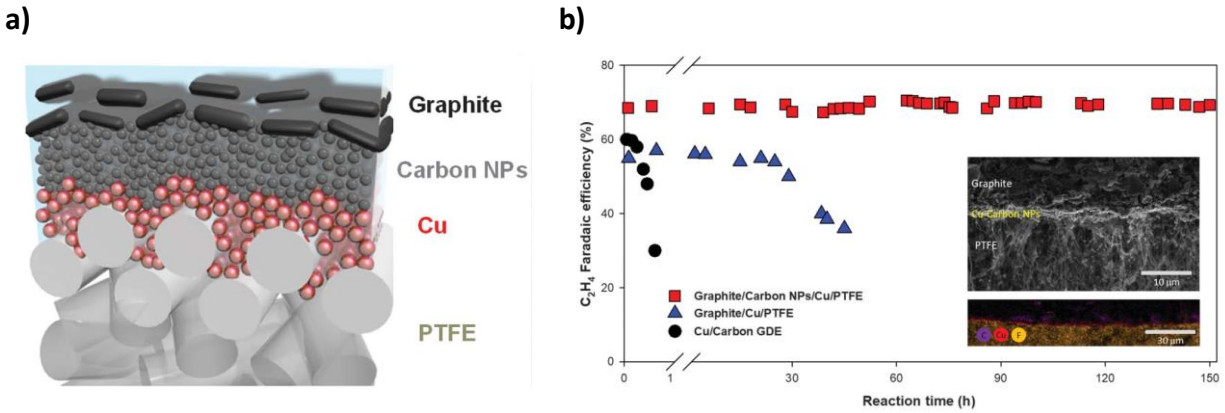

Figure 28. a) Illustration of graphite/carbon NPs/Cu/PTFE-based GDE; b) Stability tests for the different GDEs employed for CO_2R to ethylene (Electrolyte: 7 M KOH, applied voltage: -0.55 V versus the RHE); Insets show the cross-section SEM and energy-dispersive x-ray spectroscopy mapping of the sample after operation of the COR cells for 150 [354].

Membranes could also play a role in determining the stability of CO_2R cells [62, 137, 141, 367]. Although efforts have been undertaken majorly to improve the transport properties of the membranes, the search for membranes based on stable backbones and functionalities has been a point of interest. As discussed in section 4.4.2, one of the notable discovery is the work by Dioxide Materials reporting new AEMs, now available under the commercial name `Sustainion®,´ which has shown a stable CO_2R operation for up to1000's of hours under specific operating conditions [137, 141, 367]. It should be noted that the operating condition and hence the transport properties and stabilities are interrelated. For instance, for operations in anion buffering solutions like $KHCO_3$, the membranes could be damaged due to the precipitation of electrolyte as a result of the accumulation of buffering ions and co-ions in the membrane, which might also damage the GDE

itself. Configuration based on BPMs which allows keeping a pH balance has also been shown as a promising route towards stable CO_2 operations [62].

However, further investigation is required for a better understanding of the degradation of the catalytic layer as well as the membrane in CO_2 electrolyzers. Preliminary techno-economic assessments show that further effort is required to demonstrate stable long-term operations of > 420,000 h at a current density of up to >200 mA cm^{-2} to implement an economically viable electrochemical CO_2 conversion systems [21, 368, 369]. Overall, tuning the type and compositions of the whole MEA, from catalytic and ionomer composition in the GDE to the structure and functionalities of membrane materials, can be the key strategy to enhance the stability of CO_2R cells.

Table 5. CO_2 electrolyzers based on the different system designs: the dependence of cell performance on type of membrane (a: AEM), b: CEM, c: BPM) and electrocatalysts under conditions of varying electrolyte phases (liquid and gaseous electrolytes).

a) AEM

Cell design	System components					Desired product	Cell voltage or cathode potential vs RHE[b] (V)	FE[e] (%)	*J* (mA cm^{-2})	Ref
		Electrodes/catalysts		Electrolyte						
	Membranes	Cathodes	Anode	Anolyte	Catholyte					
FL-C[a]	Composite PAA with PVA/GA/KOH	CP/Cu_2O	Pt/C	Deionized water	CO_2 (g)	CH_4	2 [d]	10.38	4.1	[117]
FL-C	Sustainion X37-50	Porous Ag membranes	CP/IrO_2	0.1 M $KHCO_3$	CO_2 (g)	CO	3.3 [d]	>85	200	[142]
FL-C	Fumasep FAA-3-PK-130	Ag/Cu bimettalic	Pt wire	1 M KOH	1 M KOH	C_2H_4	-0.67	41	250	[144]
FL-C	Sustainion X37-50	Sn	IrO_2	10 mM $KHCO_3$	HM CO_2 (g)	$HCOO^-$	2.89 [d]	99.2	100	[139]
FL-C	Sustainion X37-50	Pt/Ti alloy	Co phthalocyanine	1 M KOH	1 M KOH	CO	-0.92	95	165	[147]
FL-C	Sustainion X24	Ag	IrO_2	10 mM $KHCO_3$	HM[f] CO_2 (g)	CO	3 [d]	98	200	[141]
FL-C	PSMIM AEM	2D-Bi	IrO_2/C	0.5 M H_2SO_4	HM CO_2 (g)	HCOOH	3.21 [d]	>90	>30	[370]

Table 5. Cont´d

FL-C	Fumasep AA30	Au black	IrO_2-TiO_2	pure H_2	50/50 vol.% CO_2/Ar (g)	CO	~0.125	~12	-50	[150]
FL-C	AMI-7001	Cu_2O/C	Pt/C	DI H_2O	CO_2 (g)	CH_4	2.5 [d]	32	5.4	[330]
FL-C	AMI-7001S	In-Pb/C	Pt/C	DI H_2O	1 M $NaHCO_3$	$HCOO^-$	>2.5 [d]	80	40	[130]
FL-C	Sustainion X37-50	Sn/PTFE	IrO_2/PTFE	DI H_2O	CO_2 (g)	HCOOH	3.5 [d]	94	140	[367]
FL-C	Sustainion PSMIM	Ag	IrO_2	Open air	HM CO_2 (g)	CO	3 [d]	95	>100	[137]

b) CEM

Cell design	Membranes	System components: Electrodes/catalysts: Cathodes	Anode	Electrolyte: Anolyte	Catholyte	Desired product	Cell voltage or cathode potential vs RHE[b] (V)	FE (%)	*J* (mA cm^{-2})	Ref
H-C[c]	Nafion N115	Au	Pt mesh	0.25 M KCl + 0.25 M $KHCO_3$	0.25 M KCl + 0.25 M $KHCO_3$	CO	-0.7	82	-	[119]
H-C	Nafion 117	Au	Pt	0.5 M $KHCO_3$	0.5 M $KHCO_3$	CO	-0.79	>90	16	[120]
FL-C	Nafion 117	HKUST-1	Pt	0.5 M $KHCO_3$	0.5 M $KHCO_3$	CH_3OH	-0.78	54.8	~ -30	[117]
H-C	Nafion 117	SnO_2	Pt foil	0.5 M $KHCO_3$	0.5 M $KHCO_3$	$HCOO^-$	-0.59	~ 62	-	[118]
FL-C	Nafion 117	Ag	Pt-Ir Alloy	DI water	0.5 M $KHCO_3$	CO	-0.5	82	20	[124]
H-C	Nafion 117	Cu	Pt	0.5 M $KHCO_3$	0.5 M $KHCO_3$	HCOOH	0.31	~60	-	[109]
H-C	Nafion 117	Fe (II)-Ti	Pt	0.5 M $KHCO_3$	0.5 M $KHCO_3$	CH_3COOH	-0.24	~48	-	[109]
H-C	Nafion 117	Fe (II)-Ti	Pt	0.5 M $KHCO_3$	0.5 M $KHCO_3$	CO	0.21	~30	-	[109]
FL-C	Nafion 117	HKUST-1	Pt	0.5 M $KHCO_3$	0.5 M $KHCO_3$	C_2H_5OH	-0.55	31.4	-	[117]
FL-C	Nafion 117	Sn	DSA-O_2	1 M KOH	0.45 M $KHCO_3$ + 0.5 M KCl	$HCOO^-$	-1.39	68.8	90	[122]

Table 5. Cont´d

FL-C	Nafion 115	In/Pb	Pt	1 M NaOH	1 M $NaHCO_3$	$HCOO^-$	2 [d]	80	40	[130]
FL-C	Nafion 212	Sn	Pt/C	1 M KOH	0.1 M $KHCO_3$	$HCOO^-$	-1.7	90	-9	[112]
H-C	Nafion 117	PANI/Cu_2O	Pt	0.1 M TBAP/CH_3OH	0.1 M TBAP/CH_3OH	CH_3COOH	0.35	63	~ 0.05	[123]
H-C	Nafion 211	Sn	Pt	0.1 M $KHCO_3$	0.1 M $KHCO_3$	$HCOO^-$	-0.75	91	15	[115]
H-C	Nafion N117	Nano Dendritic Cu	Pt sheet	0.1 M $KHCO_3$	0.1 M KBr	C_2H_4	-1.04	57	170	[116]
H-C	Nafion 117	Au	Pt	0.5 M $KHCO_3$	0.5 M $KHCO_3$	CO	-0.59	78	-0.8	[114]
FL-C	Fumasep FKB-PK	Sn	Ir-MMO	0.5 M H_2SO_4	1 M $KHCO_3$	$HCOO^-$	3.5 [d]	90	~30	[113]
H-C	Nafion 117	SnO_2	Pt foil	0.5 M $KHCO_3$	0.5 M $KHCO_3$	$HCOO^-$	-1.29	62	12.5	[121]
FL-C	Nafion 115	Ag	Ir-DSA	0.5 M K_2SO_4 + 1.0 M $KHCO_3$	0.5 M K_2SO_4	CO	3.25 [d]	90	225	[135]

c) BPM										
Cell design	System components					Desired product	Cell voltage or cathode potential vs RHE[b] (V)	FE (%)	*J* (mA cm^{-2})	Ref
	Membranes	Electrodes/catalysts		Electrolyte						
		Cathodes	Anode	Anolyte	Catholyte					
FL-C	Fumasep FBM	Ag	Ni foam	1 M KOH	1 M K_2CO_3	CO	2.2 [d]	28	100	[151]
FL-C	Fumatech FBM	Au black	IrO_2-TiO_2	Pure H_2	50/50 vol.% CO_2/Ar (g)	CO	~0.125	~13.5	-50	[150]
FL-C	Fumatech FBM	Ag	Ni foam	1 M NaOH	HD CO_2	CO	3 [d]	67	100	[62]
FL-C	Fumatech FBM	Ag	$NiFeO_x$	1 M KOH	0.5 M $KHCO_3$	CO	-0.4	50	30	[63]
FL-C	Fumasep FBM-PK	Sn	Ir-MMO	1 M KOH	0.5 M $KHCO_3$	$HCOO^-$	3.5[d]	90	~30	[113]
H-C	Fumasep FBM	Pd/C	Tandem GaAs/InGaP/TiO_2/Ni	1.0 M KOH	2.8 M $KHCO_3$	$HCOO^-$	-0.077	~100	8.5	[149]
FL-C	Fumasep FBM	Ag	NiFe	1 M NaOH	0.1 M $KHCO_3$	CO	−1.1	~78%	-	[148]

[a] Flow cell ; [b] Cathode potentials reported with different references were converted to potentials versus reversible hydrogen electrode (RHE) at pH =7 using the following equations: $E_{RHE} = 0.197 + E_{Ag/AgCl} + 0.059$ pH, $E_{RHE} = 0.241 + E_{SCE} + 0.059$ pH, $E_{RHE} = E_{SHE} + 0.059$ pH; [c] H-cell ; [d] Cell voltage; [e]The FE values are for the products indicated; [f]HM: Humidified.

5. Computational approaches in CO_2 electrolysis

Early transition-metal-centered complexes have been reported to show catalytic activity for CO_2R reactions. In this regard, low-valent early transition metals are highly reactive due to their strong tendency towards oxidation to more stable high-valent states [371]. Such strongly reducing complexes for productive reactivity are potentially powerful for the activation of CO_2. Besides this, early transition metals are highly reactive and earth-abundant [371, 372]. This has made them to be excellent candidates for the catalytic transformation of CO_2. However, the limited energy efficiency, uncontrollable selectivity of catalysts, low stability at different conditions, and uncertain reaction mechanisms remain to be major challenges [373-375].

Computational investigation of catalytic CO_2R into energy-rich products has attracted much attention [376-389]. Most importantly, the understanding of the challenging catalytic reaction mechanisms can be made easier and safer by using synergistic experimental and computational approaches. Moreover, the design of metal-free and metal-containing catalysts can be facilitated by accurate computational simulations [385, 390-392]. The catalytic activity is determined from the binding energies of the reaction intermediates bound to the catalyst active site in their lowest energy conformations [386, 390, 393, 394]. Reaction energy barriers can be determined from the calculations performed on the reactants, products and transition state geometries. Analysis of the spontaneity of the overall catalytic reactions can be determined from the change in free energies obtained from the frequency calculations performed for the different states [380, 383, 386-388, 395-397]. In many of these aspects, density functional theory (DFT) has been playing a vital role among the computational approaches [379, 380, 385-387, 391, 392, 394, 395, 398, 399]. Hence, this section of the review is aimed to analyze the contributions of computational approaches in alleviating the challenges of CO_2 activation and its electrocatalytic reduction reactions. Namely, the computational aspects of the design and modification of catalysts and the corresponding reaction mechanisms are highlighted.

5.1. Computational design and modification of catalysts

DFT calculations have been used to study the activity and selectivity of catalysts used for eCO_2RR. This helps to improve the reduction process by either modifying the ligands or changing the metal centres. For instance, Rawat *et al* [376] used DFT (UB3LYP/6-31G** for the light atoms and LanL2DZ for Mn) to study the role of bipyridine substituents on eCO_2RR by Mn(I) complexes

in which the electron-donating (^{t}Bu) groups attached to the main ligand showed minimum barrier (9.8 kcal/mol) compared to the electron-withdrawing (CN) substituent [376]. DFT calculations also showed that iron is an inefficient CO_2 electroreduction catalyst, despite being active for thermal CO/CO_2R catalysis [382]. A DFT analysis of low-coverage reaction intermediate energies for the production of CH_4 and CH_3OH from CO_2 also suggests that iron could be more active than copper, which is a good metallic catalyst with good selectivity towards hydrocarbon formation [382].

Martin Head-Gordon and co-workers [400] used DFT calculations (using the revised PBE functional, RPBE) for screening 28 single-atom alloys with isolated single atoms, M (M = Pd, Cu, Ni, Co, Ir, Rh and Pt), embedded into the (100) and (111) surfaces of Au or Ag for CO_2R (Fig. 29a and 29b). The calculations indicated that the feedstock CO_2 is first reduced to *CO by Au or Ag catalysts and is subsequently captured and further reduced to single carbon products by the metals (Fig. 28c). From the reaction mechanism studies, the authors found that Rh@Au(100) and Rh@Ag(100) reduce CO_2 to methane, although the reduction occurs through different pathways.

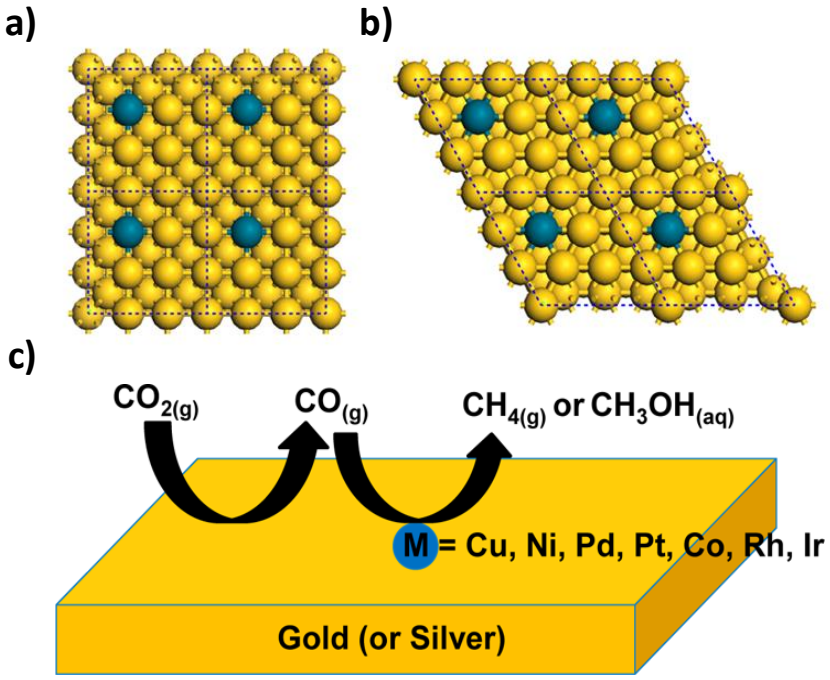

Fig. 29. (Top) Surface models for simulation of the single-atom alloys: (a) M@Au(111), M@Ag(111), and (b) M@Au(100), M@Ag(100). c) Schematic illustration of the proposed one-pot tandem catalytic reaction which is composed primarily of gold or silver (colored gold), alloyed

with small amounts of M (M = Cu, Ni, Pd, Pt, Co, Rh, and Ir). The feedstock CO_2 is first reduced to *CO by Au or Ag, and is subsequently captured and further reduced to C1 products by M. Reprinted with permission from [400]. Copyright 2014, American Chemical Society.

The combination of early and late transition metals may be the key to develop stable and active systems for CO_2R. For instance, the DFT calculations reported by Isegawa and Sharma [387] suggest the importance of catalytic systems composed of two Lewis acids (Mg^{2+}) and one transition metal (Mn) for a highly efficient CO_2R process. On the other hand, due to their low cost, copper-based nanoparticles are considered to be promising candidates for the catalytic hydrogenation of CO_2. In this regard, the study by Dean *et al* [385] demonstrated that computational studies based on DFT calculations can be efficiently used to identify Cu-based bimetallic nanoparticles that are able to adsorb and activate CO_2.

Product selectivity is another challenge in the field. Here, the contribution from DFT takes the lion-share in screening, modifying and identifying a specific type of catalyst for a specific product. A study performed using a combined density functional and rate theory by Hussain *et al.* [383] demonstrated the ability of the calculations in solving challenging problems in eCO_2R reactions. The authors used the calculated results to explain the significant yield of hydrocarbons and alcohols by copper electrodes, demonstrating that such calculations have the potential to develop criteria for identifying new and improved catalysts for eCO_2RR [383, 385, 387, 390]. Moreover, Yuhan Mei [401] used DFT calculations to study the catalytic activity of M-N_4-graphene (Fig. 30a) and M-N_4-carbon nanotube (Fig. 30b) catalytic model systems. The author showed that HER is preferred over the *CO formation pathway of CO_2R reaction for M = Fe, Co, Ni and Mn, whereas, CO_2R reaction pathway to form HCOOH is preferred over the HER pathway for the Ni-N_4-graphene catalyst.

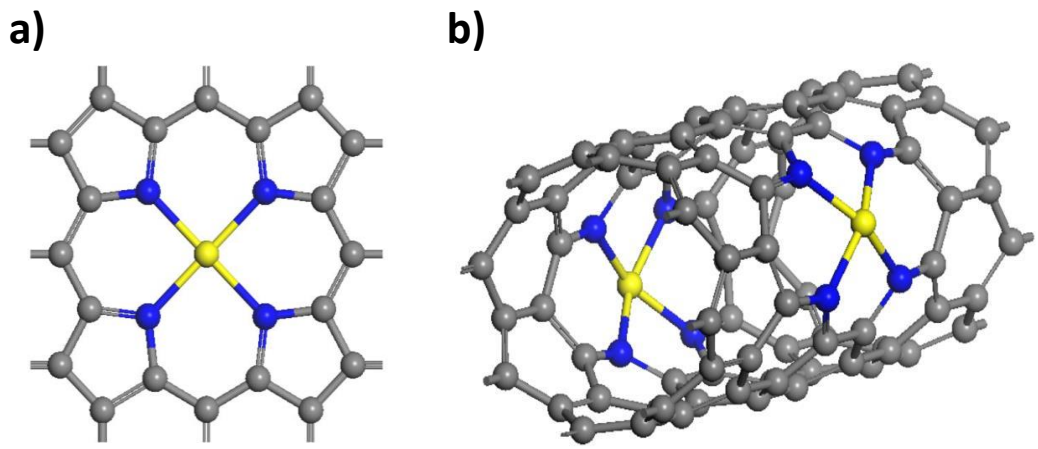

Fig. 30. (a) Part of the metal-nitrogen-doped graphene, and (b) part of the metal-nitrogen-doped carbon nanotube catalysts. The metal centres are yellow, nitrogen atoms are blue, and carbon atoms are in grey. Reprinted with permission from [401, 402]. Copyright 2018, State University of New York.

Because of the ease of mixing with the reactants, homogeneous catalysts are preferred for CO_2R compared to heterogeneous catalysts, but it is difficult to separate the products and recycle the catalysts. The key factor for the heterogeneous catalytic mechanism is that the interaction between CO_2 and the metal surface is mainly determined by the d-band levels of the catalyst [403]. Computationally, it is possible to modify the catalyst by adjusting the location of the d-band centres as well as doping the electrodes [404]. Not only this, the bonding strength of the adsorbed intermediates and the energy barriers of the rate-determining steps would be calculated and optimized to enhance the catalytic performance, selectivity as well as the conversion rates [376, 384, 403, 405].

5.2. Computational study of the reaction mechanisms

Experimental identification of low cost, stable, selective and highly active catalysts based on the most feasible reaction mechanisms is challenging; However, such efforts can be minimized and enhanced by following synergistic experimental and computational approaches. A computational reaction mechanism study performed on the M-N_4-graphene and carbon nanotube catalytic model systems (Fig. 29) by Yuhan Mei [401] showed that all $\Delta G_{(*COOH)}$ energies are larger than $\Delta G_{(*H)}$ for M = Fe, Co, Ni and Mn, demonstrating that HER is preferred over the CO formation pathway of CO_2R reaction. On the other hand, however, for the Ni-N_4-graphene catalyst,

$\Delta G_{(*COOH)}$ is 1.45 eV, which is lower than $\Delta G_{(H)}$ (1.82 eV) suggesting that CO_2R reaction pathway to form HCOOH is preferred over the HER pathway for the Ni-N_4-Graphene catalyst. DFT calculations performed by Bernstein *et al.* [382] on the reaction mechanism of CO_2R reactions catalysed by iron and copper catalysts also suggested that Iron catalysts show considerable selectivity for the formation of hydrocarbons than Copper ones. The authors demonstrated that the adsorption energy of CO_2 on the surface (Fig. 31a) was determined to be -0.25 eV, indicating a stable adsorbate surface complex of *COOH (Fig. 31b) and *CO (Fig. 31c), which are formed by protonation of an oxygen atom of CO_2.

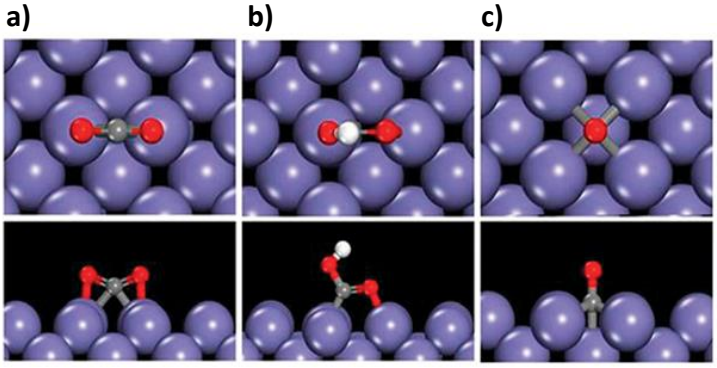

Fig. 31. Top and side view of optimized reduction intermediates (a) adsorption of CO_2, (b) formation of *COOH and (c) adsorbed *CO. Atom species are: Fe (purple), C (grey), O (red) and H (white). Reprinted with permission from [382]. Copyright 2014, Royal Society of Chemistry.

Density functional theory calculations also indicated the reduction of CO_2 to C_2 products on copper electrodes [406-408]. The computed results demonstrated that C–C bond formation during CO_2RR proceeds via the formation of a *COCO dimer at low overpotentials, whereas, C–C coupling occurs via the reaction of *CO with *CHO at high overpotentials [406-411]. For instance, Goodpaster *et al*. [408] used periodic Kohn–Sham DFT (using the RPBE functional) for the identification of possible pathways for C–C bond formation during eCO_2RR on Cu(100) using a model that includes the effects of the electrochemical potential, electrolyte and solvent. The authors showed that C–C bond formation occurs through a *CO dimer at low-applied potential, (Fig. 32a), whereas a large activation barrier blocks this pathway at high applied potentials; and hence, C–C bond is formed by the reaction of adsorbed *CHO and *CO (Fig. 32b). In another study, Garza *et al*. [406] investigated CO_2RR on Cu(100) and Cu(111) facets using DFT

calculations (using the RPBE functional). The calculated results showed that the free energy for the *CO dimerization reaction on Cu(100) was computed to be close to zero, and further hydrogenation to *COCHO is thermodynamically favorable. On the other hand, the *COCO dimer is highly unstable on Cu(111) surface, while reduction of *CO to *CHO has a ΔG reaction of 0.60 eV, implying the formation of *COCHO species from the reaction between *CHO and *CO.

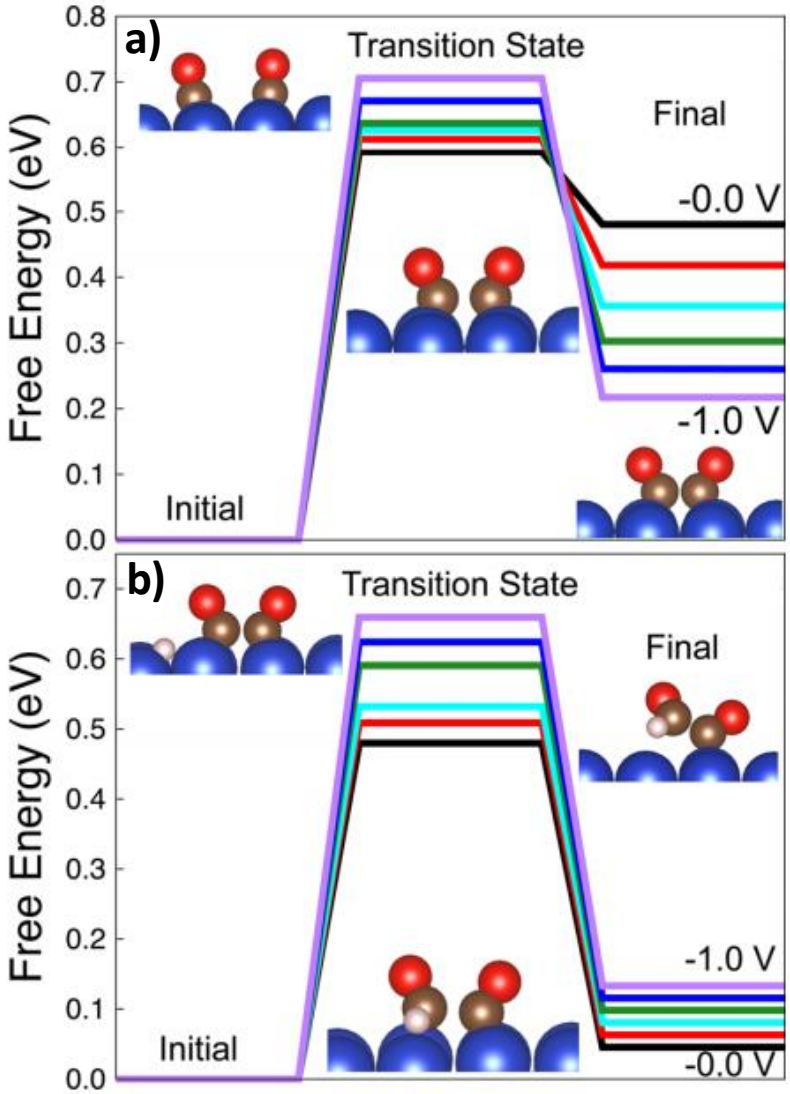

Fig. 32. Relative free energy of the initial configuration, transition state, and final configuration for (a) the formation of *CO dimer and (b) the formation of adsorbed *OCCHO as predicted from the authors' electrochemical model for -1.0 V (purple), -0.8 V (blue), -0.6 V (green), -0.4 V (cyan),

-0.2 V (red), and 0.0 V (black). All potentials are presented versus RHE at pH 7. Reprinted with permission from [408]. Copyright 2016, American Chemical Society.

5.3. Challenges related to the computational approaches

Besides the very promising progress and opportunities related to the contribution of computational methods, especially the DFT approaches in eCO_2RR [379, 380, 385-387, 391, 392, 394, 395, 398, 399], there are still related challenges. Complicated electrochemical systems such as surface structure of the electrodes, charge distribution at the solid-liquid interface, and solvation effect of the electrolytes make it difficult to accurately consider all the aspects in the calculations. Since CO_2 is typically a weakly adsorbed molecule, the treatment of the weak long-range interactions may cause non-negligible errors in the calculated results. Most of the existing computational methods are still not perfect to consider the weak interactions efficiently and accurately, hence one needs to take care of designing and choosing the computational methods. In this aspect, the most commonly used approach to treat such weak interactions is to include empirical dispersion corrections [412, 413]. The other challenge is the treatment of electrode-electrolyte interfaces. There are possibilities to treat this by using either explicit or implicit solvent models. The former is too expensive to consider the dynamic explicit solvation environment with numerous solvent molecules, whereas the implicit solvent model can lose hydrogen bonds and other important interactions in which the solvent molecules participate. The other important challenge to be carefully considered during the calculations is the treatment of relativistic effects [414]. The catalysts mainly involve transition metals, where relativistic effects can cause considerable errors on the calculated results. Such effects, for instance, have the potential to dictate the reaction mechanisms [415]. Therefore, the use of relativistic Hamiltonian is required to consider the relativistic corrections due to both the scalar (spin-free) and spin-orbit relativistic effects. When the use of relativistic Hamiltonian is a challenge, the use of relativistic effective core potentials, designed mainly to capture scalar relativistic effects, for the metal atoms is one of the approaches to partially treat the relativistic effects [414, 416].

6. Economic and commercial aspects

Despite being under intensive investigation for several years now, the eCO_2RR is still confined to laboratory-based investigations and only in recent years, some pilot units are being installed and operated. Part of the reason for this seeming gap between the lab and a successful

commercial process is the low current densities (leading to high capital expenditure (CPAEX)) and non-selective nature of the conversion process thus leading to reduced Faradaic efficiencies (resulting in high operational expenditure (OPEX)). In recent years, the research on this topic has expanded globally partly in response to the increasing awareness about global climate change and political willingness to respond to it by finding technological breakthroughs. This has led to significant improvement in the eCO_2RR process and performance. The most recent breakthrough, in this case, was reported recently by the Sargent group, who described the CO_2 electrolysis on copper in 7 M potassium hydroxide electrolyte to ethylene at a partial current density of 1.3 A/cm^2 at 45% cathodic energy efficiency [417]. Such high current densities lead to better economics especially in large scale devices (>100 cm² active area) even when the real operational current densities are lower and in the order of 200 mA/cm^2, thus bringing CO_2 electrolysis one step closer towards commercialization [42].

In 2016, a detailed techno-economic analysis of electrochemical CO_2 conversion was carried out by the group of Prof. Paul Kenis [418]. According to them, CO and HCOOH are the most profitable products of CO_2R reaction at then electricity prices (6-12 cents per kWh). Of course, this was subject to certain conditions like benchmarks in catalyst and electrode durability (thousands of hours) being met. Later on, in 2019, revised figures for formic acid production from CO_2R reaction were proposed by De Luna et al. [419]. It was suggested that for an electricity cost of 4 cents/kWh, Faradaic efficiency of 90% and the energy conversion efficiency of 70%, electrocatalysis can become cost-competitive with fossil fuel–derived sources and more economical than biocatalytic processes. Of course, all of these processes still need a stable operation for a significant amount of time. A proposal has been made that CO_2R reaction systems would need to match lifetime ranges exhibited by PEM electrolyzers (beyond 20000 h) [420]. However, this economical feasible life time will also be determined by the 1) the value final product, 2) the evolution of the equipment's productivity and 3) the cost of replacement parts and outage time to bring the unit back into pristine operational mode .. As such, for a high-value product, shorter minimum lifetimes might be acceptable as well, since in that case, the early replacement cost of electrolyzer components will be offset by the profit margins. Finally, this operational period is inherently linked to the current density and faradaic efficiency towards the desired product. For a shorter operational lifetime,higher productivities (current densities and

selectivities) are needed while longer operational periods allow for a lower partial current density of the desired product for economically feasible operation [420].

On the other hand, the technologies related to CO_2 capture, including direct air capture (DAC) seem to be more developed and closer to the market [421]. There are several companies commercially operating in this domain such as CO_2 Solutions (Canada; founded 1997), Carbon Engineering (Canada; founded 2009), Global Thermostat (USA; founded 2010), Climeworks (Switzerland; founded 2009), Infinitree (USA; founded 2014), Skytree (Netherlands; founded 2010) [422]. Eventually, the CO_2 and renewable energy-based industrial systems are being envisaged taking into account the CO_2 air capture as well. A case study for CO_2 electrolyzers producing 10,000 tons of methanol/day was recently investigated by [423]. One of the key findings of the study was that a six order-of-magnitude gap exists between current operational catalyst areas and real industry-sized applications, which in fact matches with the limited number of industrial level pilots.

Several of the pilot studies and projects currently being undertaken were recently reported by Gutiérrez Sánchez *et al*. [33], who mentioned that most of the eCO_2RR demonstrators are currently at pre-commercial stage and most of these pilots are the outcome of publicly funded research projects. There certainly seems to be commercial interest in the technology, which is evident by the participation of large companies (such as Covestro, Solvay, Siemens, Arkema, Evonik, ArcelorMittal, Audi etc.) in such projects. Beyond eCO_2RR, there are several companies which are engaged in the direct use of CO_2 (such as Praxair, DyeCoo Textile Systems and Great Point Energy) or its conversion to value-added products (eg. Novemer, Newlight, Skyonic Corporation, CO_2 Solutions' Inc. technology, Algenol and Joule). These were described by ElMekawy *et al*. [424] who also described a preliminary techno-economic analysis of a CO_2 electrorefinery for three main CO_2 conversion products namely, formic acid, acetic acid and oxalic acid by comparing Net Present Value of the investment for 20 years at 10% nominal discount rate. It was observed that in case of formic and acetic acid, the low conversion rates of 10 and 25 g/m² h results in insufficient revenue streams to compensate the CAPEX and OPEX while oxalic acid had the largest profit margin, the positive NPV20 values were obtained for a long electrode lifetime.

In any of the CO_2 conversion processes including eCO_2RR, the reaction conditions need to be carefully selected in order to ensure that the reaction should not become a net CO_2 producer instead of overall consuming CO_2 and thus will not contribute to avoiding CO_2 [425].

7. Conclusions and outlook

The electrochemical CO_2R represents a great prospect to address the current energy and climate issues by closing the carbon cycle. The electrochemical CO_2RR reaction allows for direct, one-step production of useful chemical feedstocks or fuels from CO_2, driven by the renewable electricity, which is stored as chemical energy in the form of liquid or gaseous fuels and used for different purposes including transport, mobility households and various industrial processes. Impressive research advances have been demonstrated by the scientific and engineering community, particularly in terms of developing new electrocatalysts for a highly efficient CO_2 conversion. However, further developments are still required both from material and process design perspectives to reach the performance targets for the implementation of CO_2 electrolyzers on a commercial scale. The eCO_2RR activities are highly influenced by the competing HER, which creates a trade-off between the activity and selectivity for most of the catalysts claimed to be promising for CO_2 electrolysis.

Flow cell reactors for CO_2 electrolysis generally represent a better alternative for the practical implementation of the fundamental lab discoveries into practice. The key challenges for low-cost CO_2R that can be addressed by these factors together with the catalyst materials are reducing the required cell voltages, improving selectivity, and lowering product separation costs. CO_2 electrolyzers with better designs are required for a high performance CO_2 electro-reduction. The large majority of the research works on CO_2R are focused on the catalyst and catalytic activities with only a few studies that have been focused on cell design as well as different operational modes like batch or continuous flow modes. Careful optimization of these parameters is required for better stability and energy efficiency of the CO_2 electrolytic cells. In particular, a broad prospect is forseen to enhance the performance of the gas-phase CO_2 through membrane and catalyst development, which represents the most promising approach to reduce the mass-transfer limitations observed for the liquid-phase CO_2 electrolysis. Membranes-based gas-phase CO_2 electrolysis can also be engineered to reduce the distance between the electrodes (forming zero-gap arrangement), which decreases the internal cell resistance, thereby increasing the energy efficiency of the cell. In the case of liquid-phase water electrolyzers, the designs of the electrode flow field plate with varying

path lengths, cell numbers and channel thicknesses highly influence the hydrodynamics across the MEA and hence the performance of the electrolysis. Thus, systematic optimization of these geometric parameters supported by the computational fluid dynamics plays a key role in designing highly efficient cell configurations. In addition to CO_2 solubility issues, the other limitations of performing CO_2R in a liquid phase are the complex CO_2/carbonate/bicarbonate buffering equilibria and the fluctuation of the local pH and hence the difficulty in optimizing the chemical properties of the catalyst-electrolyte interface. Overall, cell design optimization supported by computational modeling also enables a better understanding of the interactive effect of process parameters such as pH, temperature, pressure and gas/liquid flow rates on the performance of CO_2 electrolyzers.

Elucidation of the structure-property relationship of membranes optimally designed to function under the CO_2R conditions is also very important for tuning the CO_2 conversion reaction to the desired product. For this purpose, the concept used in designing the polymer electrolyte membranes that are used for the other relevant technologies such as PEM fuel cells and electrolyzers can be adopted for CO_2 electrolyzers to reach the performance metrics required for commercial implementations. The key parameters required for optimal performance of the monopolar membranes are stability, good swelling property, ionic conductivity, and selectivity. In the case of bipolar membranes, enhanced selectivity and swelling properties are crucial for efficient water splitting at its interface which also reduces the membrane voltage, thereby increasing the energy efficiency of the cell. Moreover, the success in the development and use of optimal polymer electrolytes membranes enables the operability of CO_2 electrolyzers over a broad range of operating parameters such as pH and pressures.

Catalyst discovery is one of the key steps determining the commercial success of electrochemical CO_2R technologies. To mitigate the current issue associated with the availability of suitable catalysts, the following major challenges needed to be addressed: i) Catalytically active centers of the CO_2 or CO activation need to be identified by, for example, computational studies and reveal the least energy reaction pathway. DFT guided synthesis method is required to generate the defects of the catalysts that can create more CO_2 or CO activation sites and subsequently lowering the free energy of the reaction; ii) developing an in situ/operando spectroscopies characterization could be a useful tool to identify the catalytically active sites for eCO_2R reactions, indicating a new roadmap for development of the efficient electrocatalyst; iii) further look into the electrolyte, which affects the activity and selectivity of the eCO_2R reaction, allows for a controlled

way of proton supply which might prevent the competing HER and enhances the eCO_2R selectivity; iv) advancing new catalyst synthesis routes, for example, by using covalent organic framework (COF) and Mxenes, could be a good prospect for developing next-generation electrocatalysts for electrochemical CO_2R. Along with the catalyst synthesis, the stability of the catalysts under CO_2R conditions is very crucial which remains a less investigated topic. Thus, further study on the degradation mechanisms and deactivation of existing catalysts is essential for a better understanding of the stability issues in CO_2R systems.

Fundamental research focused on the processes occurring on GDEs and at the GDEs-electrolyte interfaces along with the optimal catalyst and cell design approaches is required for a better understanding of factors influencing the selectivity of the CO_2RRs and energy efficiency of the cells. In line with this, new achievements in the development of ion-exchange membranes can be adopted to the design and development of ionomers that can be used along with GDE to create interconnected pathways for ionic conduction. The chemical and physical properties of ionomer properties highly influence CO_2R activity and selectivity. Optimal tuning of the structural property of the ionomer not only facilitates the charge species transport along the three-dimensional GDEs but also allows for the effective utilization of the active sites in the reaction zone.

Despite the promising research progress on the different areas of research in CO_2R, there are still some research gaps within some areas which are given less attention so far. Some of these include the OER which is crucial for the reduction of the overall cell resistance and overpotential demands. Therefore, optimally designed oxygen evolution electrocatalysts for OER remains a topic of further investigation for better energy efficiency of the CO_2 electrolyzers. Membranes prevent the crossover of the CO_2R products preventing the passage to the OER compartment and reoxidation on the anode. However, the literature lacks detailed studies on the crossover of the different types of ion-exchange membranes under different operating conditions. Moreover, elucidation of the impact of operational parameters such as flow rates, relative humidity, temperature, and cell voltage on the conversion rates and efficiency of CO_2 electrolyzers are also among the poorly investigated topics.

Hybrid applications of CO_2 electrolyzers combined with other electrochemical energy systems can be extended beyond the use of renewable energy from intermittent renewable energy sources such as the wind and sun. Emerging membrane-based, non-intermittent energy technologies like reverse electrodialysis and pressure retarded osmosis, which can generate

electricity from mixing water solutions like seawater and river water or brine exhausts from desalination industries can drive CO_2 electrolyzers. Reverse electrodialysis can also capture energy from waste resources, e.g. brine discharge from desalination technologies and/or SO_4^{-2}-rich industrial waste streams [426]. Therefore, there is a huge potential for the implementation of hybrid electrolyzer systems for an indirect, un-interrupted conversion of the electrochemical potential of waste resources including CO_2 into valuable chemical and fuel production, in line with the logic of process intensification and the circular economy. Moreover, the anodic reactions in CO_2 electrolyzers can be manipulated by using a low-overpotential oxidation reaction involving organic pollutants to design a process for the simultaneous CO_2R and wastewater treatment [25, 427].

Acknowledgments

The financial support of the European Union's Horizon 2020 research and innovation program under the Marie Sklodowska-Curie grant agreement no. 713683 (COFUND fellows DTU) is gratefully acknowledged. This work was also supported by ECOEthylene project from the Innovation Fund Denmark (grant# 8057-00018B) and by the European Union's Horizon 2020 research and innovation program under the grant agreement no. 761093, project LOTER.CO2M.

References

[1] NOAA. Earth's CO2 home page. Accessed on January 2, 2020.
[2] Agency IE. Energy Technology Perspectives 2014. Paris Cedex, France2014.
[3] Birdja YY. Electrocatalytic CO2 reduction toward liquid fuels: on heterogeneous electrocatalysts and heterogenized molecular catalysts, PhD thesis, 2018.
[4] Aresta M, Dibenedetto A, Angelini A. Catalysis for the Valorization of Exhaust Carbon: from CO2 to Chemicals, Materials, and Fuels. Technological Use of CO2. Chemical Reviews. 2014;114:1709-42.
[5] Lim XJNN. How to make the most of carbon dioxide. 2015;526:628.
[6] Rotstein BH, Liang SH, Holland JP, Collier TL, Hooker JM, Wilson AA, et al. 11 CO 2 fixation: a renaissance in PET radiochemistry. Chemical Communications. 2013;49:5621-9.
[7] Mikkelsen M, Jørgensen M, Krebs FC. The teraton challenge. A review of fixation and transformation of carbon dioxide. Energy & Environmental Science. 2010;3:43-81.
[8] Maidan R, Willner I. Photoreduction of carbon dioxide to methane in aqueous solutions using visible light. Journal of the American Chemical Society. 1986;108:8100-1.
[9] Olah GA, Goeppert A, Prakash GKS. Chemical Recycling of Carbon Dioxide to Methanol and Dimethyl Ether: From Greenhouse Gas to Renewable, Environmentally Carbon Neutral Fuels and Synthetic Hydrocarbons. The Journal of Organic Chemistry. 2009;74:487-98.
[10] Benson EE, Kubiak CP, Sathrum AJ, Smieja JM. Electrocatalytic and homogeneous approaches to conversion of CO2 to liquid fuels. Chemical Society Reviews. 2009;38:89-99.

[11] Barton EE, Rampulla DM, Bocarsly ABJJotACS. Selective solar-driven reduction of CO2 to methanol using a catalyzed p-GaP based photoelectrochemical cell. Journal of the Amercan Chemical Society. 2008;130:6342-4.
[12] Yi Q, Li W, Feng J, Xie K. Carbon cycle in advanced coal chemical engineering. Chemical Society Reviews. 2015;44:5409-45.
[13] Olajire AA. Valorization of greenhouse carbon dioxide emissions into value-added products by catalytic processes. Journal of CO2 Utilization. 2013;3-4:74-92.
[14] Bushuyev OS, De Luna P, Dinh CT, Tao L, Saur G, van de Lagemaat J, et al. What Should We Make with CO2 and How Can We Make It? Joule. 2018;2:825-32.
[15] Coates GW, Moore DR. Discrete Metal-Based Catalysts for the Copolymerization of CO2 and Epoxides: Discovery, Reactivity, Optimization, and Mechanism. Angewandte Chemie. 2004;43:6618-39.
[16] Olejník R, Bílek M, Růžičková Z, Hoštálek Z, Merna J, Růžička A. Zinc complexes chelated by bifunctional ketiminate ligands: Structure, reactivity and possible applications in initiation of ROP and copolymerization of epoxides with carbon dioxide. Journal of Organometallic Chemistry. 2015;794:237-46.
[17] Aresta M, Dibenedetto A. The contribution of the utilization option to reducing the CO2 atmospheric loading: research needed to overcome existing barriers for a full exploitation of the potential of the CO2 use. Catalysis Today. 2004;98:455-62.
[18] Peterson AA, Abild-Pedersen F, Studt F, Rossmeisl J, Nørskov JK. How copper catalyzes the electroreduction of carbon dioxide into hydrocarbon fuels. Energy & Environmental Science. 2010;3:1311-5.
[19] Seh ZW, Kibsgaard J, Dickens CF, Chorkendorff I, Nørskov JK, Jaramillo TF. Combining theory and experiment in electrocatalysis: Insights into materials design. Science. 2017;355:eaad4998.
[20] Weekes DM, Salvatore DA, Reyes A, Huang A, Berlinguette CP. Electrolytic CO2 Reduction in a Flow Cell. Accounts of Chemical Research. 2018;51:910-8.
[21] Jouny M, Luc W, Jiao F. General Techno-Economic Analysis of CO2 Electrolysis Systems. Industrial & Engineering Chemistry Research. 2018;57:2165-77.
[22] Chen C, Khosrowabadi Kotyk JF, Sheehan SW. Progress toward Commercial Application of Electrochemical Carbon Dioxide Reduction. Chem. 2018;4:2571-86.
[23] Vennekoetter J-B, Sengpiel R, Wessling M. Beyond the catalyst: How electrode and reactor design determine the product spectrum during electrochemical CO2 reduction. Chemical Engineering Journal. 2019;364:89-101.
[24] Kortlever R, Shen J, Schouten KJP, Calle-Vallejo F, Koper MTM. Catalysts and Reaction Pathways for the Electrochemical Reduction of Carbon Dioxide. The Journal of Physical Chemistry Letters. 2015;6:4073-82.
[25] Endrődi B, Bencsik G, Darvas F, Jones R, Rajeshwar K, Janáky C. Continuous-flow electroreduction of carbon dioxide. Progress in Energy and Combustion Science. 2017;62:133-54.
[26] Durst J, Rudnev A, Dutta A, Fu Y, Herranz J, Kaliginedi V, et al. Electrochemical CO2 reduction–a critical view on fundamentals, materials and applications. CHIMIA International Journal for Chemistry. 2015;69:769-76.
[27] Lu Q, Jiao F. Electrochemical CO2 reduction: Electrocatalyst, reaction mechanism, and process engineering. Nano Energy. 2016;29:439-56.
[28] Kibria MG, Edwards JP, Gabardo CM, Dinh C-T, Seifitokaldani A, Sinton D, et al. Electrochemical CO2 Reduction into Chemical Feedstocks: From Mechanistic Electrocatalysis Models to System Design. Advanced Materials. 2019;31:1807166.
[29] Jhong H-RM, Ma S, Kenis PJA. Electrochemical conversion of CO2 to useful chemicals: current status, remaining challenges, and future opportunities. Current Opinion in Chemical Engineering. 2013;2:191-9.

[30] Zhang W, Hu Y, Ma L, Zhu G, Wang Y, Xue X, et al. Progress and Perspective of Electrocatalytic CO2 Reduction for Renewable Carbonaceous Fuels and Chemicals. Advanced Science. 2018;5:1700275.
[31] Zheng T, Jiang K, Wang H. Recent Advances in Electrochemical CO2-to-CO Conversion on Heterogeneous Catalysts. Advanced Materials. 2018;30:1802066.
[32] Sánchez OG, Birdja YY, Bulut M, Vaes J, Breugelmans T, Pant D. Recent advances in industrial CO2 electroreduction. Current Opinion in Green and Sustainable Chemistry. 2019;16:47-56.
[33] Bevilacqua M, Filippi J, Miller HA, Vizza F. Recent Technological Progress in CO2 Electroreduction to Fuels and Energy Carriers in Aqueous Environments. Energy Technology. 2015;3:197-210.
[34] Wang H, Sun S, Ge W, Zhao L, Hou B, Wang K, et al. Horizontal gene transfer of Fhb7 from fungus underlies Fusarium head blight resistance in wheat. 2020;368:eaba5435.
[35] Garg S, Li M, Weber AZ, Ge L, Li L, Rudolph V, et al. Advances and challenges in electrochemical CO2 reduction processes: an engineering and design perspective looking beyond new catalyst materials. Journal of Materials Chemistry A. 2020.
[36] Merino-Garcia I, Alvarez-Guerra E, Albo J, Irabien A. Electrochemical membrane reactors for the utilisation of carbon dioxide. Chemical Engineering Journal. 2016;305:104-20.
[37] Voiry D, Shin HS, Loh KP, Chhowalla M. Low-dimensional catalysts for hydrogen evolution and CO2 reduction. Nature Reviews Chemistry. 2018;2:0105.
[38] Yang W, Dastafkan K, Jia C, Zhao C. Design of Electrocatalysts and Electrochemical Cells for Carbon Dioxide Reduction Reactions. 2018;3:1700377.
[39] Zhu DD, Liu JL, Qiao SZJAm. Recent advances in inorganic heterogeneous electrocatalysts for reduction of carbon dioxide. 2016;28:3423-52.
[40] Li F, MacFarlane DR, Zhang J. Recent advances in the nanoengineering of electrocatalysts for CO2 reduction. Nanoscale. 2018;10:6235-60.
[41] Wang Y, Liu J, Wang Y, Al‐Enizi AM, Zheng GJS. Tuning of CO2 reduction selectivity on metal electrocatalysts. 2017;13:1701809.
[42] Burdyny T, Smith WA. CO2 reduction on gas-diffusion electrodes and why catalytic performance must be assessed at commercially-relevant conditions. Energy & Environmental Science. 2019;12:1442-53.
[43] Higgins D, Hahn C, Xiang C, Jaramillo TF, Weber AZ. Gas-Diffusion Electrodes for Carbon Dioxide Reduction: A New Paradigm. ACS Energy Letters. 2019;4:317-24.
[44] Weng L-C, Bell AT, Weber AZ. Towards membrane-electrode assembly systems for CO2 reduction: a modeling study. Energy & Environmental Science. 2019;12:1950-68.
[45] Schwartz M, Cook RL, Kehoe VM, MacDuff RC, Patel J, Sammells AFJJotES. Carbon Dioxide Reduction to Alcohols using Perovskite‐Type Electrocatalysts. 1993;140:614-8.
[46] Cook RL, MacDuff RC, Sammells AFJJotES. On the electrochemical reduction of carbon dioxide at in situ electrodeposited copper. 1988;135:1320-6.
[47] Cook R, Sammells AJPU. Electrochemical reduction of CO2 to CH4 and C2H4. 1990.
[48] Cook RL, MacDuff RC, Sammells AFJJoES. Efficient high rate carbon dioxide reduction to methane and ethylene at in situ electrodeposited copper electrode. 1987.
[49] Qin B, Li Y, Wang H, Yang G, Cao Y, Yu H, et al. Efficient electrochemical reduction of CO2 into CO promoted by sulfur vacancies. Nano Energy. 2019;60:43-51.
[50] Daiyan R, Lovell EC, Bedford NM, Saputera WH, Wu K-H, Lim S, et al. Modulating Activity through Defect Engineering of Tin Oxides for Electrochemical CO2 Reduction. Advanced Science. 2019;6:1900678.
[51] Luo W, Zhang J, Li M, Züttel A. Boosting CO Production in Electrocatalytic CO2 Reduction on Highly Porous Zn Catalysts. ACS Catalysis. 2019;9:3783-91.

[52] Kibria MG, Dinh C-T, Seifitokaldani A, De Luna P, Burdyny T, Quintero-Bermudez R, et al. A Surface Reconstruction Route to High Productivity and Selectivity in CO2 Electroreduction toward C2+ Hydrocarbons. Advanced Materials. 2018;30:1804867.
[53] Garg S, Li M, Rufford TE, Ge L, Rudolph V, Knibbe R, et al. Catalyst–Electrolyte Interactions in Aqueous Reline Solutions for Highly Selective Electrochemical CO2 Reduction. ChemSusChem.n/a.
[54] Ju W, Bagger A, Wang X, Tsai Y, Luo F, Möller T, et al. Unraveling Mechanistic Reaction Pathways of the Electrochemical CO2 Reduction on Fe–N–C Single-Site Catalysts. ACS Energy Letters. 2019;4:1663-71.
[55] Klingan K, Kottakkat T, Jovanov ZP, Jiang S, Pasquini C, Scholten F, et al. Reactivity Determinants in Electrodeposited Cu Foams for Electrochemical CO2 Reduction. ChemSusChem. 2018;11:3449-59.
[56] Liu S, Yang H, Huang X, Liu L, Cai W, Gao J, et al. Identifying Active Sites of Nitrogen-Doped Carbon Materials for the CO2 Reduction Reaction. Advanced Functional Materials. 2018;28:1800499.
[57] Clark EL, Bell AT. Direct Observation of the Local Reaction Environment during the Electrochemical Reduction of CO2. Journal of the American Chemical Society. 2018;140:7012-20.
[58] Li YC, Yan Z, Hitt J, Wycisk R, Pintauro PN, Mallouk TE. Bipolar Membranes Inhibit Product Crossover in CO2 Electrolysis Cells. Advanced Sustainable Systems. 2018;2:1700187.
[59] Whipple DT, Finke EC, Kenis PJ. Microfluidic reactor for the electrochemical reduction of carbon dioxide: the effect of pH. Electrochemical and Solid-State Letters. 2010;13:B109-B11.
[60] Jayashree RS, Mitchell M, Natarajan D, Markoski LJ, Kenis PJA. Microfluidic Hydrogen Fuel Cell with a Liquid Electrolyte. Langmuir. 2007;23:6871-4.
[61] Alvarez-Guerra M, Del Castillo A, Irabien A. Continuous electrochemical reduction of carbon dioxide into formate using a tin cathode: Comparison with lead cathode. Chemical Engineering Research and Design. 2014;92:692-701.
[62] Salvatore DA, Weekes DM, He J, Dettelbach KE, Li YC, Mallouk TE, et al. Electrolysis of Gaseous CO2 to CO in a Flow Cell with a Bipolar Membrane. ACS Energy Letters. 2018;3:149-54.
[63] Li YC, Zhou D, Yan Z, Gonçalves RH, Salvatore DA, Berlinguette CP, et al. Electrolysis of CO2 to Syngas in Bipolar Membrane-Based Electrochemical Cells. ACS Energy Letters. 2016;1:1149-53.
[64] Merino‐Garcia I, Albo J, Irabien A. Productivity and Selectivity of Gas‐Phase CO2 Electroreduction to Methane at Copper Nanoparticle‐Based Electrodes. Energy Technology. 2017;5:922-8.
[65] Cook RL, MacDuff RC, Sammells AF. High rate gas phase CO 2 reduction to ethylene and methane using gas diffusion electrodes. Journal of The Electrochemical Society. 1990;137:607-8.
[66] Gutiérrez-Guerra N, Moreno-López L, Serrano-Ruiz JC, Valverde JL, de Lucas-Consuegra A. Gas phase electrocatalytic conversion of CO2 to syn-fuels on Cu based catalysts-electrodes. Applied Catalysis B: Environmental. 2016;188:272-82.
[67] Pérez-Rodríguez S, Barreras F, Pastor E, Lázaro MJ. Electrochemical reactors for CO2 reduction: From acid media to gas phase. International Journal of Hydrogen Energy. 2016;41:19756-65.
[68] Patru A, Binninger T, Pribyl B, Schmidt TJ. Design principles of bipolar electrochemical co-electrolysis cells for efficient reduction of carbon dioxide from gas phase at low temperature. Journal of the Electrochemical Society. 2019;166:F34-F43.
[69] Wang G, Pan J, Jiang SP, Yang H. Gas phase electrochemical conversion of humidified CO2 to CO and H2 on proton-exchange and alkaline anion-exchange membrane fuel cell reactors. Journal of CO2 Utilization. 2018;23:152-8.
[70] Xu S, Li S, Yao W, Dong D, Xie K. Direct electrolysis of CO2 using an oxygen-ion conducting solid oxide electrolyzer based on La0.75Sr0.25Cr0.5Mn0.5O3 − δ electrode. Journal of Power Sources. 2013;230:115-21.
[71] Zhang L, Hu S, Zhu X, Yang W. Electrochemical reduction of CO2 in solid oxide electrolysis cells. Journal of Energy Chemistry. 2017;26:593-601.

[72] Zhang X, Song Y, Wang G, Bao X. Co-electrolysis of CO2 and H2O in high-temperature solid oxide electrolysis cells: Recent advance in cathodes. Journal of Energy Chemistry. 2017;26:839-53.
[73] Lim RJ, Xie M, Sk MA, Lee J-M, Fisher A, Wang X, et al. A review on the electrochemical reduction of CO2 in fuel cells, metal electrodes and molecular catalysts. Catalysis Today. 2014;233:169-80.
[74] Ebbesen SD, Jensen SH, Hauch A, Mogensen MB. High Temperature Electrolysis in Alkaline Cells, Solid Proton Conducting Cells, and Solid Oxide Cells. Chemical Reviews. 2014;114:10697-734.
[75] Nikiforov AV, Petrushina IM, Christensen E, Berg RW, Bjerrum NJ. Voltammetric study of one-step electrochemical methane production during water and CO2 co-electrolysis in molten CsH2PO4. Renewable Energy. 2020;145:508-13.
[76] Soli AL, Byrne RH. CO2 system hydration and dehydration kinetics and the equilibrium CO2/H2CO3 ratio in aqueous NaCl solution. Marine Chemistry. 2002;78:65-73.
[77] Zhong H, Fujii K, Nakano Y, Jin F. Effect of CO2 Bubbling into Aqueous Solutions Used for Electrochemical Reduction of CO2 for Energy Conversion and Storage. The Journal of Physical Chemistry C. 2015;119:55-61.
[78] König M, Vaes J, Klemm E, Pant D. Solvents and Supporting Electrolytes in the Electrocatalytic Reduction of CO2. iScience. 2019;19:135-60.
[79] Lee S, Ocon JD, Son Y-i, Lee J. Alkaline CO2 Electrolysis toward Selective and Continuous HCOO– Production over SnO2 Nanocatalysts. The Journal of Physical Chemistry C. 2015;119:4884-90.
[80] Pérez-Gallent E, Marcandalli G, Figueiredo MC, Calle-Vallejo F, Koper MTM. Structure- and Potential-Dependent Cation Effects on CO Reduction at Copper Single-Crystal Electrodes. Journal of the American Chemical Society. 2017;139:16412-9.
[81] Hori Y, Murata A, Takahashi R. Formation of hydrocarbons in the electrochemical reduction of carbon dioxide at a copper electrode in aqueous solution. Journal of the Chemical Society, Faraday Transactions 1: Physical Chemistry in Condensed Phases. 1989;85:2309-26.
[82] Kumar B, Llorente M, Froehlich J, Dang T, Sathrum A, Kubiak CP. Photochemical and Photoelectrochemical Reduction of CO2. 2012;63:541-69.
[83] Sreekanth N, Phani KL. Selective reduction of CO2 to formate through bicarbonate reduction on metal electrodes: new insights gained from SG/TC mode of SECM. Chemical Communications. 2014;50:11143-6.
[84] Kortlever R, Tan KH, Kwon Y, Koper MTM. Electrochemical carbon dioxide and bicarbonate reduction on copper in weakly alkaline media. Journal of Solid State Electrochemistry. 2013;17:1843-9.
[85] Dunwell M, Lu Q, Heyes JM, Rosen J, Chen JG, Yan Y, et al. The Central Role of Bicarbonate in the Electrochemical Reduction of Carbon Dioxide on Gold. Journal of the American Chemical Society. 2017;139:3774-83.
[86] Wuttig A, Yoon Y, Ryu J, Surendranath Y. Bicarbonate Is Not a General Acid in Au-Catalyzed CO2 Electroreduction. Journal of the American Chemical Society. 2017;139:17109-13.
[87] Resasco J, Lum Y, Clark E, Zeledon JZ, Bell AT. Effects of Anion Identity and Concentration on Electrochemical Reduction of CO2. 2018;5:1064-72.
[88] Tomita Y, Teruya S, Koga O, Hori Y. Electrochemical reduction of carbon dioxide at a platinum electrode in acetonitrile-water mixtures. Journal of the Electrochemical Society. 2000;147:4164-7.
[89] Matsubara Y, Grills DC, Kuwahara Y. Thermodynamic Aspects of Electrocatalytic CO2 Reduction in Acetonitrile and with an Ionic Liquid as Solvent or Electrolyte. ACS Catalysis. 2015;5:6440-52.
[90] Díaz-Duque Á, Sandoval-Rojas AP, Molina-Osorio AF, Feliu JM, Suárez-Herrera MF. Electrochemical reduction of CO2 in water-acetonitrile mixtures on nanostructured Cu electrode. Electrochemistry Communications. 2015;61:74-7.
[91] Rudnev AV, Zhumaev UE, Kuzume A, Vesztergom S, Furrer J, Broekmann P, et al. The promoting effect of water on the electroreduction of CO2 in acetonitrile. Electrochimica Acta. 2016;189:38-44.

[92] Mendieta-Reyes NE, Díaz-García AK, Gómez R. Simultaneous Electrocatalytic CO2 Reduction and Enhanced Electrochromic Effect at WO3 Nanostructured Electrodes in Acetonitrile. ACS Catalysis. 2018;8:1903-12.
[93] Berto TC, Zhang L, Hamers RJ, Berry JF. Electrolyte Dependence of CO2 Electroreduction: Tetraalkylammonium Ions Are Not Electrocatalysts. ACS Catalysis. 2015;5:703-7.
[94] Figueiredo MC, Ledezma-Yanez I, Koper MTM. In Situ Spectroscopic Study of CO2 Electroreduction at Copper Electrodes in Acetonitrile. ACS Catalysis. 2016;6:2382-92.
[95] Oh Y, Vrubel H, Guidoux S, Hu X. Electrochemical reduction of CO2 in organic solvents catalyzed by MoO2. Chemical Communications. 2014;50:3878-81.
[96] Sun L, Ramesha GK, Kamat PV, Brennecke JF. Switching the Reaction Course of Electrochemical CO2 Reduction with Ionic Liquids. Langmuir. 2014;30:6302-8.
[97] Zhu Q, Ma J, Kang X, Sun X, Liu H, Hu J, et al. Efficient Reduction of CO2 into Formic Acid on a Lead or Tin Electrode using an Ionic Liquid Catholyte Mixture. 2016;55:9012-6.
[98] Kai T, Zhou M, Duan Z, Henkelman GA, Bard AJ. Detection of CO2•– in the Electrochemical Reduction of Carbon Dioxide in N,N-Dimethylformamide by Scanning Electrochemical Microscopy. Journal of the American Chemical Society. 2017;139:18552-7.
[99] Shi J, Shen F-x, Shi F, Song N, Jia Y-J, Hu Y-Q, et al. Electrochemical reduction of CO2 into CO in tetrabutylammonium perchlorate/propylene carbonate: Water effects and mechanism. Electrochimica Acta. 2017;240:114-21.
[100] Aydin R, Köleli F. Electrochemical reduction of CO2 on a polyaniline electrode under ambient conditions and at high pressure in methanol. Journal of Electroanalytical Chemistry. 2002;535:107-12.
[101] Kaneco S, Iiba K, Katsumata H, Suzuki T, Ohta K. Effect of sodium cation on the electrochemical reduction of CO2 at a copper electrode in methanol. Journal of Solid State Electrochemistry. 2007;11:490-5.
[102] Kaneco S, Iiba K, Yabuuchi M, Nishio N, Ohnishi H, Katsumata H, et al. High efficiency electrochemical CO2-to-methane conversion method using methanol with lithium supporting electrolytes. Industrial and Engineering Chemistry Research. 2002;41:5165-70.
[103] Kaneco S, Katsumata H, Suzuki T, Ohta K. Electrochemical Reduction of CO2 to Methane at the Cu Electrode in Methanol with Sodium Supporting Salts and Its Comparison with Other Alkaline Salts. Energy & Fuels. 2006;20:409-14.
[104] Kaneco S, Ueno Y, Katsumata H, Suzuki T, Ohta K. Electrochemical reduction of CO2 in copper particle-suspended methanol. Chemical Engineering Journal. 2006;119:107-12.
[105] Murugananthan M, Kumaravel M, Katsumata H, Suzuki T, Kaneco S. Electrochemical reduction of CO2 using Cu electrode in methanol/LiClO4 electrolyte. International Journal of Hydrogen Energy. 2015;40:6740-4.
[106] Faggion D, Gonçalves WDG, Dupont J. CO2 Electroreduction in Ionic Liquids. 2019;7.
[107] Lim H-K, Kim H. The Mechanism of Room-Temperature Ionic-Liquid-Based Electrochemical CO2 Reduction: A Review. 2017;22:536.
[108] Sharma PP, Zhou X-D. Electrocatalytic conversion of carbon dioxide to fuels: a review on the interaction between CO2 and the liquid electrolyte. WIREs Energy and Environment. 2017;6:e239.
[109] Marepally BC, Ampelli C, Genovese C, Tavella F, Quadrelli EA, Perathoner S, et al. Electrocatalytic reduction of CO2 over dendritic-type Cu- and Fe-based electrodes prepared by electrodeposition. Journal of CO2 Utilization. 2019.
[110] Jeanty P, Scherer C, Magori E, Wiesner-Fleischer K, Hinrichsen O, Fleischer M. Upscaling and continuous operation of electrochemical CO2 to CO conversion in aqueous solutions on silver gas diffusion electrodes. Journal of CO2 Utilization. 2018;24:454-62.

[111] Marepally BC, Ampelli C, Genovese C, Tavella F, Veyre L, Quadrelli EA, et al. Role of small Cu nanoparticles in the behaviour of nanocarbon-based electrodes for the electrocatalytic reduction of CO2. Journal of CO2 Utilization. 2017;21:534-42.
[112] Wu J, Risalvato FG, Sharma PP, Pellechia PJ, Ke F-S, Zhou X-DJJoTES. Electrochemical reduction of carbon dioxide II. Design, assembly, and performance of low temperature full electrochemical cells. Journal of The Electrochemical

Society. 2013;160:F953-F7.
[113] Ramdin M, Morrison ART, de Groen M, van Haperen R, de Kler R, van den Broeke LJP, et al. High Pressure Electrochemical Reduction of CO2 to Formic Acid/Formate: A Comparison between Bipolar Membranes and Cation Exchange Membranes. Industrial & Engineering Chemistry Research. 2019;58:1834-47.
[114] Nursanto EB, Jeon HS, Kim C, Jee MS, Koh JH, Hwang YJ, et al. Gold catalyst reactivity for CO2 electro-reduction: From nano particle to layer. Catalysis Today. 2016;260:107-11.
[115] Zhao C, Wang J. Electrochemical reduction of CO2 to formate in aqueous solution using electro-deposited Sn catalysts. Chemical Engineering Journal. 2016;293:161-70.
[116] Reller C, Krause R, Volkova E, Schmid B, Neubauer S, Rucki A, et al. Selective Electroreduction of CO2 toward Ethylene on Nano Dendritic Copper Catalysts at High Current Density. Advanced Energy Materials. 2017;7:1602114.
[117] Albo J, Vallejo D, Beobide G, Castillo O, Castaño P, Irabien A. Copper-Based Metal–Organic Porous Materials for CO2 Electrocatalytic Reduction to Alcohols. ChemSusChem. 2017;10:1100-9.
[118] Liu Y, Fan M, Zhang X, Zhang Q, Guay D, Qiao J. Design and engineering of urchin-like nanostructured SnO2 catalysts via controlled facial hydrothermal synthesis for efficient electro-reduction of CO2. Electrochimica Acta. 2017;248:123-32.
[119] Hong S, Lee S, Kim S, Lee JK, Lee J. Anion dependent CO/H2 production ratio from CO2 reduction on Au electro-catalyst. Catalysis Today. 2017;295:82-8.
[120] Kim H, Jeon HS, Jee MS, Nursanto EB, Singh JP, Chae K, et al. Contributors to Enhanced CO2 Electroreduction Activity and Stability in a Nanostructured Au Electrocatalyst. ChemSusChem. 2016;9:2097-102.
[121] Fu Y, Li Y, Zhang X, Liu Y, Qiao J, Zhang J, et al. Novel hierarchical SnO2 microsphere catalyst coated on gas diffusion electrode for enhancing energy efficiency of CO2 reduction to formate fuel. Applied Energy. 2016;175:536-44.
[122] Del Castillo A, Alvarez-Guerra M, Solla-Gullón J, Sáez A, Montiel V, Irabien A. Electrocatalytic reduction of CO2 to formate using particulate Sn electrodes: Effect of metal loading and particle size. Applied Energy. 2015;157:165-73.
[123] Grace AN, Choi SY, Vinoba M, Bhagiyalakshmi M, Chu DH, Yoon Y, et al. Electrochemical reduction of carbon dioxide at low overpotential on a polyaniline/Cu2O nanocomposite based electrode. Applied Energy. 2014;120:85-94.
[124] Delacourt C, Ridgway PL, Kerr JB, Newman JJJoTES. Design of an electrochemical cell making syngas (CO+ H2) from CO2 and H2O reduction at room temperature. Journal of the Electrochemical Society. 2008;155:B42-B9.
[125] Sebastián D, Palella A, Baglio V, Spadaro L, Siracusano S, Negro P, et al. CO2 reduction to alcohols in a polymer electrolyte membrane co-electrolysis cell operating at low potentials. Electrochimica Acta. 2017;241:28-40.
[126] Maeda M, Kitaguchi Y, Ikeda S, Ito K. Reduction of carbon dioxide on partially-immersed Au plate electrode and Au-SPE electrode. Journal of Electroanalytical Chemistry and Interfacial Electrochemistry. 1987;238:247-58.

[127] Aeshala LM, Rahman SU, Verma A. Effect of solid polymer electrolyte on electrochemical reduction of CO2. Separation and Purification Technology. 2012;94:131-7.
[128] Cook RL, MacDuff RC, Sammells AFJJotES. Ambient temperature gas phase CO 2 reduction to hydrocarbons at solid polymer electrolyte cells. Journal of the Electrochemical Society. 1988;135:1470-1.
[129] Komatsu S, Tanaka M, Okumura A, Kungi A. Preparation of cu-solid polymer electrolyte composite electrodes and application to gas-phase electrochemical reduction of CO2. Electrochimica Acta. 1995;40:745-53.
[130] Narayanan S, Haines B, Soler J, Valdez TJJoTES. Electrochemical conversion of carbon dioxide to formate in alkaline polymer electrolyte membrane cells. Journal of the Electrochemical Society. 2011;158:A167-A73.
[131] Dewulf DW, Bard AJ. The electrochemical reduction of CO2 to CH4 and C2H4 at Cu/Nafion electrodes (solid polymer electrolyte structures). Catalysis Letters. 1988;1:73-9.
[132] Cook RL, MacDuff RC, Sammells AFJJoTES. Gas‐Phase CO 2 Reduction to Hydrocarbons at Metal/Solid Polymer Electrolyte Interface. Journal of the Electrochemical Society. 1990;137:187-9.
[133] Scott K, Cheng H, Samuel SJE. Reduction of carbon dioxide to formic acid in a solid polymer electrolyte (SPE) reactor. Electrochemical Processes for a Cleaner Environment, Proceedings. 2001;2001:351-61.
[134] Vennekötter J-B, Scheuermann T, Sengpiel R, Wessling M. The electrolyte matters: Stable systems for high rate electrochemical CO2 reduction. Journal of CO2 Utilization. 2019;32:202-13.
[135] Dufek EJ, Lister TE, Stone SG, McIlwain MEJJoTES. Operation of a pressurized system for continuous reduction of CO2. Journal of the Electrochemical Society. 2012;159:F514-F7.
[136] Aeshala LM, Uppaluri R, Verma A. Electrochemical conversion of CO2 to fuels: tuning of the reaction zone using suitable functional groups in a solid polymer electrolyte. Physical Chemistry Chemical Physics. 2014;16:17588-94.
[137] Kutz RB, Chen Q, Yang H, Sajjad SD, Liu Z, Masel IR. Sustainion Imidazolium-Functionalized Polymers for Carbon Dioxide Electrolysis. Energy Technology. 2017;5:929-36.
[138] Liu Z, Masel RI, Chen Q, Kutz R, Yang H, Lewinski K, et al. Electrochemical generation of syngas from water and carbon dioxide at industrially important rates. Journal of CO2 Utilization. 2016;15:50-6.
[139] Kaczur JJ, Yang H, Liu Z, Sajjad SD, Masel RI. Carbon Dioxide and Water Electrolysis Using New Alkaline Stable Anion Membranes. Frontiers in Chemistry. 2018;6.
[140] Endrődi B, Kecsenovity E, Samu A, Darvas F, Jones RV, Török V, et al. Multilayer Electrolyzer Stack Converts Carbon Dioxide to Gas Products at High Pressure with High Efficiency. ACS Energy Letters. 2019;4:1770-7.
[141] Liu Z, Yang H, Kutz R, Masel RIJJoTES. CO2 Electrolysis to CO and O2 at High Selectivity, Stability and Efficiency Using Sustainion Membranes. Journal of the Electrochemical Society. 2018;165:J3371-J7.
[142] Larrazábal GO, Strøm-Hansen P, Heli JP, Zeiter K, Therkildsen KT, Chorkendorff I, et al. Analysis of Mass Flows and Membrane Cross-over in CO2 Reduction at High Current Densities in an MEA-Type Electrolyzer. ACS Applied Materials & Interfaces. 2019;11:41281-8.
[143] Luc W, Ko BH, Kattel S, Li S, Su D, Chen JG, et al. SO2-Induced Selectivity Change in CO2 Electroreduction. Journal of the American Chemical Society. 2019;141:9902-9.
[144] Li YC, Wang Z, Yuan T, Nam D-H, Luo M, Wicks J, et al. Binding Site Diversity Promotes CO2 Electroreduction to Ethanol. Journal of the American Chemical Society. 2019;141:8584-91.
[145] Aeshala LM, Verma A. Amines as Reaction Environment Regulator for CO2 Electrochemical Reduction to CH4. Macromolecular Symposia. 2015;357:79-85.
[146] Nishimura Y, Yoshida D, Mizuhata M, Asaka K, Oguro K, Takenaka H. Solid polymer electrolyte CO2 reduction. Energy Conversion and Management. 1995;36:629-32.
[147] Wang M, Torbensen K, Salvatore D, Ren S, Joulié D, Dumoulin F, et al. CO 2 electrochemical catalytic reduction with a highly active cobalt phthalocyanine. Nature Communication. 2019;10:1-8.

[148] Vermaas DA, Smith WA. Synergistic Electrochemical CO2 Reduction and Water Oxidation with a Bipolar Membrane. ACS Energy Letters. 2016;1:1143-8.
[149] Zhou X, Liu R, Sun K, Chen Y, Verlage E, Francis SA, et al. Solar-Driven Reduction of 1 atm of CO2 to Formate at 10% Energy-Conversion Efficiency by Use of a TiO2-Protected III–V Tandem Photoanode in Conjunction with a Bipolar Membrane and a Pd/C Cathode. ACS Energy Letters. 2016;1:764-70.
[150] Pătru A, Binninger T, Pribyl B, Schmidt TJJJoTES. Design principles of bipolar electrochemical co-electrolysis cells for efficient reduction of carbon dioxide from gas phase at low temperature. Journal of the Electrochemical Society. 2019;166:F34-F43.
[151] Li YC, Lee G, Yuan T, Wang Y, Nam D-H, Wang Z, et al. CO2 Electroreduction from Carbonate Electrolyte. ACS Energy Letters. 2019;4:1427-31.
[152] Chen Y, Vise A, Klein WE, Cetinbas FC, Myers DJ, Smith WA, et al. A Robust, Scalable Platform for the Electrochemical Conversion of CO2 to Formate: Identifying Pathways to Higher Energy Efficiencies. ACS Energy Letters. 2020:1825-33.
[153] Unnikrishnan EK, Kumar SD, Maiti B. Permeation of inorganic anions through Nafion ionomer membrane. Journal of Membrane Science. 1997;137:133-7.
[154] Mohanty AD, Tignor SE, Krause JA, Choe Y-K, Bae C. Systematic Alkaline Stability Study of Polymer Backbones for Anion Exchange Membrane Applications. Macromolecules. 2016;49:3361-72.
[155] Vargas-Barbosa NM, Geise GM, Hickner MA, Mallouk TE. Assessing the Utility of Bipolar Membranes for use in Photoelectrochemical Water-Splitting Cells. 2014;7:3017-20.
[156] Strathmann H, Krol JJ, Rapp HJ, Eigenberger G. Limiting current density and water dissociation in bipolar membranes. Journal of Membrane Science. 1997;125:123-42.
[157] Sheldeshov N, Zabolotskii V, Pis-menskaya N, Gnusin NJSE. Catalysis of water dissociation by the phosphoric-acid groups of an MB-3 bipolar membrane. Sov Electrochem (Engl Transl). 1986;22.
[158] Strathmann H, Rapp HJ, Bauer B, Bell CM. Theoretical and practical aspects of preparing bipolar membranes. Desalination. 1993;90:303-23.
[159] Simons R. A novel method for preparing bipolar membranes. Electrochimica Acta. 1986;31:1175-7.
[160] Simons R. Preparation of a high performance bipolar membrane. Journal of Membrane Science. 1993;78:13-23.
[161] Hohenadel A, Powers D, Wycisk R, Adamski M, Pintauro P, Holdcroft S. Electrochemical Characterization of Hydrocarbon Bipolar Membranes with Varying Junction Morphology. ACS Applied Energy Materials. 2019;2:6817-24.
[162] Shen C, Wycisk R, Pintauro PN. High performance electrospun bipolar membrane with a 3D junction. Energy & Environmental Science. 2017;10:1435-42.
[163] Jeevananda T, Yeon K-H, Moon S-H. Synthesis and characterization of bipolar membrane using pyridine functionalized anion exchange layer. Journal of Membrane Science. 2006;283:201-8.
[164] Manohar M, Shahi VK. Graphene Oxide–Polyaniline as a Water Dissociation Catalyst in the Interfacial Layer of Bipolar Membrane for Energy-Saving Production of Carboxylic Acids from Carboxylates by Electrodialysis. ACS Sustainable Chemistry & Engineering. 2018;6:3463-71.
[165] McDonald MB, Freund MS. Graphene Oxide as a Water Dissociation Catalyst in the Bipolar Membrane Interfacial Layer. ACS Applied Materials & Interfaces. 2014;6:13790-7.
[166] Strathmann H, Krol J, Rapp H-J, Eigenberger GJJoMS. Limiting current density and water dissociation in bipolar membranes. 1997;125:123-42.
[167] Mafé S, Manzanares JA, Ramrez P. Model for ion transport in bipolar membranes. Physical Review A. 1990;42:6245-8.
[168] Ramírez P, Aguilella VM, Manzanares JA, Mafé S. Effects of temperature and ion transport on water splitting in bipolar membranes. Journal of Membrane Science. 1992;73:191-201.
[169] Simons R, Khanarian GJTJoMB. Water dissociation in bipolar membranes: Experiments and theory. 1978;38:11-30.

[170] Simons R. A mechanism for water flow in bipolar membranes. Journal of Membrane Science. 1993;82:65-73.
[171] Shimizu K, Tanioka AJP. Effect of interface structure and amino groups on water splitting and rectification effects in bipolar membranes. 1997;38:5441-6.
[172] Chou T-J, Tanioka AJTJoPCB. Current− Voltage Curves of Composite Bipolar Membrane in Alcohol− Water Solutions. 1998;102:7866-70.
[173] Chou T-J, Tanioka AJJoEC. Current–voltage curves of a composite bipolar membrane in organic acid–water solutions. 1999;462:12-8.
[174] Bassignana I, Reiss HJJoMS. Ion transport and water dissociation in bipolar ion exchange membranes. 1983;15:27-41.
[175] Franken TJMT. Bipolar membrane technology and its applications. 2000;2000:8-11.
[176] Martinez RJ, Farrell J. Quantifying Electric Field Enhancement of Water Dissociation Rates in Bipolar Membranes. Industrial & Engineering Chemistry Research. 2019;58:782-9.
[177] Reiter RS, White W, Ardo SJJoTES. Communication—Electrochemical Characterization of Commercial Bipolar Membranes under Electrolyte Conditions Relevant to Solar Fuels Technologies. 2016;163:H3132-H4.
[178] McDonald MB, Ardo S, Lewis NS, Freund MS. Use of Bipolar Membranes for Maintaining Steady-State pH Gradients in Membrane-Supported, Solar-Driven Water Splitting. 2014;7:3021-7.
[179] Schreier M, Héroguel F, Steier L, Ahmad S, Luterbacher JS, Mayer MT, et al. Solar conversion of CO2 to CO using Earth-abundant electrocatalysts prepared by atomic layer modification of CuO. Nature Energy. 2017;2:17087.
[180] Li T, Lees EW, Goldman M, Salvatore DA, Weekes DM, Berlinguette CP. Electrolytic Conversion of Bicarbonate into CO in a Flow Cell. Joule. 2019;3:1487-97.
[181] Ma M, Clark EL, Therkildsen KT, Dalsgaard S, Chorkendorff I, Seger B. Insights into the carbon balance for CO2 electroreduction on Cu using gas diffusion electrode reactor designs. Energy & Environmental Science. 2020.
[182] Alcaraz A, Ramírez P, Mafé S, Holdik H, Bauer B. Ion selectivity and water dissociation in polymer bipolar membranes studied by membrane potential and current–voltage measurements. Polymer. 2000;41:6627-34.
[183] Luo J, Vermaas DA, Bi D, Hagfeldt A, Smith WA, Grätzel M. Bipolar Membrane-Assisted Solar Water Splitting in Optimal pH. Advanced Energy Materials. 2016;6:1600100.
[184] Vermaas DA, Sassenburg M, Smith WA. Photo-assisted water splitting with bipolar membrane induced pH gradients for practical solar fuel devices. Journal of Materials Chemistry A. 2015;3:19556-62.
[185] Sun K, Liu R, Chen Y, Verlage E, Lewis NS, Xiang CJAEM. A Stabilized, Intrinsically Safe, 10% Efficient, Solar‐Driven Water‐Splitting Cell Incorporating Earth‐Abundant Electrocatalysts with Steady‐State pH Gradients and Product Separation Enabled by a Bipolar Membrane. Advanced Energy Materials. 2016;6:1600379.
[186] Hori Yi. Electrochemical CO 2 reduction on metal electrodes. Modern aspects of electrochemistry: Springer; 2008. p. 89-189.
[187] Hori Y, Kikuchi K, Suzuki S. Production of CO and CH4 in electrochemical reduction of CO2 at metal electrodes in aqueous hydrogencarbonate solution. Chemistry Letters. 1985;14:1695-8.
[188] Hori Y, Wakebe H, Tsukamoto T, Koga O. Electrocatalytic process of CO selectivity in electrochemical reduction of CO2 at metal electrodes in aqueous media. Electrochimica Acta. 1994;39:1833-9.
[189] Hoshi N, Kato M, Hori Y. Electrochemical reduction of CO2 on single crystal electrodes of silver Ag (111), Ag (100) and Ag (110). Journal of electroanalytical chemistry. 1997;440:283-6.

[190] Hori Y, Takahashi I, Koga O, Hoshi N. Selective formation of C2 compounds from electrochemical reduction of CO2 at a series of copper single crystal electrodes. The Journal of Physical Chemistry B. 2002;106:15-7.
[191] Kuhl KP, Hatsukade T, Cave ER, Abram DN, Kibsgaard J, Jaramillo TF. Electrocatalytic conversion of carbon dioxide to methane and methanol on transition metal surfaces. Journal of the American Chemical Society. 2014;136:14107-13.
[192] De Gregorio GL, Burdyny T, Loiudice A, Iyengar P, Smith WA, Buonsanti R. Facet-Dependent Selectivity of Cu Catalysts in Electrochemical CO2 Reduction at Commercially Viable Current Densities. ACS Catalysis. 2020;10:4854-62.
[193] Yang F, Elnabawy AO, Schimmenti R, Song P, Wang J, Peng Z, et al. Bismuthene for highly efficient carbon dioxide electroreduction reaction. Nature Communications. 2020;11:1088.
[194] Hansen HA, Varley JB, Peterson AA, Norskov JK. Understanding Trends in the Electrocatalytic Activity of Metals and Enzymes for CO2 Reduction to CO. J Phys Chem Lett. 2013;4:388-92.
[195] Zhu W, Michalsky R, Metin O, Lv H, Guo S, Wright CJ, et al. Monodisperse Au nanoparticles for selective electrocatalytic reduction of CO2 to CO. J Am Chem Soc. 2013;135:16833-6.
[196] Zhu W, Zhang YJ, Zhang H, Lv H, Li Q, Michalsky R, et al. Active and selective conversion of CO2 to CO on ultrathin Au nanowires. J Am Chem Soc. 2014;136:16132-5.
[197] Hatsukade T, Kuhl KP, Cave ER, Abram DN, Jaramillo TF. Insights into the electrocatalytic reduction of CO(2) on metallic silver surfaces. Phys Chem Chem Phys. 2014;16:13814-9.
[198] Chen Y, Kanan MW. Tin oxide dependence of the CO2 reduction efficiency on tin electrodes and enhanced activity for tin/tin oxide thin-film catalysts. J Am Chem Soc. 2012;134:1986-9.
[199] Lu Q, Rosen J, Zhou Y, Hutchings GS, Kimmel YC, Chen JG, et al. A selective and efficient electrocatalyst for carbon dioxide reduction. Nat Commun. 2014;5:3242.
[200] Rosen J, Hutchings GS, Lu Q, Rivera S, Zhou Y, Vlachos DG, et al. Mechanistic Insights into the Electrochemical Reduction of CO2 to CO on Nanostructured Ag Surfaces. ACS Catalysis. 2015;5:4293-9.
[201] Hsieh Y-C, Senanayake SD, Zhang Y, Xu W, Polyansky DE. Effect of Chloride Anions on the Synthesis and Enhanced Catalytic Activity of Silver Nanocoral Electrodes for CO2Electroreduction. ACS Catalysis. 2015;5:5349-56.
[202] Ma M, Liu K, Shen J, Kas R, Smith WA. In Situ Fabrication and Reactivation of Highly Selective and Stable Ag Catalysts for Electrochemical CO2 Conversion. ACS Energy Lett. 2018;3:1301-6.
[203] Dinh C-T, García de Arquer FP, Sinton D, Sargent EH. High Rate, Selective, and Stable Electroreduction of CO2 to CO in Basic and Neutral Media. ACS Energy Letters. 2018;3:2835-40.
[204] Rosen J, Hutchings GS, Lu Q, Forest RV, Moore A, Jiao F. Electrodeposited Zn Dendrites with Enhanced CO Selectivity for Electrocatalytic CO2 Reduction. ACS Catalysis. 2015;5:4586-91.
[205] Won da H, Shin H, Koh J, Chung J, Lee HS, Kim H, et al. Highly Efficient, Selective, and Stable CO2 Electroreduction on a Hexagonal Zn Catalyst. Angew Chem Int Ed Engl. 2016;55:9297-300.
[206] Quan F, Zhong D, Song H, Jia F, Zhang L. A highly efficient zinc catalyst for selective electroreduction of carbon dioxide in aqueous NaCl solution. Journal of Materials Chemistry A. 2015;3:16409-13.
[207] Zhang T, Li X, Qiu Y, Su P, Xu W, Zhong H, et al. Multilayered Zn nanosheets as an electrocatalyst for efficient electrochemical reduction of CO2. Journal of Catalysis. 2018;357:154-62.
[208] Peterson AA, Abild-Pedersen F, Studt F, Rossmeisl J, Nørskov JK. How copper catalyzes the electroreduction of carbon dioxide into hydrocarbon fuels. Energy & Environmental Science. 2010;3.
[209] Peterson AA, Nørskov JK. Activity Descriptors for CO2 Electroreduction to Methane on Transition-Metal Catalysts. The Journal of Physical Chemistry Letters. 2012;3:251-8.
[210] Tang W, Peterson AA, Varela AS, Jovanov ZP, Bech L, Durand WJ, et al. The importance of surface morphology in controlling the selectivity of polycrystalline copper for CO2 electroreduction. Phys Chem Chem Phys. 2012;14:76-81.

[211] Kuhl KP, Cave ER, Abram DN, Jaramillo TF. New insights into the electrochemical reduction of carbon dioxide on metallic copper surfaces. Energy & Environmental Science. 2012;5.
[212] Ma M, Djanashvili K, Smith WA. Selective electrochemical reduction of CO2 to CO on CuO-derived Cu nanowires. Phys Chem Chem Phys. 2015;17:20861-7.
[213] Reske R, Mistry H, Behafarid F, Roldan Cuenya B, Strasser P. Particle size effects in the catalytic electroreduction of CO(2) on Cu nanoparticles. J Am Chem Soc. 2014;136:6978-86.
[214] Li CW, Kanan MW. CO2 reduction at low overpotential on Cu electrodes resulting from the reduction of thick Cu2O films. J Am Chem Soc. 2012;134:7231-4.
[215] Kas R, Kortlever R, Milbrat A, Koper MT, Mul G, Baltrusaitis J. Electrochemical CO2 reduction on Cu2O-derived copper nanoparticles: controlling the catalytic selectivity of hydrocarbons. Phys Chem Chem Phys. 2014;16:12194-201.
[216] Sen S, Liu D, Palmore GTR. Electrochemical Reduction of CO2at Copper Nanofoams. ACS Catalysis. 2014;4:3091-5.
[217] Ma M, Djanashvili K, Smith WA. Controllable Hydrocarbon Formation from the Electrochemical Reduction of CO2 over Cu Nanowire Arrays. Angew Chem Int Ed Engl. 2016;55:6680-4.
[218] Handoko AD, Chan KW, Yeo BS. –CH3 Mediated Pathway for the Electroreduction of CO2 to Ethane and Ethanol on Thick Oxide-Derived Copper Catalysts at Low Overpotentials. ACS Energy Letters. 2017;2:2103-9.
[219] Hori Y, Wakebe H, Tsukamoto T, Koga O. Adsorption of CO accompanied with simultaneous charge transfer on copper single crystal electrodes related with electrochemical reduction of CO2 to hydrocarbons. Surface science. 1995;335:258-63.
[220] Schouten KJ, Qin Z, Perez Gallent E, Koper MT. Two pathways for the formation of ethylene in CO reduction on single-crystal copper electrodes. J Am Chem Soc. 2012;134:9864-7.
[221] Schouten KJP, Pérez Gallent E, Koper MTM. The influence of pH on the reduction of CO and CO2 to hydrocarbons on copper electrodes. Journal of Electroanalytical Chemistry. 2014;716:53-7.
[222] Loiudice A, Lobaccaro P, Kamali EA, Thao T, Huang BH, Ager JW, et al. Tailoring Copper Nanocrystals towards C2 Products in Electrochemical CO2 Reduction. Angew Chem Int Ed Engl. 2016;55:5789-92.
[223] Li CW, Ciston J, Kanan MW. Electroreduction of carbon monoxide to liquid fuel on oxide-derived nanocrystalline copper. Nature. 2014;508:504-7.
[224] Verdaguer-Casadevall A, Li CW, Johansson TP, Scott SB, McKeown JT, Kumar M, et al. Probing the Active Surface Sites for CO Reduction on Oxide-Derived Copper Electrocatalysts. J Am Chem Soc. 2015;137:9808-11.
[225] Chen Y, Li CW, Kanan MW. Aqueous CO2 reduction at very low overpotential on oxide-derived Au nanoparticles. J Am Chem Soc. 2012;134:19969-72.
[226] Feng X, Jiang K, Fan S, Kanan MW. Grain-boundary-dependent CO2 electroreduction activity. J Am Chem Soc. 2015;137:4606-9.
[227] Ma M, Trzesniewski BJ, Xie J, Smith WA. Selective and Efficient Reduction of Carbon Dioxide to Carbon Monoxide on Oxide-Derived Nanostructured Silver Electrocatalysts. Angew Chem Int Ed Engl. 2016;55:9748-52.
[228] Kim D, Resasco J, Yu Y, Asiri AM, Yang P. Synergistic geometric and electronic effects for electrochemical reduction of carbon dioxide using gold-copper bimetallic nanoparticles. Nat Commun. 2014;5:4948.
[229] Siahrostami S, Verdaguer-Casadevall A, Karamad M, Deiana D, Malacrida P, Wickman B, et al. Enabling direct H2O2 production through rational electrocatalyst design. Nat Mater. 2013;12:1137-43.
[230] Rasul S, Anjum DH, Jedidi A, Minenkov Y, Cavallo L, Takanabe K. A highly selective copper-indium bimetallic electrocatalyst for the electrochemical reduction of aqueous CO2 to CO. Angew Chem Int Ed Engl. 2015;54:2146-50.

[231] Sarfraz S, Garcia-Esparza AT, Jedidi A, Cavallo L, Takanabe K. Cu–Sn Bimetallic Catalyst for Selective Aqueous Electroreduction of CO2 to CO. ACS Catalysis. 2016;6:2842-51.
[232] Li M, Wang J, Li P, Chang K, Li C, Wang T, et al. Mesoporous palladium–copper bimetallic electrodes for selective electrocatalytic reduction of aqueous CO2to CO. Journal of Materials Chemistry A. 2016;4:4776-82.
[233] Ren D, Ang BS-H, Yeo BS. Tuning the Selectivity of Carbon Dioxide Electroreduction toward Ethanol on Oxide-Derived CuxZn Catalysts. ACS Catalysis. 2016;6:8239-47.
[234] Jiang K, Sandberg RB, Akey AJ, Liu X, Bell DC, Nørskov JK, et al. Metal ion cycling of Cu foil for selective C–C coupling in electrochemical CO2 reduction. Nature Catalysis. 2018;1:111-9.
[235] Ma S, Sadakiyo M, Heima M, Luo R, Haasch RT, Gold JI, et al. Electroreduction of Carbon Dioxide to Hydrocarbons Using Bimetallic Cu-Pd Catalysts with Different Mixing Patterns. J Am Chem Soc. 2017;139:47-50.
[236] Ma M, Hansen HA, Valenti M, Wang Z, Cao A, Dong M, et al. Electrochemical reduction of CO2 on compositionally variant Au-Pt bimetallic thin films. Nano Energy. 2017;42:51-7.
[237] Hahn C, Abram DN, Hansen HA, Hatsukade T, Jackson A, Johnson NC, et al. Synthesis of thin film AuPd alloys and their investigation for electrocatalytic CO2 reduction. Journal of Materials Chemistry A. 2015;3:20185-94.
[238] Kortlever R, Peters I, Koper S, Koper MTM. Electrochemical CO2 Reduction to Formic Acid at Low Overpotential and with High Faradaic Efficiency on Carbon-Supported Bimetallic Pd–Pt Nanoparticles. ACS Catalysis. 2015;5:3916-23.
[239] Asadi M, Kumar B, Behranginia A, Rosen BA, Baskin A, Repnin N, et al. Robust carbon dioxide reduction on molybdenum disulphide edges. Nature Communications. 2014;5:4470.
[240] Xu J, Li X, Liu W, Sun Y, Ju Z, Yao T, et al. Carbon Dioxide Electroreduction into Syngas Boosted by a Partially Delocalized Charge in Molybdenum Sulfide Selenide Alloy Monolayers. Angewandte Chemie International Edition. 2017;56:9121-5.
[241] Abbasi P, Asadi M, Liu C, Sharifi-Asl S, Sayahpour B, Behranginia A, et al. Tailoring the Edge Structure of Molybdenum Disulfide toward Electrocatalytic Reduction of Carbon Dioxide. ACS Nano. 2017;11:453-60.
[242] Sun X, Kang X, Zhu Q, Ma J, Yang G, Liu Z, et al. Very highly efficient reduction of CO2 to CH4 using metal-free N-doped carbon electrodes. Chemical Science. 2016;7:2883-7.
[243] Wang H, Chen Y, Hou X, Ma C, Tan T. Nitrogen-doped graphenes as efficient electrocatalysts for the selective reduction of carbon dioxide to formate in aqueous solution. Green Chemistry. 2016;18:3250-6.
[244] Wu J, Liu M, Sharma PP, Yadav RM, Ma L, Yang Y, et al. Incorporation of Nitrogen Defects for Efficient Reduction of CO2 via Two-Electron Pathway on Three-Dimensional Graphene Foam. Nano Letters. 2016;16:466-70.
[245] Sreekanth N, Nazrulla MA, Vineesh TV, Sailaja K, Phani KL. Metal-free boron-doped graphene for selective electroreduction of carbon dioxide to formic acid/formate. Chemical Communications. 2015;51:16061-4.
[246] Liu Y, Zhang Y, Cheng K, Quan X, Fan X, Su Y, et al. Selective Electrochemical Reduction of Carbon Dioxide to Ethanol on a Boron- and Nitrogen-Co-doped Nanodiamond. Angewandte Chemie International Edition. 2017;56:15607-11.
[247] Li W, Seredych M, Rodríguez-Castellón E, Bandosz TJ. Metal-free Nanoporous Carbon as a Catalyst for Electrochemical Reduction of CO2 to CO and CH4. ChemSusChem. 2016;9:606-16.
[248] Pan F, Li B, Deng W, Du Z, Gang Y, Wang G, et al. Promoting electrocatalytic CO2 reduction on nitrogen-doped carbon with sulfur addition. Applied Catalysis B: Environmental. 2019;252:240-9.

[249] Sharma PP, Wu J, Yadav RM, Liu M, Wright CJ, Tiwary CS, et al. Nitrogen-Doped Carbon Nanotube Arrays for High-Efficiency Electrochemical Reduction of CO2: On the Understanding of Defects, Defect Density, and Selectivity. Angewandte Chemie International Edition. 2015;54:13701-5.
[250] Li C, Wang Y, Xiao N, Li H, Ji Y, Guo Z, et al. Nitrogen-doped porous carbon from coal for high efficiency CO2 electrocatalytic reduction. Carbon. 2019;151:46-52.
[251] Xie J, Zhao X, Wu M, Li Q, Wang Y, Yao J. Metal-Free Fluorine-Doped Carbon Electrocatalyst for CO2 Reduction Outcompeting Hydrogen Evolution. Angewandte Chemie International Edition. 2018;57:9640-4.
[252] Wang R, Sun X, Ould-Chikh S, Osadchii D, Bai F, Kapteijn F, et al. Metal-Organic-Framework-Mediated Nitrogen-Doped Carbon for CO2 Electrochemical Reduction. ACS Applied Materials & Interfaces. 2018;10:14751-8.
[253] Pan F, Li B, Xiang X, Wang G, Li Y. Efficient CO2 Electroreduction by Highly Dense and Active Pyridinic Nitrogen on Holey Carbon Layers with Fluorine Engineering. ACS Catalysis. 2019;9:2124-33.
[254] Wu J, Ma S, Sun J, Gold JI, Tiwary C, Kim B, et al. A metal-free electrocatalyst for carbon dioxide reduction to multi-carbon hydrocarbons and oxygenates. Nature Communications. 2016;7:13869.
[255] Liu Y, Chen S, Quan X, Yu H. Efficient Electrochemical Reduction of Carbon Dioxide to Acetate on Nitrogen-Doped Nanodiamond. Journal of the American Chemical Society. 2015;137:11631-6.
[256] Nakata K, Ozaki T, Terashima C, Fujishima A, Einaga Y. High-Yield Electrochemical Production of Formaldehyde from CO2 and Seawater. Angewandte Chemie International Edition. 2014;53:871-4.
[257] Jhong H-RM, Tornow CE, Smid B, Gewirth AA, Lyth SM, Kenis PJA. A Nitrogen-Doped Carbon Catalyst for Electrochemical CO2 Conversion to CO with High Selectivity and Current Density. ChemSusChem. 2017;10:1094-9.
[258] Lu X, Tan TH, Ng YH, Amal R. Highly Selective and Stable Reduction of CO2 to CO by a Graphitic Carbon Nitride/Carbon Nanotube Composite Electrocatalyst. Chemistry – A European Journal. 2016;22:11991-6.
[259] Almeida Paz FA, Klinowski J, Vilela SMF, Tomé JPC, Cavaleiro JAS, Rocha J. Ligand design for functional metal–organic frameworks. Chemical Society Reviews. 2012;41:1088-110.
[260] Elgrishi N, Chambers MB, Wang X, Fontecave M. Molecular polypyridine-based metal complexes as catalysts for the reduction of CO2. Chemical Society Reviews. 2017;46:761-96.
[261] Leung K, Nielsen IMB, Sai N, Medforth C, Shelnutt JA. Cobalt−Porphyrin Catalyzed Electrochemical Reduction of Carbon Dioxide in Water. 2. Mechanism from First Principles. The Journal of Physical Chemistry A. 2010;114:10174-84.
[262] Yao CL, Li JC, Gao W, Jiang Q. Cobalt-porphine catalyzed CO2 electro-reduction: a novel protonation mechanism. Physical Chemistry Chemical Physics. 2017;19:15067-72.
[263] Nichols Eva M, Derrick JS, Nistanaki SK, Smith PT, Chang CJ. Positional effects of second-sphere amide pendants on electrochemical CO2 reduction catalyzed by iron porphyrins. Chemical Science. 2018;9:2952-60.
[264] Lieber CM, Lewis NS. Catalytic reduction of carbon dioxide at carbon electrodes modified with cobalt phthalocyanine. Journal of the American Chemical Society. 1984;106:5033-4.
[265] Zhang X, Wu Z, Zhang X, Li L, Li Y, Xu H, et al. Highly selective and active CO2 reduction electrocatalysts based on cobalt phthalocyanine/carbon nanotube hybrid structures. Nature Communications. 2017;8:14675.
[266] Choi J, Kim J, Wagner P, Gambhir S, Jalili R, Byun S, et al. Energy efficient electrochemical reduction of CO2 to CO using a three-dimensional porphyrin/graphene hydrogel. Energy & Environmental Science. 2019;12:747-55.
[267] Yao SA, Ruther RE, Zhang L, Franking RA, Hamers RJ, Berry JF. Covalent Attachment of Catalyst Molecules to Conductive Diamond: CO2 Reduction Using “Smart” Electrodes. Journal of the American Chemical Society. 2012;134:15632-5.

[268] Isaacs M, Armijo F, Ramírez G, Trollund E, Biaggio SR, Costamagna J, et al. Electrochemical reduction of CO2 mediated by poly-M-aminophthalocyanines (M=Co, Ni, Fe): poly-Co-tetraaminophthalocyanine, a selective catalyst. Journal of Molecular Catalysis A: Chemical. 2005;229:249-57.
[269] Zhu M, Chen J, Huang L, Ye R, Xu J, Han Y-F. Covalently Grafting Cobalt Porphyrin onto Carbon Nanotubes for Efficient CO2 Electroreduction. Angewandte Chemie International Edition. 2019;58:6595-9.
[270] Kornienko N, Zhao Y, Kley CS, Zhu C, Kim D, Lin S, et al. Metal–Organic Frameworks for Electrocatalytic Reduction of Carbon Dioxide. Journal of the American Chemical Society. 2015;137:14129-35.
[271] Liu H, Chu J, Yin Z, Cai X, Zhuang L, Deng H. Covalent Organic Frameworks Linked by Amine Bonding for Concerted Electrochemical Reduction of CO2. Chem. 2018;4:1696-709.
[272] Su P, Iwase K, Harada T, Kamiya K, Nakanishi S. Covalent triazine framework modified with coordinatively-unsaturated Co or Ni atoms for CO2 electrochemical reduction. Chemical Science. 2018;9:3941-7.
[273] Shen J, Kortlever R, Kas R, Birdja YY, Diaz-Morales O, Kwon Y, et al. Electrocatalytic reduction of carbon dioxide to carbon monoxide and methane at an immobilized cobalt protoporphyrin. Nature Communications. 2015;6:8177.
[274] Wang Y, Marquard SL, Wang D, Dares C, Meyer TJ. Single-Site, Heterogeneous Electrocatalytic Reduction of CO2 in Water as the Solvent. ACS Energy Letters. 2017;2:1395-9.
[275] Maurin A, Robert M. Noncovalent Immobilization of a Molecular Iron-Based Electrocatalyst on Carbon Electrodes for Selective, Efficient CO2-to-CO Conversion in Water. Journal of the American Chemical Society. 2016;138:2492-5.
[276] Kang P, Zhang S, Meyer TJ, Brookhart M. Rapid Selective Electrocatalytic Reduction of Carbon Dioxide to Formate by an Iridium Pincer Catalyst Immobilized on Carbon Nanotube Electrodes. Angewandte Chemie International Edition. 2014;53:8709-13.
[277] Morlanés N, Takanabe K, Rodionov V. Simultaneous Reduction of CO2 and Splitting of H2O by a Single Immobilized Cobalt Phthalocyanine Electrocatalyst. ACS Catalysis. 2016;6:3092-5.
[278] Weng Z, Jiang J, Wu Y, Wu Z, Guo X, Materna KL, et al. Electrochemical CO2 Reduction to Hydrocarbons on a Heterogeneous Molecular Cu Catalyst in Aqueous Solution. Journal of the American Chemical Society. 2016;138:8076-9.
[279] Wu Y, Jiang J, Weng Z, Wang M, Broere DLJ, Zhong Y, et al. Electroreduction of CO2 Catalyzed by a Heterogenized Zn–Porphyrin Complex with a Redox-Innocent Metal Center. ACS Central Science. 2017;3:847-52.
[280] Zhu M, Chen J, Guo R, Xu J, Fang X, Han Y-F. Cobalt phthalocyanine coordinated to pyridine-functionalized carbon nanotubes with enhanced CO2 electroreduction. Applied Catalysis B: Environmental. 2019;251:112-8.
[281] Smith PT, Benke BP, Cao Z, Kim Y, Nichols EM, Kim K, et al. Iron Porphyrins Embedded into a Supramolecular Porous Organic Cage for Electrochemical CO2 Reduction in Water. Angewandte Chemie International Edition. 2018;57:9684-8.
[282] Dou S, Song J, Xi S, Du Y, Wang J, Huang Z-F, et al. Boosting Electrochemical CO2 Reduction on Metal–Organic Frameworks via Ligand Doping. Angewandte Chemie International Edition. 2019;58:4041-5.
[283] Lee JH, Kattel S, Xie Z, Tackett BM, Wang J, Liu C-J, et al. Understanding the Role of Functional Groups in Polymeric Binder for Electrochemical Carbon Dioxide Reduction on Gold Nanoparticles. Advanced Functional Materials. 2018;28:1804762.
[284] Lee J, Lim J, Roh C-W, Whang HS, Lee H. Electrochemical CO2 reduction using alkaline membrane electrode assembly on various metal electrodes. Journal of CO2 Utilization. 2019;31:244-50.

[285] Bard AJ, Faulkner LR, Leddy J, Zoski CG. Electrochemical methods: fundamentals and applications: wiley New York; 1980.
[286] Shen M, Bennett N, Ding Y, Scott K. A concise model for evaluating water electrolysis. International Journal of Hydrogen Energy. 2011;36:14335-41.
[287] Ni M, Leung MK, Leung DYJPotW. Electrochemistry modeling of proton exchange membrane (PEM) water electrolysis for hydrogen production. 2006;16.
[288] Zeng K, Zhang D. Recent progress in alkaline water electrolysis for hydrogen production and applications. Progress in Energy and Combustion Science. 2010;36:307-26.
[289] Haas T, Krause R, Weber R, Demler M, Schmid G. Technical photosynthesis involving CO2 electrolysis and fermentation. Nature Catalysis. 2018;1:32-9.
[290] Mahmood MN, Masheder D, Harty CJ. Use of gas-diffusion electrodes for high-rate electrochemical reduction of carbon dioxide. I. Reduction at lead, indium- and tin-impregnated electrodes. Journal of Applied Electrochemistry. 1987;17:1159-70.
[291] Prakash GKS, Viva FA, Olah GA. Electrochemical reduction of CO2 over Sn-Nafion® coated electrode for a fuel-cell-like device. Journal of Power Sources. 2013;223:68-73.
[292] Del Castillo A, Alvarez-Guerra M, Solla-Gullón J, Sáez A, Montiel V, Irabien A. Sn nanoparticles on gas diffusion electrodes: Synthesis, characterization and use for continuous CO2 electroreduction to formate. Journal of CO2 Utilization. 2017;18:222-8.
[293] Weng L-C, Bell AT, Weber AZ. Modeling gas-diffusion electrodes for CO2 reduction. Physical Chemistry Chemical Physics. 2018;20:16973-84.
[294] Hori Y, Takahashi R, Yoshinami Y, Murata A. Electrochemical reduction of CO at a copper electrode. The Journal of Physical Chemistry B. 1997;101:7075-81.
[295] Hori Y, Murata A, Takahashi R, Suzuki S. Enhanced formation of ethylene and alcohols at ambient temperature and pressure in electrochemical reduction of carbon dioxide at a copper electrode. Journal of the Chemical Society, Chemical Communications. 1988:17-9.
[296] Dinh C-T, Burdyny T, Kibria MG, Seifitokaldani A, Gabardo CM, De Arquer FPG, et al. CO2 electroreduction to ethylene via hydroxide-mediated copper catalysis at an abrupt interface. Science. 2018;360:783-7.
[297] Ganesh I. Conversion of carbon dioxide into methanol – a potential liquid fuel: Fundamental challenges and opportunities (a review). Renewable and Sustainable Energy Reviews. 2014;31:221-57.
[298] Murata A, Hori YJBotCSoJ. Product selectivity affected by cationic species in electrochemical reduction of CO2 and CO at a Cu electrode. Bulletin of the Chemical Society of Japan. 1991;64:123-7.
[299] Hori Y. Electrochemical CO2 Reduction on Metal Electrodes. In: Vayenas CG, White RE, Gamboa-Aldeco ME, editors. Modern Aspects of Electrochemistry. New York, NY: Springer New York; 2008. p. 89-189.
[300] Resasco J, Chen LD, Clark E, Tsai C, Hahn C, Jaramillo TF, et al. Promoter Effects of Alkali Metal Cations on the Electrochemical Reduction of Carbon Dioxide. J Am Chem Soc. 2017;139:11277-87.
[301] Perez-Gallent E, Marcandalli G, Figueiredo MC, Calle-Vallejo F, Koper MTM. Structure- and Potential-Dependent Cation Effects on CO Reduction at Copper Single-Crystal Electrodes. J Am Chem Soc. 2017;139:16412-9.
[302] Varela AS, Kroschel M, Reier T, Strasser P. Controlling the selectivity of CO2 electroreduction on copper: The effect of the electrolyte concentration and the importance of the local pH. Catalysis Today. 2016;260:8-13.
[303] Zhu S, Jiang B, Cai W-B, Shao M. Direct Observation on Reaction Intermediates and the Role of Bicarbonate Anions in CO2 Electrochemical Reduction Reaction on Cu Surfaces. Journal of the American Chemical Society. 2017;139:15664-7.

[304] Wuttig A, Yaguchi M, Motobayashi K, Osawa M, Surendranath Y. Inhibited proton transfer enhances Au-catalyzed CO-to-fuels selectivity. Proceedings of the National Academy of Sciences of the United States of America. 2016;113:E4585-E93.
[305] Chen CS, Handoko AD, Wan JH, Ma L, Ren D, Yeo BS. Stable and selective electrochemical reduction of carbon dioxide to ethylene on copper mesocrystals. Catalysis Science & Technology. 2015;5:161-8.
[306] Gao D, Scholten F, Roldan Cuenya B. Improved CO2 Electroreduction Performance on Plasma-Activated Cu Catalysts via Electrolyte Design: Halide Effect. ACS Catalysis. 2017;7:5112-20.
[307] Varela AS, Ju W, Reier T, Strasser P. Tuning the Catalytic Activity and Selectivity of Cu for CO2 Electroreduction in the Presence of Halides. ACS Catalysis. 2016;6:2136-44.
[308] Singh MR, Goodpaster JD, Weber AZ, Head-Gordon M, Bell AT. Mechanistic insights into electrochemical reduction of CO2 over Ag using density functional theory and transport models. Proceedings of the National Academy of Sciences of the United States of America. 2017;114:E8812-E21.
[309] Dufek EJ, Lister TE, Stone SG, McIlwain ME. Operation of a Pressurized System for Continuous Reduction of CO2. Journal of The Electrochemical Society. 2012;159:F514-F7.
[310] Kohjiro H, Tadayoshi S. Large Current Density CO2 Reduction under High Pressure Using Gas Diffusion Electrodes. Bulletin of the Chemical Society of Japan. 1997;70:571-6.
[311] Hara K. High Efficiency Electrochemical Reduction of Carbon Dioxide under High Pressure on a Gas Diffusion Electrode Containing Pt Catalysts. Journal of The Electrochemical Society. 1995;142:L57.
[312] Hara K, Kudo A, Sakata T. Electrochemical reduction of carbon dioxide under high pressure on various electrodes in an aqueous electrolyte. Journal of Electroanalytical Chemistry. 1995;391:141-7.
[313] Todoroki M, Hara K, Kudo A, Sakata T. Electrochemical reduction of high pressure CO2 at Pb, Hg and In electrodes in an aqueous KHCO3 solution. Journal of Electroanalytical Chemistry. 1995;394:199-203.
[314] Kas R, Kortlever R, Yılmaz H, Koper MTM, Mul G. Manipulating the Hydrocarbon Selectivity of Copper Nanoparticles in CO2 Electroreduction by Process Conditions. ChemElectroChem. 2015;2:354-8.
[315] Mizuno T, Ohta K, Sasaki A, Akai T, Hirano M, Kawabe A. Effect of Temperature on Electrochemical Reduction of High-Pressure CO2 with In, Sn, and Pb Electrodes. Energy Sources. 1995;17:503-8.
[316] Nakagawa S, Kudo A, Azuma M, Sakata T. Effect of pressure on the electrochemical reduction of CO2 on Group VIII metal electrodes. Journal of Electroanalytical Chemistry and Interfacial Electrochemistry. 1991;308:339-43.
[317] De Jesús-Cardona H, del Moral C, Cabrera CR. Voltammetric study of CO2 reduction at Cu electrodes under different KHCO3 concentrations, temperatures and CO2 pressures. Journal of Electroanalytical Chemistry. 2001;513:45-51.
[318] Hara K, Kudo A, Sakata T. Electrochemical CO2 reduction on a glassy carbon electrode under high pressure. Journal of Electroanalytical Chemistry. 1997;421:1-4.
[319] Hara K, Kudo A, Sakata T. Electrochemical reduction of high pressure carbon dioxide on Fe electrodes at large current density. Journal of Electroanalytical Chemistry. 1995;386:257-60.
[320] Sonoyama N, Kirii M, Sakata T. Electrochemical reduction of CO2 at metal-porphyrin supported gas diffusion electrodes under high pressure CO2. Electrochemistry Communications. 1999;1:213-6.
[321] Hara K. Electrochemical Reduction of CO[sub 2] on a Cu Electrode under High Pressure. Journal of The Electrochemical Society. 1994;141:2097.
[322] Jhong H-RM, Brushett FR, Kenis PJA. The Effects of Catalyst Layer Deposition Methodology on Electrode Performance. Advanced Energy Materials. 2013;3:589-99.
[323] Verma S, Lu X, Ma S, Masel RI, Kenis PJA. The effect of electrolyte composition on the electroreduction of CO2 to CO on Ag based gas diffusion electrodes. Physical Chemistry Chemical Physics. 2016;18:7075-84.

[324] Lu X, Leung DYC, Wang H, Maroto-Valer MM, Xuan J. A pH-differential dual-electrolyte microfluidic electrochemical cells for CO2 utilization. Renewable Energy. 2016;95:277-85.
[325] Leonard ME, Clarke LE, Forner-Cuenca A, Brown SM, Brushett FR. Investigating Electrode Flooding in a Flowing Electrolyte, Gas-Fed Carbon Dioxide Electrolyzer. ChemSusChem. 2020;13:400-11.
[326] Rosen BA, Salehi-Khojin A, Thorson MR, Zhu W, Whipple DT, Kenis PJA, et al. Ionic Liquid–Mediated Selective Conversion of CO2 to CO at Low Overpotentials. Science. 2011;334:643-4.
[327] Lu X, Leung DY, Wang H, Xuan J. Microfluidics-based pH-differential reactor for CO2 utilization: A mathematical study. Applied Energy. 2018;227:525-32.
[328] Kannan V, Raman KA, Fisher A, Birgersson E. Correlating Uncertainties of a CO2 to CO Microfluidic Electrochemical Reactor: A Monte Carlo Simulation. Industrial & Engineering Chemistry Research. 2019;58:19361-76.
[329] Wang H, Leung DYC, Xuan J. Modeling of a microfluidic electrochemical cell for CO2 utilization and fuel production. Applied Energy. 2013;102:1057-62.
[330] Aeshala LM, Uppaluri RG, Verma A. Effect of cationic and anionic solid polymer electrolyte on direct electrochemical reduction of gaseous CO2 to fuel. Journal of CO2 Utilization. 2013;3-4:49-55.
[331] Zhang F, Zhang H, Qu C. Imidazolium functionalized polysulfone anion exchange membrane for fuel cell application. Journal of Materials Chemistry. 2011;21:12744-52.
[332] Lin B, Dong H, Li Y, Si Z, Gu F, Yan F. Alkaline Stable C2-Substituted Imidazolium-Based Anion-Exchange Membranes. Chemistry of Materials. 2013;25:1858-67.
[333] Wang B, Sun W, Bu F, Li X, Na H, Zhao C. Comparison of alkaline stability of benzyltrimethylammonium, benzylmethylimidazolium and benzyldimethylimidazolium functionalized poly(arylene ether ketone) anion exchange membranes. International Journal of Hydrogen Energy. 2016;41:3102-12.
[334] Wang C, Xu C, Shen B, Zhao X, Li J. Stable poly(arylene ether sulfone)s anion exchange membranes containing imidazolium cations on pendant phenyl rings. Electrochimica Acta. 2016;190:1057-65.
[335] Liu M, Wang Z, Mei J, Xu J, Xu L, Han H, et al. A facile functionalized routine for the synthesis of imidazolium-based anion-exchange membrane with excellent alkaline stability. Journal of Membrane Science. 2016;505:138-47.
[336] Zhuo YZ, Lai AL, Zhang QG, Zhu AM, Ye ML, Liu QL. Enhancement of hydroxide conductivity by grafting flexible pendant imidazolium groups into poly(arylene ether sulfone) as anion exchange membranes. Journal of Materials Chemistry A. 2015;3:18105-14.
[337] Xu Y, Yang J, Ye N, Teng M, He R. Modification of poly(aryl ether ketone) using imidazolium groups as both pendants and bridging joints for anion exchange membranes. European Polymer Journal. 2015;73:116-26.
[338] Si Z, Qiu L, Dong H, Gu F, Li Y, Yan F. Effects of Substituents and Substitution Positions on Alkaline Stability of Imidazolium Cations and Their Corresponding Anion-Exchange Membranes. ACS Applied Materials & Interfaces. 2014;6:4346-55.
[339] Yang Y, Wang J, Zheng J, Li S, Zhang S. A stable anion exchange membrane based on imidazolium salt for alkaline fuel cell. Journal of Membrane Science. 2014;467:48-55.
[340] Gao Y, Song F, Qiao J, Chen S, Zhao X, Zhang J. Imidazolium-Functionalized Anion Exchange Polymer Electrolytes with High Tensile Strength and Stability for Alkaline Membrane Fuel Cells. Electrochimica Acta. 2015;177:201-8.
[341] Li Z, Jiang Z, Tian H, Wang S, Zhang B, Cao Y, et al. Preparing alkaline anion exchange membrane with enhanced hydroxide conductivity via blending imidazolium-functionalized and sulfonated poly(ether ether ketone). Journal of Power Sources. 2015;288:384-92.
[342] Zhao S-F, Horne M, Bond AM, Zhang J. Is the Imidazolium Cation a Unique Promoter for Electrocatalytic Reduction of Carbon Dioxide? The Journal of Physical Chemistry C. 2016;120:23989-4001.

[343] Masel RI, Salehi-khojin A. Electrocatalysts for carbon dioxide conversion. Google Patents; 2015.
[344] Cook RL, MacDuff RC, Sammells AFJJES. Electrochemical reduction of carbon dioxide to methane at high current densities. Journal of Electroanalytical Chemistry. 1987;134:1873-4.
[345] Jähne B, Heinz G, Dietrich WJJoGRO. Measurement of the diffusion coefficients of sparingly soluble gases in water. Journal of Geophysical Research. 1987;92:10767-76.
[346] Varcoe JR, Atanassov P, Dekel DR, Herring AM, Hickner MA, Kohl PA, et al. Anion-exchange membranes in electrochemical energy systems. Energy & Environmental Science. 2014;7:3135-91.
[347] Merle G, Wessling M, Nijmeijer K. Anion exchange membranes for alkaline fuel cells: A review. Journal of Membrane Science. 2011;377:1-35.
[348] Vincent I, Bessarabov DJR, Reviews SE. Low cost hydrogen production by anion exchange membrane electrolysis: A review. 2018;81:1690-704.
[349] David M, Ocampo-Martínez C, Sánchez-Peña RJJoES. Advances in alkaline water electrolyzers: a review. 2019;23:392-403.
[350] Carmo M, Fritz DL, Mergel J, Stolten DJIjohe. A comprehensive review on PEM water electrolysis. International Journal of Hydrogen Energy. 2013;38:4901-34.
[351] Merle G, Wessling M, Nijmeijer KJJoMS. Anion exchange membranes for alkaline fuel cells: A review. 2011;377:1-35.
[352] Vermaas DA, Wiegman S, Nagaki T, Smith WA. Ion transport mechanisms in bipolar membranes for (photo)electrochemical water splitting. Sustainable Energy & Fuels. 2018;2:2006-15.
[353] Popović S, Smiljanić M, Jovanovič P, Vavra J, Buonsanti R, Hodnik NJACIE. Stability and degradation mechanisms of copper‐based catalysts for electrochemical CO2 reduction. 2020.
[354] Dinh C-T, Burdyny T, Kibria MG, Seifitokaldani A, Gabardo CM, García de Arquer FP, et al. CO₂ electroreduction to ethylene via hydroxide-mediated copper catalysis at an abrupt interface. 2018;360:783-7.
[355] Qiao J, Liu Y, Zhang J. Electrochemical reduction of carbon dioxide: fundamentals and technologies: CRC Press; 2016.
[356] Hori Y, Konishi H, Futamura T, Murata A, Koga O, Sakurai H, et al. “Deactivation of copper electrode” in electrochemical reduction of CO2. 2005;50:5354-69.
[357] Wasmus S, Cattaneo E, Vielstich W. Reduction of carbon dioxide to methane and ethene—an on-line MS study with rotating electrodes. Electrochimica Acta. 1990;35:771-5.
[358] Kyriacou G, Anagnostopoulos A. Electroreduction of CO2 on differently prepared copper electrodes: The influence of electrode treatment on the current efficiences. Journal of Electroanalytical Chemistry. 1992;322:233-46.
[359] Jermann B, Augustynski J. Long-term activation of the copper cathode in the course of CO2 reduction. Electrochimica Acta. 1994;39:1891-6.
[360] Friebe P, Bogdanoff P, Alonso-Vante N, Tributsch H. A Real-Time Mass Spectroscopy Study of the (Electro)chemical Factors Affecting CO2Reduction at Copper. Journal of Catalysis. 1997;168:374-85.
[361] Hori Y, Konishi H, Futamura T, Murata A, Koga O, Sakurai H, et al. “Deactivation of copper electrode” in electrochemical reduction of CO2. Electrochimica Acta. 2005;50:5354-69.
[362] DeWulf DW. Electrochemical and Surface Studies of Carbon Dioxide Reduction to Methane and Ethylene at Copper Electrodes in Aqueous Solutions. Journal of The Electrochemical Society. 1989;136:1686.
[363] Francke R, Schille B, Roemelt M. Homogeneously Catalyzed Electroreduction of Carbon Dioxide—Methods, Mechanisms, and Catalysts. Chemical Reviews. 2018;118:4631-701.
[364] Costentin C, Di Giovanni C, Giraud M, Savéant J-M, Tard C. Nanodiffusion in electrocatalytic films. Nature Materials. 2017;16:1016-21.
[365] Guntern YT, Pankhurst JR, Vávra J, Mensi M, Mantella V, Schouwink P, et al. Nanocrystal/Metal–Organic Framework Hybrids as Electrocatalytic Platforms for CO2 Conversion. 2019;58:12632-9.

[366] Zhang L, Wei Z, Thanneeru S, Meng M, Kruzyk M, Ung G, et al. A Polymer Solution To Prevent Nanoclustering and Improve the Selectivity of Metal Nanoparticles for Electrocatalytic CO2 Reduction. 2019;58:15834-40.
[367] Yang H, Kaczur JJ, Sajjad SD, Masel RI. Electrochemical conversion of CO2 to formic acid utilizing Sustainion™ membranes. Journal of CO2 Utilization. 2017;20:208-17.
[368] Shaner MR, Atwater HA, Lewis NS, McFarland EW. A comparative technoeconomic analysis of renewable hydrogen production using solar energy. Energy & Environmental Science. 2016;9:2354-71.
[369] Verma S, Kim B, Jhong H-RM, Ma S, Kenis PJA. A Gross-Margin Model for Defining Technoeconomic Benchmarks in the Electroreduction of CO2. ChemSusChem. 2016;9:1972-9.
[370] Xia C, Zhu P, Jiang Q, Pan Y, Liang W, Stavitski E, et al. Continuous production of pure liquid fuel solutions via electrocatalytic CO2 reduction using solid-electrolyte devices. Nature Energy. 2019;4:776-85.
[371] Beaumier EP, Pearce AJ, See XY, Tonks IA. Modern applications of low-valent early transition metals in synthesis and catalysis. Nat Rev Chem. 2019;3:15-34.
[372] Greenwood NN, Earnshaw A. Chemistry of the Elements Second ed. Oxford: Butterworth-Heinemann; 1997.
[373] Zheng Y, WZ, Yifeng Li, Jing Chen, BoYu, Jianchen Wang, et al. Energy Related CO2 Conversion and Utilization: Advanced Materials/Nanomaterials, Reaction Mechanisms and Technologies. Nano Energy. 2017;40: 512–39.
[374] Ju W, Bagger A, Hao G-P, Varela AS, Sinev I, Bon V, et al. Understanding activity and selectivity of metal-nitrogen-doped carbon catalysts for electrochemical reduction of CO_2. Nat Commun. 2017;8.
[375] Xuelu M, Yanhui T, Ming L. Mechanistic Studies on the Carboxylation of Hafnocene and ansa-Zirconocene Dinitrogen Complexes with CO_2. Organometallics. 2013;32:7077−82.
[376] Kuber SR, Shyama CM, Pathak B. A computational study of electrocatalytic CO_2 reduction by Mn(I) complexes: Role of bipyridine substituents. Electrochim Act. 2019;297:606-12.
[377] Ning Zhang, Ran Long CG, Xiong Y. Recent progress on advanced design for photoelectrochemical reduction of CO2 to fuels. Sci China Mater. 2018;61:771–805.
[378] Yusuke Kuramochi, Ishitani O. Reaction Mechanisms of Catalytic Photochemical CO_2 Reduction Using Re(I) and Ru(II) Complexes. Coord Chem Rev. 2018;373:333–56.
[379] Wang Y, Tian Y, Yan L, Su Z. DFT Study on Sulfur-Doped g-C3N4 Nanosheets as a Photocatalyst for CO2 Reduction Reaction. J Phys Chem C. 2018;122:7712-9.
[380] Shen J, Kolb MJ, Göttle AJ, Koper MTM. DFT Study on the Mechanism of the Electrochemical Reduction of CO2 Catalyzed by Cobalt Porphyrins. J Phys Chem C. 2016;120:15714-21.
[381] Rodriguez MM, Peng X, Liu L, Li Y, Andino JM. A Density Functional Theory and Experimental Study of CO2 Interaction with Brookite TiO2. J Phys Chem C. 2012;116:19755-64.
[382] Nicole J. Bernstein, Sneha A. Akhade, Janik MJ. Density Functional Theory Study of Carbon Dioxide Electrochemical Reduction on the Fe(100) Surface. Phys Chem Chem Phys. 2014;16: 13708--17.
[383] Hussain J, Skúlason E, Jónsson H. Computational Study of Electrochemical CO2 Reduction at Transition Metal Electrodes. Procedia Comput Sci. 2015;51:1865-71.
[384] Hussain J, Jónsson H, Skúlason E. Calculations of Product Selectivity in Electrochemical CO2 Reduction. ACS Catalysis. 2018;8:5240-9.
[385] Dean J, Yang Y, Austin N, Veser G, Mpourmpakis G. Design of Copper-Based Bimetallic Nanoparticles for Carbon Dioxide Adsorption and Activation. ChemSusChem. 2018;11:1169-78.
[386] Guo C, Zhang T, Deng X, Liang X, Guo W, Lu X, et al. Electrochemical CO2 Reduction to C1 Products on Single Nickel/Cobalt/Iron-Doped Graphitic Carbon Nitride: A DFT Study. ChemSusChem. 2019;12:5126-32.
[387] Isegawa M, Sharma AK. CO2 reduction by a Mn electrocatalyst in the presence of a Lewis acid: a DFT study on the reaction mechanism. Sustain Energ Fuels. 2019;3:1730-8.

[388] Singh MR, Goodpaster JD, Weber AZ, Head-Gordon M, Bell AT. Mechanistic insights into electrochemical reduction of CO2 over Ag using density functional theory and transport models. PNAS. 2017;114:E8812-E21.
[389] Zhong M, Tran K, Min Y, Wang C, Wang Z, Dinh C-T, et al. Accelerated discovery of CO2 electrocatalysts using active machine learning. Nature. 2020;581:178-83.
[390] Nørskov JK, Abild-Pedersen F, Studt F, Bligaard T. Density functional theory in surface chemistry and catalysis. PNAS. 2011;108:937-43.
[391] Weijing D, Weihong Z, Xiaodong Z, Baofeng Z, Lei C, Laizhi S, et al. The application of DFT in catalysis and adsorption reaction system. Energy Procedia. 2018;152:997-1002.
[392] Du X, Gao X, Hu W, Yu J, Luo Z, Cen K. Catalyst Design Based on DFT Calculations: Metal Oxide Catalysts for Gas Phase NO Reduction. J Phys Chem C. 2014;118:13617-22.
[393] Viasus CJ, Alderman NP, Licciulli S, Korobkov I, Gambarotta S. Radical Behavior of CO_2 versus its Deoxygenation Promoted by Vanadium Aryloxide Complexes: How the Geometry of Intermediate CO_2-Adducts Determines the Reactivity. Chem Eur J. 2017;23:17269 – 78.
[394] Zhu C-Y, Zhang Y-Q, Liao R-Z, Xia W, Hu J-C, Wu J, et al. Photocatalytic reduction of CO2 to CO and formate by a novel Co(ii) catalyst containing a cis-oxygen atom: photocatalysis and DFT calculations. Dalton Trans. 2018;47:13142-50.
[395] Zhang C, Lu Y, Zhao R, Menberu W, Guo J, Wang Z-X. A comparative DFT study of TBD-catalyzed reactions of amines with CO2 and hydrosilane: the effect of solvent polarity on the mechanistic preference and the origins of chemoselectivities. Chem Commun. 2018;54:10870-3.
[396] Shunichi Fukuzumi, Yong-Min Lee, Hyun S. Ahn, authora W. Mechanisms of Catalytic Reduction of CO_2 with Heme And Nonheme Metal Complexes. Chem Sci. 2018;9:6017–34.
[397] Liu J-Y, Gong X-Q, Alexandrova AN. Mechanism of CO2 Photocatalytic Reduction to Methane and Methanol on Defected Anatase TiO2 (101): A Density Functional Theory Study. J Phys Chem C. 2019;123:3505-11.
[398] Alnald Javiera, Jack Hess Baricuatrob, Soriagab. Electrocatalytic Reduction of CO2 on Cu and Au/W Electrode Surfaces: Empirical (DEMS) Confirmation of Computational (DFT) Predictions. ECS Trans. 2017; 75:1-17.
[399] Poudyal S, Laursen S. Photocatalytic CO2 reduction by H2O: insights from modeling electronically relaxed mechanisms. Catal Sci Technol. 2019;9:1048-59.
[400] Cheng M-J, Clark EL, Pham HH, Bell AT, Head-Gordon M. Quantum Mechanical Screening of Single-Atom Bimetallic Alloys for the Selective Reduction of CO2 to C1 Hydrocarbons. ACS Catalysis. 2016;6:7769-77.
[401] Mei Y. Theoretical investigations of Metal-N_4-Graphene and Metal-C_3N_4 catalysts for CO_2 reduction State University of New York; 2018.
[402] Cheng M-J, Kwon Y, Head-Gordon M, Bell AT. Tailoring Metal-Porphyrin-Like Active Sites on Graphene to Improve the Efficiency and Selectivity of Electrochemical CO2 Reduction. The Journal of Physical Chemistry C. 2015;119:21345-52.
[403] Wenjun Zhang, Yi Hu, Lianbo Ma, Guoyin Zhu, Yanrong Wang, Xiaolan Xue, et al. Progress and Perspective of Electrocatalytic CO_2 Reduction for Renewable Carbonaceous Fuels and Chemicals. Adv Sci. 2018;5:1-24.
[404] Saravanan K, Basdogan Y, Dean J, Keith JA. Computational investigation of CO2 electroreduction on tin oxide and predictions of Ti, V, Nb and Zr dopants for improved catalysis. J Mater Chem A. 2017;5:11756-63.
[405] Abdulhadi A. Al-Omari, Nguyen HL. Electrocatalytic CO_2 Reduction: From Homogeneous Catalysts to Heterogeneous-Based Reticular Chemistry. Molecules. 2018;23:1-12
[406] Garza AJ, Bell AT, Head-Gordon M. Mechanism of CO2 Reduction at Copper Surfaces: Pathways to C2 Products. ACS Catalysis. 2018;8:1490-9.

[407] Todorova TK, Schreiber MW, Fontecave M. Mechanistic Understanding of CO2 Reduction Reaction (CO2RR) Toward Multicarbon Products by Heterogeneous Copper-Based Catalysts. ACS Catalysis. 2020;10:1754-68.
[408] Goodpaster JD, Bell AT, Head-Gordon M. Identification of Possible Pathways for C–C Bond Formation during Electrochemical Reduction of CO2: New Theoretical Insights from an Improved Electrochemical Model. The Journal of Physical Chemistry Letters. 2016;7:1471-7.
[409] Xiao H, Cheng T, Goddard WA. Atomistic Mechanisms Underlying Selectivities in C1 and C2 Products from Electrochemical Reduction of CO on Cu(111). Journal of the American Chemical Society. 2017;139:130-6.
[410] Luo W, Nie X, Janik MJ, Asthagiri A. Facet Dependence of CO2 Reduction Paths on Cu Electrodes. ACS Catalysis. 2016;6:219-29.
[411] Cheng T, Xiao H, Goddard WA. Full atomistic reaction mechanism with kinetics for CO reduction on Cu(100) from ab initio molecular dynamics free-energy calculations at 298 K. Proceedings of the National Academy of Sciences. 2017;114:1795-800.
[412] Grimme S. J Chem Phys. 2003;118:9095-102.
[413] Grimme S. J Comput Chem. 2004;25:1463-73.
[414] Pyykko P. Relativistic Effects in Chemistry: More Common Than You Thought. Annual Review of Physical Chemistry 2012;63:45-64.
[415] Demissie TB, Garabato BD, Ruud K, Kozlowski PM. Mercury Methylation by Cobalt Corrinoids: Relativistic Effects Dictate the Reaction Mechanism. Angew Chem Int Ed. 2016;55:11503-6.
[416] Liu W. Handbook of Relativistic Quantum Chemistry. Springer, Berlin, Heidelberg; 2017.
[417] García de Arquer FP, Dinh C-T, Ozden A, Wicks J, McCallum C, Kirmani AR, et al. CO2 electrolysis to multicarbon products at activities greater than 1 A cm-2. Science. 2020;367:661-6.
[418] Verma S, Kim B, Jhong H-RM, Ma S, Kenis PJA. A Gross-Margin Model for Defining Technoeconomic Benchmarks in the Electroreduction of CO2. 2016;9:1972-9.
[419] De Luna P, Hahn C, Higgins D, Jaffer SA, Jaramillo TF, Sargent EH. What would it take for renewably powered electrosynthesis to displace petrochemical processes? Science. 2019;364.
[420] Nwabara UO, Cofell ER, Verma S, Negro E, Kenis PJA. Durable Cathodes and Electrolyzers for the Efficient Aqueous Electrochemical Reduction of CO2. 2020;13:855-75.
[421] Sanz-Pérez ES, Murdock CR, Didas SA, Jones CW. Direct Capture of CO2 from Ambient Air. Chemical Reviews. 2016;116:11840-76.
[422] Chalmin A. Direct air capture: recent developments and future plans. Geoengineering Monitor. 2019.
[423] Smith WA, Burdyny T, Vermaas DA, Geerlings H. Pathways to Industrial-Scale Fuel Out of Thin Air from CO2 Electrolysis. Joule. 2019;3:1822-34.
[424] ElMekawy A, Hegab HM, Mohanakrishna G, Elbaz AF, Bulut M, Pant D. Technological advances in CO2 conversion electro-biorefinery: A step toward commercialization. Bioresource Technology. 2016;215:357-70.
[425] Aresta M, Dibenedetto A, Dutta A. Energy issues in the utilization of CO2 in the synthesis of chemicals: The case of the direct carboxylation of alcohols to dialkyl-carbonates. Catalysis Today. 2017;281:345-51.
[426] Tufa RA, Hnát J, Němeček M, Kodým R, Curcio E, Bouzek K. Hydrogen production from industrial wastewaters: An integrated reverse electrodialysis - Water electrolysis energy system. Journal of Cleaner Production. 2018;203:418-26.
[427] Sabatino S, Galia A, Saracco G, Scialdone O. Development of an Electrochemical Process for the Simultaneous Treatment of Wastewater and the Conversion of Carbon Dioxide to Higher Value Products. ChemElectroChem. 2017;4:150-9.